Investigation and Characterization of Eco-friendly Limestone-rich Concretes and their Carbonation Behavior

TECHNISCHE UNIVERSITÄT DARMSTADT

Vom Fachbereich Chemie

der Technischen Universität Darmstadt

zur Erlangung des Grades

Doktor-Ingenieurs

(Dr.-Ing.)

Dissertation

von Halil YILDIRIM, M.Sc.

Erstgutachterin: Prof. Dr. Barbara Albert

Zweitgutachter: Prof. Dr. -Ing. Carl-Alexander Graubner

Darmstadt 2018

Tag der Einreichung: 18. Dezember 2017

Tag der mündlichen Prüfung: 23. April 2018

YILDIRIM, Halil: Investigation and Characterization of Eco-friendly Limestone-rich Concretes and their Carbonation Behavior
Darmstadt, Technische Universität Darmstadt,
Jahr der Veröffentlichung der Dissertation auf TUprints: 2018

For my family

ACKNOWLEDGEMENT

I would like to thank Prof. Dr. Barbara Albert for allowing me to be a part of her research group, her competent and friendly support, as well as her discussion and helpfulness during every stage of my research.

I am grateful to Dr. Kathrin Hofmann for her invaluable help, interesting ideas, and supporting professional discussions through my doctorate.

I reserve my special thanks to Prof. Dr. Carl-Alexander Graubner from Institut für Massivbau TU Darmstadt, his group members Dr. Tilo Proske, Dr. Stefan Hainer, Dr. Moein Rezvani and Sarah Steiner for their collaboration and helpful support and allowing me to use the laboratories.

I would like to thank all of my colleagues for their friendship, scientific comments and suggestions as well as their pleasant cooperation and nice activities both inside and outside the university.

I am also thankful to Dr. Franziska Emmerling from BAM (Bundesanstalt für Materialforschung und –prüfung, Berlin) and her group members Dr. Julia Stroh and Dr. Ana Guilherme Buzanich for their support for the neutron diffraction measurements at ESRF (European Synchrotron Radiation Facility) in France.

I thank to my friends and flat mates in Germany for their friendship and help.

The greatest thanks go to my family: my parents Yusuf and Emine YILDIRIM, my brothers Mustafa and Halit YILDIRIM for their endless love, moral and support during my stay in Germany.

This work was carried out during the period from September 2012 to September 2016 in the work group of Prof. Barbara Albert at the Eduard-Zintl-Institute of Inorganic and Physical Chemistry at the Technische Universität Darmstadt. Parts of this work have already been published, or have been presented on the occasion of a series of conferences.

Conference Presentations and Procedings:

16-18 September 2015, 19. Internationale Baustofftagung: **Yildirim, H., Hainer, S., Hofmann, K., Albert, B. R.; Graubner, C.-A.,** Carbonation of Hydrated Clinker Phases, Weimar, Germany, ISBN 978-3-00-050225-5 Band 1 (Poster, Conference Proceedings)

4-9 October 2015, Sustainable Industrial Processing Summit and Exhibition: Yildirim, H., Hainer, S., Hofmann, K., Albert, B. R.; Graubner, C.-A., Investigation of Carbonation Reactions in Eco-friendly Cements, Volume 6, Coating, Cement, Rare Earth and Ferro-alloys, ISBN 978-1-987-820-29-4. (Oral Presentation, Conference Proceedings)

Kurzzusammenfassung

Untersuchung und Charakterisierung von klimaschonenden, kalksteinmehlreichen Betonen und deren Karbonatisierungsverhalten

Diese Arbeit resultiert aus einer interdisziplinären Studie zum Karbonatisierungsverhalten klinkerreduzierter, umweltfreundlicher Zemente und Betone, die in Zusammenarbeit mit dem Institut für Massivbau der Technischen Universität Darmstadt durchgeführt wurde. Im Fokus dieser Zusammenarbeit stand das Karbonatisierungsverhalten von Zementen mit hohen Kalksteinmehlgehalten (bis zu 50 %). Die Verwendung von Kalksteinmehl erlaubt eine Reduzierung von Portlandzementklinker, dessen Herstellung für die hohen CO_2-Emissionen bei der Zementproduktion verantwortlich ist. Durch einen reduzierten Anteil an Portlandzementklinker in Zement und Beton werden allerdings auch weniger Hydratationsprodukte wie Calciumhydroxid und C-S-H-Phasen gebildet. Eine Mindestmenge an Calciumhydroxid und eine hohe Dichtigkeit des Zementsteins sind jedoch für die Passivierung des Bewehrungsstahls notwendig. Daher ergeben sich hinsichtlich der Anwendung sehr kalksteinreicher Zemente und Betone viele Fragen bezüglich der Dauerhaftigkeit gegenüber karbonatisierungsinduzierter Bewehrungskorrosion.

Im Rahmen dieser Arbeit wurden die Reaktionen der wichtigsten Hydratationsprodukte von Zement mit CO_2 untersucht. Dazu wurden im ersten Teil der Arbeit Zementleimproben aus kommerziell erhältlichen Zementen mit und ohne Zusatz von Kalksteinmehl präpariert und das Karbonatisierungsverhalten untersucht. Um ein tieferes Verständnis der ablaufenden Reaktionen in diesem komplexen Material zu erhalten, wurden zudem die wichtigsten Klinkerphasen mit hoher Reinheit im Labor synthetisiert, hydratisiert und die Reaktionsprodukte nach der Karbonatisierung untersucht. Um eine Vorstellung der zeitlichen Abläufe während der Reaktion mit CO_2 zu erhalten, wurde eine Versuchsanordnung für eine beschleunigte Karbonatisierungsreaktion entwickelt und getestet. Zusätzlich wurde auch ein Modellzement synthetisiert und untersucht. Die detaillierten Untersuchungen zeigten, dass der Karbonatisierungswiderstand nicht direkt von der Menge des gebildeten $Ca(OH)_2$ abhängt, sondern dass das Wasser/Zement-Verhältnis eine große Rolle spielt. Die zeitabhängigen Untersuchungen der Einzelphasen zeigten deutlich, dass $Ca(OH)_2$ und C-S-H-Phasen gleichzeitig karbonatisieren – anders als in gängigen Modellen angenommen, die besagen, dass die C-S-H-Phasen erst dann mit CO_2 reagieren, wenn $Ca(OH)_2$ verbraucht ist.

Abstract

Investigation and characterization of eco-friendly limestone-rich concretes and their carbonation behaviour

This work results from an interdisciplinary study on the carbonation behavior of clinker-reduced eco-friendly cements and concretes in collaboration with the Institut für Massivbau, Technische Universität Darmstadt. The focus of this study is the carbonation behavior of cements with high limestone content (up to 50 %). The use of limestone powder allows for the reduction of Portland cement clinker, whose synthesis is responsible for the high CO_2 emission during the cement production. The reduced Portland cement clinker contents in cement and concrete results in lower amounts of hydration products such as calcium hydroxide and C-S-H phases. However, a minimum amount of $Ca(OH)_2$ and a high density of the hardened cement pastes are necessary to ensure sufficient alkalinity, which is necessary for the passivation of the steel reinforcement. Therefore, questions regarding the durability against carbonation induced corrosion of the reinforcement must be answered before new limestone-rich cements and concretes will be applied in practice.

In the framework of this work the reactions of the most important hydration products of cement with CO_2 were investigated. In the first part of this work cementitious pastes of commercially available cement with and without limestone addition were prepared and the carbonation reactions investigated. To gain a deeper insight into the reactions occurring in this complex material the most important clinker phases were synthesized with high purity. The carbonation reactions of the hydrated samples were investigated in detail. To understand the time-dependence and the order of the reactions a suitable experimental setup for the accelerated carbonation reaction was established and tested. Additionally, a model cement was synthesized and investigated. The detailed investigations showed, that the carbonation resistance does not depend solely on the amount of $Ca(OH)_2$ initially formed; it reveals the important role of the water/cement-ratio. The time-dependent investigations of the single phases show that $Ca(OH)_2$ and the C-S-H phases react simultaneously with CO_2 – differently from well-established models claiming that C-S-H phases only react with CO_2 after the complete amount of $Ca(OH)_2$ is consumed.

Table of Content

1. INTRODUCTION 1

2. CEMENT AND CONCRETE 4

2.1. Definition 4

2.2. Production of Cement 4

2.3. Composition of Portland cement 5

2.3.1. Tricalcium silicate (Ca_3SiO_5) 6

2.3.2. Dicalcium silicate (Ca_2SiO_4) 7

2.3.3. Tricalcium aluminate ($Ca_3Al_2O_6$) 8

2.3.4. Tetracalcium aluminoferrite $Ca_2(Al,Fe)_2O_5$ 8

2.3.5. Calcium sulphate and other minor components 9

2.4. Hydration of Portland cement 10

2.4.1. General Remarks 10

2.4.2. Hydration of clinker phases 10

2.5. Performance and durability of Portland cement 13

2.5.1. Carbonation of concrete 14

2.6. Portland cement blends and eco –friendly cements 16

3. CHARACTERIZATION AND PREPARATION TECHNIQUES 19

3.1. X-ray powder diffraction 19

3.2. Rietveld method 20

3.3. Thermal analysis 21

3.4. Carbonation depth measurements 22

3.5. Porosimetry Measurements 23

3.6. Equipment for high temperature synthesis 24

3.7. Carbonation chamber (Carbobox) 25

4. STATE OF THE ART 26

5. INVESTIGATION OF CARBONATION REACTIONS IN LIMESTONE-RICH CEMENT PASTES 31

5.1. Experimental program 31

5.1.1. Starting materials and mix design approach 31

5.1.2. Preparation and characterization of cement pastes 32

5.1.3. Carbonation of cement pastes 39

5.1.3.1. Experimental procedure 39

5.1.3.2. Quantitative determination of $CaCO_3$ 42

5.2. Conclusion 44

6. INVESTIGATION OF PURE CLINKER PHASES 49

6.1. Preparation and synthesis of pure clinker phases 49

6.1.1. Ca_3SiO_5 49

6.1.2. Ca_2SiO_4 50

6.1.3. $Ca_3Al_2O_6$ 51

6.1.4. $Ca_2(Al,Fe)_2O_5$ 52
6.1.5. Synthesis of Ettringite 53
6.2. Hydration and carbonation of pure clinker phases 55
6.2.1. Preparation of cement pastes from pure phases 55
6.2.2. Hydration of clinker phases for direct comparison with the cement paste samples. 56
6.2.3. Time-dependent carbonation of pure clinker phases 61
6.2.4. Time-dependent carbonation of pure clinker phases in polystyrene cups 67
6.2.5. Time-dependent carbonation of a model cement 75
6.3. Comparison of the carbonated samples and discussion 78
6.4. First attempt to time-dependent in-situ investigations 80
7. CONCLUSIONS 83
8. APPENDIX 86
9. LITERATURE 97

1. INTRODUCTION

Concrete is the most important and most widely used building material of our time. Approximately 4.1 billion tons of cement, the most important component of concrete, was produced worldwide in 2015 (in Germany: approx. 32 million tons) [1]. Cement is crucial for constructing, maintaining and improving infrastructure; therefore it is of great economic and social relevance. Its mineral composition can in principle be called environmentally friendly. Otherwise, cement-based materials, like concrete, are associated with heavy air-pollution, because the production of cement accounts for approximately 5 - 7 % of the global greenhouse gas emissions [1]. The full life-cycle of a concrete structure, beginning with the extraction of the starting materials, their transport, the processing at the building site, post-treatment, maintenance and demolition at the end is associated with certain effects. The majority of the negative environmental impact of concrete is attributed to the cement. It is reported that over 90 % of the greenhouse effect related to concrete depends on the production of cement [2-4].

Due to the increase in environmental awareness among the population and to the commitments of the Kyoto Protocol (1997), eco-friendly products became more and more important. The cement industry has followed these developments. Several means are already applied by the industry to lower the environmental impact of the cement production. The methods are [5, 6]:

1) New and efficient technologies for the production of cements.
2) The use of alternative and environmentally-friendly fuels or energy sources (e.g. bio fuels).
3) Blended cements with partial substitution of clinker by filler materials or supplementary cementitious materials (SCMs) like blast furnace slag, fly ash, limestone, and pozzolans.

The easiest way to reduce the greenhouse potential of cement is replacing it with other cementitious materials. In figure 1.1 the reduction in environmental impact of Portland cement, the most used cement type, by substitution with selected supplementary materials is shown.

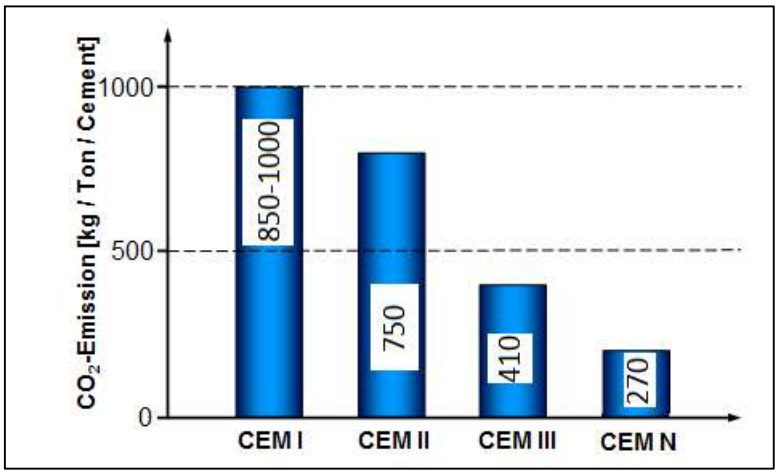

Figure 1.1: The greenhouse gas potential (in kg pro ton) of different cement types: CEM I Portland cement, CEM II Portland composite cement, CEM III Blast Furnace Cement, CEM N eco-friendly cement [7].

In recent years the cement industry launched clinker-reduced and finely ground cement types with the addition of secondary raw materials. Advantages of these cements are low production costs and a reduced environmental impact by a reduction of the amount of Portland cement clinker. To ensure that such low-clinker cements can be used in building practice, the performance of the corresponding concretes must be demonstrated with regard to their workability, compressive strength and durability. In particular, a reduction of clinker can cause a lower durability of reinforced concrete, since the carbonation resistance usually drops significantly with a lower proportion of clinker content. For this reason, the use of environmentally-friendly cements in building practice currently is very limited. The chances and limitations of concretes from these cements need to be identified in order to advance further developments in this area.

This work results from an interdisciplinary study on the carbonation behavior of clinker-reduced limestone-rich eco-friendly cements and concretes, undertaken in collaboration with the Institut für Massivbau at TU Darmstadt (group of Prof. Dr. C.-A. Graubner). One of their contributions to the development of eco-friendly cement is a drastic substitution of ordinary Portland cement with limestone. The focus of this collaboration is the carbonation behavior of cements with high addition of limestone (up to 50 %). The use of these new cement mixtures in building practice requires a sufficient durability of the reinforced concrete elements in the life-time of a building. For that reason the engineers investigate the compressive strengths, carbonation depths, and water vapor diffusion resistances dependent on the limestone addition of cementitious pastes, mortars, and cement samples in great detail. Commonly accepted

techniques like the phenolphthalein test for the determination of the carbonation depths are used. In the end a model for the predication of the carbonation behavior and a recipe for the application in practice are desired.

However, to fully understand this complex material all ongoing chemical reactions and interactions of the phases present have to be investigated, too. Another important aspect is the effect of instabilities at the nanoscale. It is important that the atomic, nanoscale, and higher lengths scale structures and the resulting properties are understood. The aim of this work was to gain insight into the reactions occurring during the carbonation of samples made from eco-friendly cement with chemical methods. In the first step cementitious pastes prepared from commercially available cement with and without limestone addition were investigated. These studies provided a first idea about the ongoing reactions due to the complex nature of the materials. In a second step the most important clinker phases were synthesized with high purity. These samples were than hydrated and carbonated to elucidate the individual reactions and clearly identify all related products. To obtain reliable data on the time-dependence and related products of accelerated carbonation reactions a suitable experimental setup was established. For that purpose different sample treatments were developed and tested. Additionally, a model cement was synthesized and investigated to transfer the results from the single phases to a real system. The results are discussed and compared to findings described in literature. The experimental data obtained as part of this work can now be used in hydrochemical modeling of the reaction processes carried out by the group of Prof. Dr. C.-A. Graubner.

2. CEMENT AND CONCRETE

2.1. Definition

Concrete is generally defined as a mixture of aggregates, water, cement, and some chemical admixtures which harden over time. A concrete can contain a wide range of materials which can be classified as hydraulic binders and filler materials. A hydraulic binder is a material which hardens due to a reaction with water. Cement acts as the hydraulic binder in concrete which holds other filler materials together and forms a strong and rigid material. The ratio of the amount of water to the amount of cement used in a concrete mix is termed water/cement (w/c) ratio. It usually refers to proportions by mass and typical values are 0.3-0.6. A hardened mixture of cement and water without filler materials is called cement paste. The cement pastes contain several crystalline, poorly crystalline or amorphous phases which result from the reaction between water and cement. Concretes are generally made using lime-based binders such as Portland cement. The filler materials are primarily sand, gravel and rock. Cement is also used in mortars which are workable pastes and mixtures of cement, water and fine aggregates. Mortars are mostly used to bind stones, bricks, and concrete masonry units together or to fill and seal irregular gaps.

2.2. Production of Cement

For the production of cement a mixture of raw materials is finely ground, blended together and fed into a rotary cement kiln which reaches high temperatures around 1450 °C.

For the desired final composition it is important to ensure adequate amounts of calcium, silicon, aluminum, and iron oxides in the raw materials. These raw materials also contain minor (or in some cases trace) amounts of alkali and alkaline earth metal oxides (potassium, strontium, sodium oxides) and heavy metal oxides. Clays are a primary and common source of silica and alumina. The cement production is a high-temperature process; a temperature of 1450 °C must be reached to obtain the highly reactive forms of the important components. The compounds formed at this temperature are called clinker phases. Finally the clinker phases are quenched and mixed with gypsum. There are different types of cement; ordinary Portland cement (OPC) is the most important and most used cement in the world. Table 2.1 shows the materials used for the production of ordinary Portland cement.

Table 2.1: General composition of ordinary Portland cement and some raw materials used in the Portland cement production.

Chemical content	Abundance in OPC, %	Raw materials
CaO	60-69	limestone, marl, chalk, ground concrete
SiO_2	20-25	clay, slag, sand, fly ash
Al_2O_3	4-7	aluminum ores, clay, fly ash
Fe_2O_3	0.2-5	iron ores, blast furnace dust, clay
SO_3	0.1-3	gypsum, $CaSO_4$ (anhydrite)
MgO	0.5-5	minor phases or traces in raw materials
$Na_2O + K_2O$	0.5-1.5	minor phases or traces in raw materials

2.3. Composition of Portland cement

Ordinary Portland cement is composed of the four main clinker phases, which are Ca_3SiO_5 (52-85%), Ca_2SiO_4 (1-27%), $Ca_3Al_2O_6$ (0-16%), and $Ca_2(Al,Fe)_2O_5$ (4-16%), and a sulphate source, generally gypsum (3-5%). In the cement chemistry some simplified chemical notations are used to refer to the oxides and compounds. S is used for SiO_2, C for CaO, A for Al_2O_3, F for Fe_2O_3, **s** for SO_3, and H for H_2O. In Table 2.2 the notations of main components of OPC and the main hydration products are given.

Table 2.2: Cement notations for the main phases [8, 9].

Phase name	Chemical formula	Cement notation	Mineral name
Tricalcium silicate	Ca_3SiO_5	C_3S	Alite
Calcium silicate	Ca_2SiO_4	C_2S	Belite
Tricalcium aluminate	$Ca_3Al_2O_6$	C_3A	Aluminate
Tetracalcium aluminoferrite	$Ca_2(Al,Fe)_2O_5$	$C_2(AF)$	Brownmillerite
Calcium hydroxide	$Ca(OH)_2$	CH	Portlandite
Calcium trisulpho- aluminonate	$Ca_6Al_2[OH]_{12}(SO_4)_3 \cdot 26H_2O$	$C_6A\mathbf{s}_3H_{32}$ (AFt)	Ettringite
Calcium silica hydrate	$Ca_xSiO_2 \cdot yH_2O$	C-S-H	Jennite, Tobermorite
Calcium sulphate dihybride	$CaSO_4 \cdot 2H_2O$	$C\mathbf{s}H_2$	Gypsum
Calcium oxide	CaO	C	Lime
Calcium Aluminum Monosulphate	$Ca_4Al_2(SO_3) \cdot 12H_2O$	$C_6A\mathbf{s}H_{12}$ (AFm)	

2.3.1. Tricalcium silicate (Ca_3SiO_5)

Ca_3SiO_5 (C_3S) is the major component of Portland cement and it is a highly hydraulic compound. Ca_3SiO_5 is stable at temperatures above 1250 °C according to the phase diagram in figure 2.1. It forms by a reaction of Ca_2SiO_4 and CaO in the liquid phase.

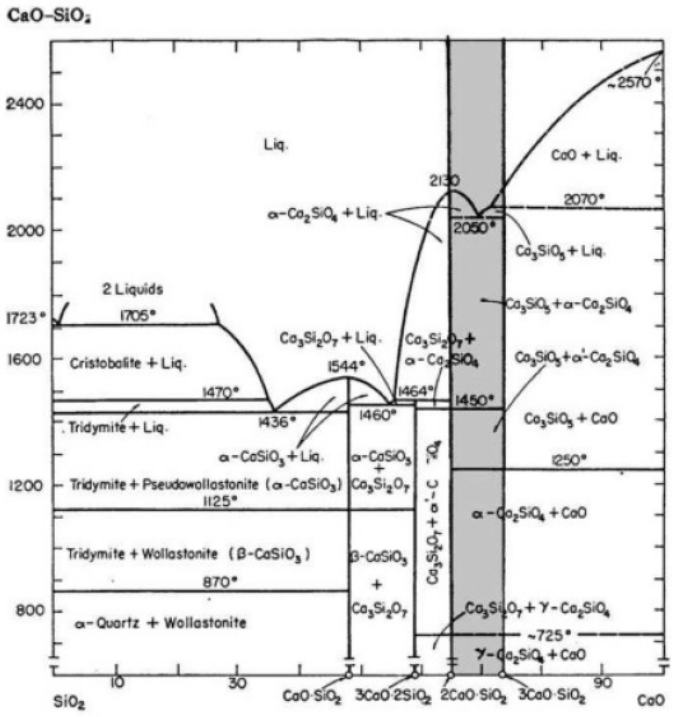

Figure 2.1: Phase diagram of CaO-SiO_2. The dark area is the only suitable field for Portland cement production [8].

Ca_3SiO_5 has seven different polymorphs that form depending on the presence of impurities or temperature. As a pure phase, C_3S is metastable at room temperature and crystallizes in the triclinic crystal system. With increasing temperatures phase transitions to monoclinic and rhombohedral modifications are observed. The transition temperatures are given in Table 2.4.

Table 2.4: Transition temperatures for C_3S [9, 10]. T refers to the triclinic, M refers to the monoclinic and R refers to the rhombohedral modifications.

Transition step	T1↔T2	T2↔T3	T3↔M1	M1↔M2	M2↔M3	M3↔R
Temperature, °C	620	920	980	990	1060	1070

Ordinary Portland cement usually contains some impurities like MgO, Al_2O_3, and Fe_2O_3. In the crystal structure of Ca_3SiO_5 Mg^{2+} and Fe^{2+} ions can replace Ca^{2+} ions, and Al^{3+} can substitute for Si^{4+}. In industrial clinkers these impurities are usually between 3–4 wt.% .

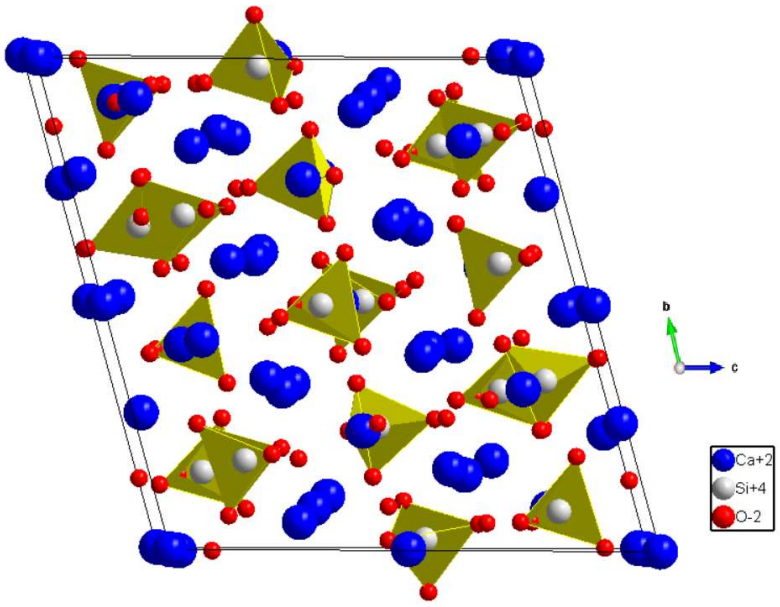

Figure 2.2: Unit cell of triclinic Ca_3SiO_5 (T_1), view along the [100] direction [11].

The monoclinic and the triclinic modifications are the most important modifications of C_3S and they are highly hydraulic.

2.3.2. Dicalcium silicate (Ca_2SiO_4)

Ca_2SiO_4 (C_2S) is stable between room temperature and its melting point at 2130 °C which can be seen in the phase diagram in figure 2.1. It has five different polymorphs in this temperature range. It is the β modification that generally occurs in Portland cement. The most stable modification at the sintering temperature is either α or α', but these high-temperature polymorphs normally transform into the β-phase during cooling and are not found in the final product. The transformation of β-C_2S into γ-C_2S is undesirable and has to be avoided because γ-C_2S is almost non-hydraulic. Transition temperatures are given in Table 2.4.

Table 2.4: Transition temperatures for C_2S [9, 10].

Transition step	$\alpha \leftrightarrow \alpha'_H$	$\alpha'_H \leftrightarrow \alpha'_L$	$\alpha'_L \leftrightarrow \beta$	$\beta \rightarrow \gamma$	$\gamma \rightarrow \alpha'_L$
Temperature, °C	1425	1160	630-680	<500	780-860

All phase transitions are reversible except the one between the β and the γ form. The γ – modification does not transform into the β-form when it is heated. It converts directly into the α'_L modification upon reaching a temperature between 780 and 860 °C.

In industrial cement C_2S can usually contain up to 4–6 wt. % impurities, mostly Al^{3+}, Fe^{3+}, SO_4^{2-}, Mg^{2+} and K^+ ions. There is also a good miscibility with both P_2O_5 and B_2O_3. Especially boron oxide has proven to increase the stability of β-C_2S.

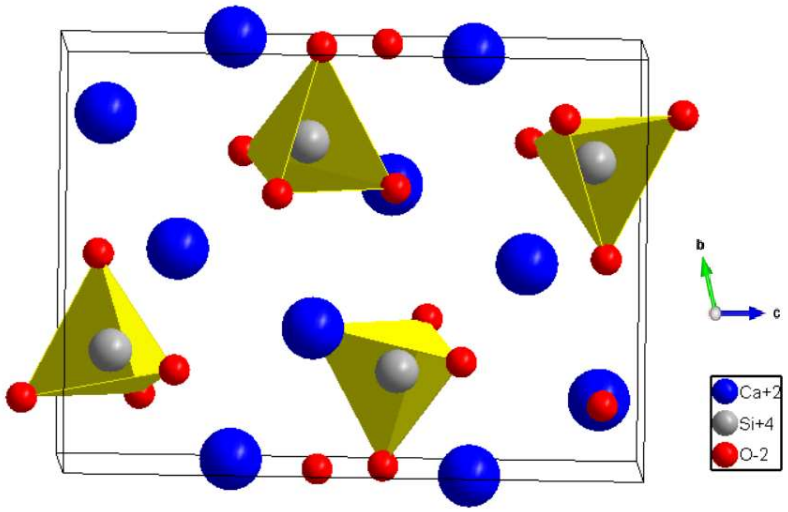

Figure 2.3: Unit cell of β-Ca_2SiO_4, view along the [100] direction [12].

2.3.3. Tricalcium aluminate ($Ca_3Al_2O_6$)

The amount of C_3A in Portland cement can reach 16 wt. %. Generally, cubic, orthorhombic and monoclinic modifications can be observed. Substitutions with other cations are possible. The most critical substituent is Na^+, since it induces changes of the modifications. In technical clinkers the cubic modification is usually present, but due to a sufficient Na_2O content, the orthorhombic modification can be observed. The Na_2O content is usually not high enough to stabilize the monoclinic modification in cement. The influence of the Na_2O concentration on the phase stability is shown in table 2.5.

Table 2.5: Stability of the modifications of $Ca_3Al_2O_6$ depending on the Na_2O content [13].

Na_2O wt. %	Modification	Crystal System
0.0-1.0	C_I	cubic
1.0-2.4	C_{II}	cubic
2.4-3.7	C_{II} +O	cubic + orthorhombic
3.7-4.6	O	orthorhombic
4.6-5.7	M	monoclinic

$Ca_3Al_2O_6$ is very reactive and plays an important role at the beginning of the hydration reaction; it gives early strength to the concrete. Its hydration is mostly influenced by the presence of sulphate-containing compounds such as gypsum.

2.3.4. Tetracalcium aluminoferrite $Ca_2(Al,Fe)_2O_5$

$Ca_2(Al,Fe)_2O_5$ ($C_2(AF)$) can be described as a solid solution between the boundary phases $Ca_2Al_2O_3$ and $Ca_2Fe_2O_3$. $Ca_2(Al,Fe)_2O_5$ is also a naturally occurring mineral called brownmillerite. The actual composition of $C_2(AF)$ in cement clinker is generally higher in

aluminum than in iron, and there is a considerable substitution with SiO_2 and MgO [14]. In the presence of gypsum or sulphate ions $C_2(AF)$ behaves like C_3A.

The structure of $C_2(AF)$ can be considered as an oxygen-deficient perovskite structure where the oxygen vacancies are ordered along the (010)-planes. This brownmillerite-type structure ($A_2B_2O_5$) consists of alternating layers of corner-sharing BO_6 octahedra and BO_4 tetrahedra. Depending on foreign ions $C_2(AF)$ can crystallize in the following space groups: *Ibm*2, *Icmm or Pnma* [14, 15].

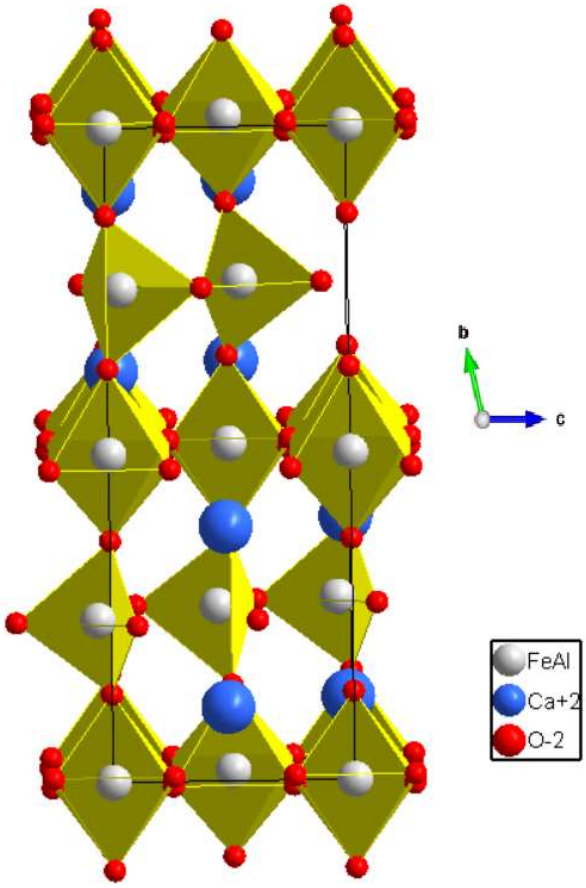

Figure 2.4: Unit cell of $Ca_2(Al,Fe)_2O_5$ in space group *Ibm*2, view along the [100] direction [15].

2.3.5. Calcium sulphate and other minor components

Gypsum is mixed with the clinker phases to slow down initial hydration reactions. The hemihydrate ($CaSO_4 \cdot 0.5H_2O$) and the water-free anhydrite ($CaSO_4$) are also observed due to the dehydration of gypsum. Besides the calcium sulphate some alkali metal sulphate like arcanite (K_2SO_4), aphthitalite ($Na_2SO_4 \cdot 3K_2SO_4$), Ca-langbeinite ($CaSO_4 \cdot K_2SO_4$), thenardite (Na_2SO_4) and syngenite ($CaK_2(SO_4)_2 \cdot H_2O$) originating from raw materials occur in cement mixtures. It may also contain oxides like MgO, Fe_2O_3, free lime (CaO), Na_2O, and K_2O [5, 8, 9, 14].

2.4. Hydration of Portland cement

2.4.1. General Remarks

Portland cement and the resulting concrete are complex chemical systems whose components react and transform during the hydration reaction. When Portland cement and water is mixed a series of reactions resulting in different hydration products occur. Some reactions are very fast causing early strength of the concrete, some will continue for a long time (days to months). The detailed reactions are described below.

2.4.2. Hydration of clinker phases

The primary hydration products of C_3S and C_2S are Portlandite ($Ca(OH)_2$) and calcium-silicate-hydrate phases (C-S-H phases) according to equations 2.1 , 2.2 and 2.3.

$$Ca_3SiO_5 + (3 - x + n)\, H_2O \rightarrow Ca_xSiO_2{\cdot}n\, H_2O + (3-x)\, Ca(OH)_2 \qquad \textbf{[2.1]}$$

When the solution is saturated with $Ca(OH)_2$, n is approximately 4 and x is about 1.7 (equation 2.3.).

$$2\, Ca_3SiO_5 + 7\, H_2O \rightarrow 3\, CaO{\cdot}2SiO_2{\cdot}4H_2O + 3\, Ca(OH)_2 \qquad \textbf{[2.2]}$$

$$2\, Ca_2SiO_4 + 5\, H_2O \rightarrow CaO{\cdot}2SiO_2{\cdot}4H_2O + Ca(OH)_2 \qquad \textbf{[2.3]}$$

Both hydration reactions are supposed to be very similar, although the hydration of C_3S is much faster than that of C_2S. The general term “calcium silicate hydrate phase” or abbreviated “C-S-H” phase refers to approximately 40 compounds with varying composition and crystalinity. The term gives no information on the composition; usually the molar ratio m (CaO)/m (SiO_2) is given. In the cement nomenclature this ratio is termed C/S ratio. Hydration of Portland cement often results in nonstoichiometric, amorphous, or semi-crystalline C-S-H phases. Numerous studies show that the Ca/Si ratio in fresh cement is between 2.8 - 1.8 and 1.2 - 0.9 in aged cement. Due to further reactions of the cement with the environment (e. g. with CO_2) lower values are obtained. The structures of many, mostly amorphous C-S-H phases are still not completely known; often crystalline calcium-silicate hydrates act as model systems. The most important crystalline calcium-silicate hydrates are shown in table 2.6.

Table 2.6: Important C-S-H phases from literature.

Phase Name	CaO/SiO_2	Chemical formula	Reference
Afwilite	1.5	$Ca_3(SiO_3OH)_2 \cdot 2H_2O$	16
α-C_2SH	2.0	$Ca_2(SiO_4) \cdot H_2O$	17
Jaffeite	3.0	$Ca_6(Si_2O_7)(OH)_6$	18
14 Å Tobermorite	0.83	$Ca_5(Si_6O_{16})(OH) \cdot 7H_2O$	19
11 Å Tobermorite	0.75	$Ca_{4.5}(Si_6O_{16})(OH) \cdot 5H_2O$	20
11 Å Tobermorite	0.66	$Ca_4\ (Si_6O_{15})(OH) \cdot 5H_2O$	20
Clinotobermorite	0.83	$Ca_5(Si_6O_{17}) \cdot 5H_2O$	20
9 Å Tobermorite	0.83	$Ca_5(Si_6O_{16})(OH)_2$	20
Jennite	1.5	$Ca_9H_2Si_6O_{18}(OH)_8 \cdot 8gH_2O$	21
Foshagite	1.33	$Ca_4(Si_3O_9)(OH)_2$	22
Hildebrandite	2.0	$Ca_2(SiO_3)(OH)_2$	23
Xonolite	1.0	$Ca_6(Si_6O_{17})(OH)$	24
Gyrolithe	0.66	$Ca_{16}Si_{24}O_{60}(OH)_8 \cdot 14H_2O$	25
K-phase	0.44	$Ca_7(Si_{16}O_{38})(OH)_2$	26
Z-phase	0.56	$Ca_9(Si_8O_{20})_2(OH)_2 \cdot 14H_2O$	27

C_3A is highly reactive and plays an important role at the beginning of the hydration reaction. It is responsible for the early strength of concrete and reacts directly with water. Its hydration is mostly influenced by the presence of sulphate-containing phases like gypsum. In the absence of sulphate ions C_3A hydrates to calcium aluminate hydrate (e.g. $Ca_3Al_2(OH)_{12}$, hydrogarnet) in form of thin crystalline plates. These can fill pores causing an intermediate hardening of cement pastes. Gypsum slows down the hydration of C_3A. The possible hydration products of C_3A are shown below in equation 2.4 and 2.7.

<u>Without gypsum</u> $Ca_3Al_2O_6 + 6\ H_2O \rightarrow Ca_3Al_2(OH)_{12}$ **[2.4]**

<u>With gypsum</u> $Ca_3Al_2O_6 + 3\ CaSO_4 \cdot 2H_2O + 26\ H_2O \rightarrow Ca_6Al_2[OH]_{12}(SO_4)_3 \cdot 26H_2O$ **[2.5]**

Ettringite ($Ca_6Al_2[OH]_{12}(SO_4)_3 \cdot 26H_2O$) is formed due to the presence of gypsum in the form of long fibrous hexagonal needles. Ettringite as a primary hydration product is only stable as long as a sufficient amount of sulphate-ions are present. Typically, the supply of SO_4^{2-} ions in cement is not high enough for a complete reaction of C_3A to ettringite. Below a certain

amount of SO_4^{2-} ions ettringite is not stable anymore and is converted to calcium aluminum monosulphate, according to equation 2.6

$$Ca_6Al_2(SO_3)_3 \cdot 32H_2O + 2\ Ca_3Al_2O_6 + 4\ H_2O \rightarrow\ 3\ Ca_4Al_2(SO_3) \cdot 12H_2O \qquad \textbf{[2.6]}$$

The hydration of $C_2(AF)$ is assumed to be similar but slower than that of C_3A. In the absence of gypsum, hydrates are formed according to equation 2.7. Additionally, some unreacted $C_2(AF)$) and or amorphous iron hydroxides can occur. In the presence of gypsum it can form Fe-substituted Ettringite (AFt) according to equation 2.8.

Without gypsum $\quad 3\ Ca_2(Al,Fe)_2O_5 + \ 6\ H_2O \ \rightarrow \ 2\ Ca_3(Al,Fe)_2(OH)_{12}$ **[2.7]**

With gypsum

$$Ca_2(Al,Fe)_2O_5 + 3\ CaSO_4 \cdot 2H_2O + Ca(OH)_2 + 26\ H_2O \rightarrow Ca_6(Al,Fe)_2(SO_3)_3 \cdot 32\ H_2O \qquad \textbf{[2.8]}$$

After mixing cement and water initially the alkali metal oxides, calcium sulphate phases and free lime are dissolved in the water. At the same time C_3A and C_3S react with water and ettringite is formed around the C_3A grains. By hydrolysis of C_3S, a C-S-H gel is formed on the surface of the C_3S grains. After the formation of these hydration products of cement a protective layer around the grains is present and the so-called dormant period begins. At this time the C-S-H gel is getting viscous and ettringite needles are growing. After several hours the mixture loses its workability and forms a harder body. This is the so-called acceleration period. It is related to the hydration of C_3S and C_2S which forms C-S-H and Portlandite. Remaining C_3A and $C_2(AF)$ also continue to hydrate. Ettringite is formed due to the reaction of C_3A and $C_2(AF)$ with gypsum and water. The sulphate concentration decreases due to the Ettringite formation. The following deceleration period is the hardening period of concrete and during this stage the hydration is mainly controlled by diffusion. Ettringite crystallizes in form of hexagonal prisms or as needle like crystals. In the unit cell the columns running along the c-axis (Fig. 6.7) consist of $Al(OH)_6$ octahedra alternating with triangular groups of edge-sharing CaO_8 polyhedra. The eight oxygen atoms in the polyhedra come from a Ca coordination with four OH^- ions shared with the $Al(OH)_6$ octahedra and from a coordination with four H_2O molecules. The crystal structure of ettringite is shown in figure 2.5.

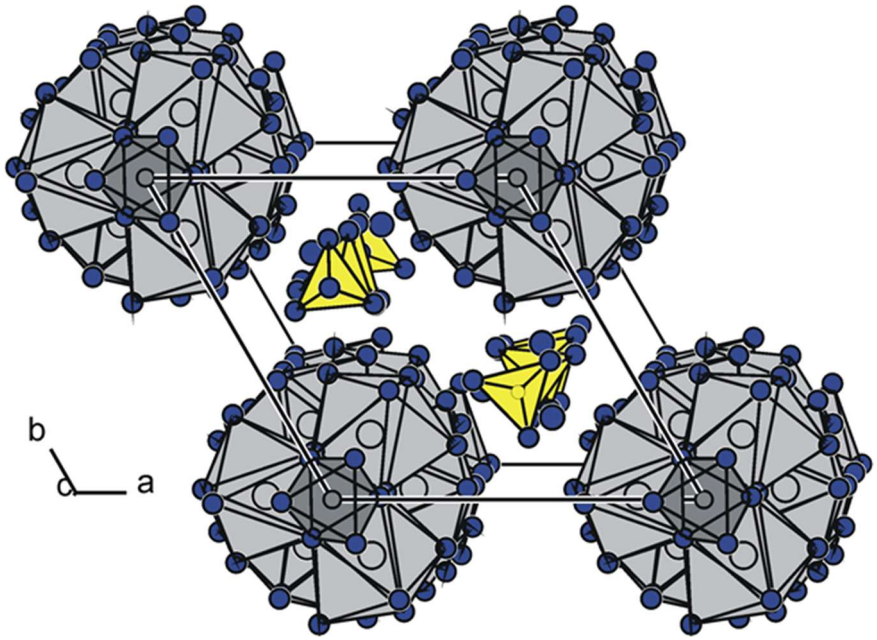

Figure 2.5: Crystal structure of ettringite. $(Al(OH)_6^{3-}$ octahedra (dark grey), CaO_8 dodecahedra (light grey), and SO_4^{2-} tetrahedra (yellow) are emphasized, the H-atoms were omitted for clarity.

2.5. Performance and durability of Portland cement

The durability of concretes depends on both environmental and internal factors. Internal factors like composition, density, aggregate, and pore structure may make the concrete vulnerable to deterioration. Also, severe environmental conditions can cause deterioration of concrete which can negatively affect the structure, the aesthetic appearance and the life-cycle of concrete. These deterioration mechanisms may be classified in different categories which are shown in table 2.7.

Tabelle 2.7: Deterioration mechanisms of concretes according to [14].

Mechanism of deterioration	Examples of deterioration
Physical	Freeze thaw
Mechanical	Abrasion
Biological	Bacterial
Chemical	Chloride ingress, carbonation, sulphate attack

These deterioration mechanisms can cause cracking, loss of color, or the corrosion of reinforcement steel in concrete. External factors are weathering conditions like temperature,

humidity, harmful gases in the air, impurity in water, abrasion and environmental conditions. Internal factors are generally related to the composition of cement, water content, kind of aggregates and filler materials.

2.5.1. Carbonation of concrete

Carbonation reactions can cause severe damages to concrete, especially to steel reinforced concrete. Therefore a detailed discussion is necessary for the different reactions. The carbonation process is a reaction between $Ca(OH)_2$ or other alkali metal hydroxides and CO_2 which forms carbonates in the concrete. Also, other hydration products that contain calcium ions and alkali metal hydroxides (for example, C-S-H, NaOH and ettringite) are susceptible to carbonation as well [5]. Gaseous CO_2 does not react directly with the cement paste. First CO_2 and $Ca(OH)_2$ must dissolve in water inside the cement pores according to equation 2.10, 2.11 and 2.12. After that, carbonate ions precipitate and form $CaCO_3$.

$$Ca(OH)_2 \rightarrow Ca^{2+} + 2\ OH^- \quad \textbf{[2.10]}$$

$$CO_2 + H_2O \rightarrow H_2CO_3 \rightarrow 2\ H^+ + CO_3^{2-} \quad \textbf{[2.11]}$$

$$Ca^{2+} + 2\ OH^- + 2\ H^+ + CO_3^{2-} \rightarrow CaCO_3 + 2\ H_2O \quad \textbf{[2.12]}$$

Alkali metal hydroxides (e.g NaOH, KOH) react also with CO_2 according to equation 2.13

$$2\ Na^+ + OH^+ + 2\ H^+ + CO_3^{2-} \rightarrow Na_2CO_3 + 2\ H_2O \quad \textbf{[2.13]}$$

Besides alkali and alkaline earth metal hydroxides other calcium-containing phases (e.g. C-S-H, ettringite) can react with CO_2. Possible carbonation reactions are shown below.

$$Ca_6Al_2(SO_3)_3{\cdot}32H_2O + 3\ CO_2 \rightarrow CaCO_3 + 2\ Al(OH)_3 + 3\ CaSO_4{\cdot}2H_2O + 23\ H_2O \quad \textbf{[2.14]}$$

$$Ca_4Al_2(SO_3){\cdot}12H_2O + 3\ CO_2 \rightarrow 3\ CaCO_3 + 2\ Al(OH)_3 + CaSO_4{\cdot}2H_2O + 7\ H_2O \quad \textbf{[2.15]}$$

$$Ca_3Al_2(OH)_{12} + 3\ CO_2 \rightarrow 3\ CaCO_3 + 2\ Al(OH)_3 + 3\ H_2O \quad \textbf{[2.16]}$$

$$Ca_2(Al_{2-x}Fe_x)(OH)_{12} + 2\ CO_2 \rightarrow 2\ CaCO_3 + 2\text{-}x\ Al(OH)_3 + x\ Fe(OH)_3 + 3\ H_2O \quad \textbf{[2.17]}$$

Theoretically, with sufficient moisture the unreacted clinker phases C_3S and C_2S could also react with CO_2. However these reactions can be neglected according to [28 - 32]. It can be seen from the equations above that all calcium containing phases like C-S-H, ettringite (AFt phases), monosulphoaluminate (AFm phases) and alkali metal hydroxides can react with CO_2 [8, 9, 33].

$CaCO_3$ occurs in three different modifications. Calcite and vaterite are the most abundant forms found in carbonated concrete. Aragonite can be observed in small amounts during the early stages of carbonation. Vaterite and aragonite transform to calcite which is thermodynamically the most stable form of $CaCO_3$. The reaction of $Ca(OH)_2$ with CO_2 causes a volume increase and reduces the pore volume by about 20 - 28 %, which is usually

beneficial for the concrete. The presence of $Ca(OH)_2$ itself provides a pH value of 12.4 and together with other alkali metal hydroxides fresh concretes reach pH values between 13 and 13.8. During the carbonation process the pH value of concrete decreases due to the consumption of $Ca(OH)_2$. The pH value of fully carbonated concrete is approximately 8.0. A high pH value is necessary especially for steel-reinforced concretes. At high pH values the steel is protected against corrosion by a passivation layer. With ongoing carbonation, the pH decreases and the reinforcement steel starts to corrode below pH 10. [8-10, 14]. This is schematically shown in figure 2.6.

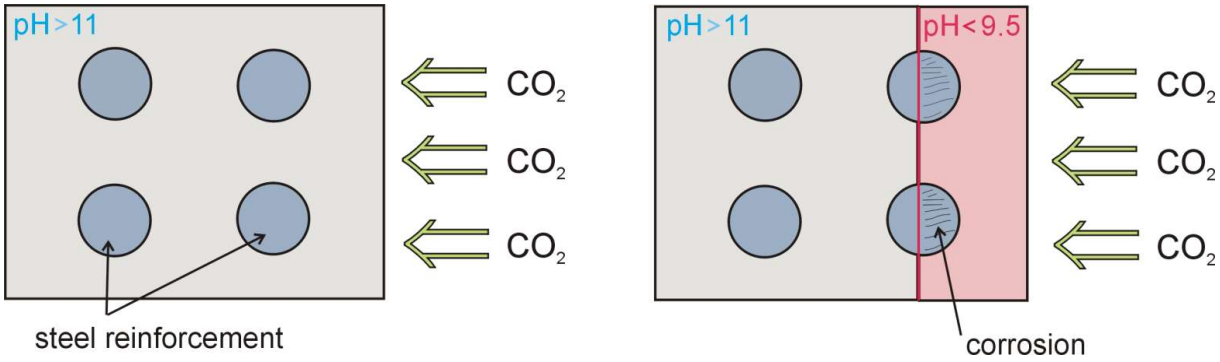

Figure 2.6: Schematic representation of the corrosion of steel in concrete as a function of the pH value.

The corrosion of steel in concrete is an electrochemical process. Fe^{2+} ions and OH^- ions react and form several corrosion products like Fe_3O_4, Fe_2O_3, α-FeOOH and γ-FeOOH. The volumes of volumes of oxides and iron hydroxide are three to six times higher than that of elemental iron in steel. The expansion produced by the formation of corrosion products causes the surrounding concrete to crack and spall [30].

The carbonation of concrete depends on several factors. Major factors which influence the carbonation are the CO_2 concentration of the environment, humidity, temperature, w/c ratio cement type, and filler materials.

The CO_2 concentration of the atmosphere is usually about 0.04 % but in some industrial regions the CO_2-concentration can reach 0.1 % or higher. The CO_2 concentration directly effects the carbonation rates.

Also humidity is needed for carbonation. Carbonation reactions in concrete are maximal in the range of 60 to 80 % humidity. In 100 % relative humidity there is almost no carbonation because the diffusion of CO_2 in water is about 10000 times slower than in air. In dry climates under 30 % humidity, the carbonation is very slow, too.

The w/c ratio is another major factor for carbonation of concrete. Concrete with higher w/c ratios contain more capillary pores. The carbonation rate is higher due to the high amount of capillary pores [5].

The substitution of clinker phases with fillers causes a reduction of hydration products which is harmful for the carbonation resistance. On the other hand, some filler materials like limestone improve the hydration and packing properties. To have a dense structure may compensate for the reduction in hydration.

2.6. Portland cement blends and eco –friendly cements

The production of cement causes about 5 to 7% of all CO_2 emissions worldwide. The aim of the cement industry is to reduce these emissions and produce eco–friendly cements. This is particularly achieved by the production of cement blends with reduced clinker content, put in to practice by replacing cements with reactive or inert filler materials. Compared with technically equivalent conventional concretes, the cement content and the greenhouse potential of these concretes can be reduced by approximately 30% [4, 5].

Commercial Portland cement can be partially replaced by e.g. limestone powder, fly ash, and blast furnace slag (BFS) in the concrete mixture. A high amount of substitution material in the Portland cement clinker is limited by conventional concrete technology, due to its low reactive potential or the low compressive strength contribution. Recent studies [34, 35] show that a significant reduction in the proportion of clinker in concrete can be achieved by various techniques. Usually reactive substances such as puzzolanic materials (mainly reactive silicon, aluminum and iron oxides) and latent-hydraulic (mainly reactive calcium, silicon and aluminum oxides) are used for clinker substitution. Since the performance of concrete is influenced partially by the water-cement ratio (w/c), a reduction of the water content compared to conventional concrete is another possibility to use the cement clinker more efficiently. This requires the simultaneous use of high-performance flow-control agents [34 - 36].

One of the most important filler materials for Portland cement blends is granulated blast furnace slag. In order to have sufficient hydration properties the liquid slag must be quenched to temperatures below 800 °C. This is done by granulation of the liquid slag in water or water spraying onto the liquid slag by high-pressure nozzles. Blast furnace slag is a lime-alumina silicate melt, mainly consisting of CaO, SiO_2 and Al_2O_3. Its composition is quite similar to Portland cement.

Pozzolans are natural or artificial materials composed of silica, alumina, limestone, iron oxide, and alkaline substances. Natural pozzolans are generally volcanic tuff. Fly ash is an artificial pozzolan. The pozzolans reacts with $Ca(OH)_2$ and form C-S-H phases as shown in equation 2.19.

$$3\ Ca(OH)_2 + 2\ SiO_2 + H_2O \rightarrow 3CaO{\cdot}2SiO_2{\cdot}4H_2O \quad \textbf{[2.19]}$$

Silica dust or fume is a very reactive pozzolan and effective filler, suitable for the production of concretes with special properties like high density and compressive strength. The cost of silica fume is high when compared to the price of Portland cement. Thus, the use of silica fume is usually limited to the production of high performance concrete.

Limestone and ground quartz are inert or quasi-inert fillers. The most important functions of these materials are to fill spaces between cement particles in concretes. Limestone is particularly effective, because it is much easier to grind than the clinker, hence the gap volume between the clinker particles can be reduced. Calcium carbonate participates to a small extent in the hydration reactions of the cements. According to the European standard EN 197-1, limestone can be used in Portland limestone cement with proportions of 6 to 35% by weight. The cement types and the amount of filler materials according to DIN EN 197-1 standard are shown in Table 2.8.

Table 2.8: Cement types and amount of filler materials according to DIN EN 197 [37].

Cement type	Clinker %	Filler Materials				
		Blast furnace slag %	Pozzolans %		Silica dust %	Limestone %
			Natural	Fly ash		
CEM I	95-100	-	-		-	-
CEM II/A	80-94	6-20 (all filler materials possible)				
CEM II/B	65-79	21-35 (all filler materials possible)				
CEM II/C*	50-64	16-44			-	6-20
CEM III/A	35-64	36-65	-		-	-
CEM III/B	20-34	66-80	-		-	-
CEM III/C	5-19	81-95	-		-	-
CEM IV/A	65-89	-	11-35		-	-
CEM IV/B	45-64	-	36-55		-	-
CEM V/A	40-64	18-30	18-30		-	-
CEM V/B	20-38	31-50	31-50		-	-
CEM VI*	35-49	31-59	-		-	6-20

3. CHARACTERIZATION AND PREPARATION TECHNIQUES

3.1. X-ray powder diffraction

X-ray diffractometry (XRD) is one of the most important characterization techniques to identify and quantify the phases that are present in cementitious materials [9, 38]. X-ray powder diffraction on solids produces patterns consisting of reflections of varying intensities at characteristic diffraction angles due to the crystal structures of the phases. The diffraction angles and positions of the reflections are determined by the symmetry and size of the unit cell. Diffraction of X-rays on crystalline material can be treated as reflection of X-rays by lattice planes if the angle of the incident beam to the planes satisfies Bragg's law (equation 3.1.). The intensities of the peaks are related to the nature and arrangement of the atoms within the unit cell of the crystalline material. By using the XRD patterns crystal structures can be determined [38].

Bragg's law: $n\lambda = 2d\sin\theta$ **[3.1]**

Where:

d = interplanar lattice spacing

θ = diffraction angle

λ = wavelength of X-rays

n = order of diffraction

X-ray powder diffraction measurements were carried out using a diffractometer (Stadi P, STOE & Cie. GmbH, Darmstadt) with transmission geometry, $Cu_{K\alpha 1}$-radiation (λ = 1.54056 Å), Ge [111] monochromator, and a flat plate sample holder with the powdered sample prepared between transparent polymer foils.

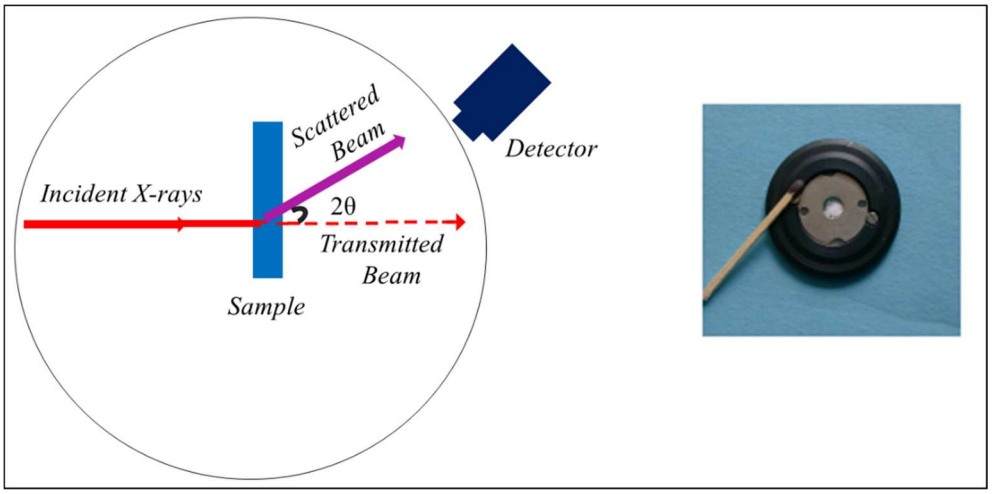

Figure 3.1: Sketch of a diffractometer with Debye-Scherer geometry (left), transmission sample holder (right) [39].

Qualitative phase analysis is based on the comparison with a pattern from a database containing data from literature. Here, qualitative phase analyses were carried out by using the program WinXpow (STOE) and the powder diffraction file database PDF published by the International Centre for Diffraction Data (ICDD) [40].

3.2. Rietveld method

The Rietveld method was described in 1966 by the Dutch physicist Hugo Rietveld who used neutron diffraction data [41, 42]. It was adapted to X-ray powder diffraction by Young et al. in 1977 [43], and Bish and Howard in 1988 [44]. This method allows a fitting of calculated and observed data using structure data to obtain a quantitative phase analysis of a reaction mixture. Alternatively, the crystal structure can be refined since the diffraction pattern (the height, width and position of the reflections) gives information about the structure of the crystalline material. Structural parameters like space group symmetry, unit cell dimensions and atomic positions as well as instrumental parameters are used for the Rietveld fitting. The Rietveld method minimizes the difference between measured and calculated patterns at each data point "i" in the diffraction pattern using a least squares approach where w_i are weighted quared differences between observed "y_{iO}" and calculated "y_{ic}" [38 ,45].

$$S_y = \Sigma_i \; w_i [y_{io} - y_{ic}]^2 \; c \qquad \textbf{[3.2]}$$

Where :

y_{iO} = observed intensity at each data point

y_{ic} = calculated intensity at each data point

w_i = weighting factor ($1/ w_i = \sigma_i^2$ standard deviation of the measured value of y_i)

The quality of measurements can be estimated from residual functions such as R_p (plain profile), R_{wp} (weighted residual) and R_{exp} (expected residual) where N is the number of observations and P are the refined parameters. These functions are shown in equation 3.3, 3.4 and 3.5. The Goodness of fit (GOF) value which is shown in equation 3.6 is calculated using these residual functions. In an ideal case the GOF value would equal to one.

$$R_p = \frac{\sum_i |y_{io} - y_{ic}|}{\sum_i y_{io}} \quad [3.3]$$

$$R_{wp} = \sqrt{\frac{\sum_i w_i (y_{io} - y_{ic})^2}{\sum_i w_i y_{io}^2}} \quad [3.4]$$

$$R_{exp} = \sqrt{\frac{(N-P)}{\sum_i w_i y_{io}^2}} \quad [3.5]$$

$$GOF = \frac{R_{wp}}{R_{exp}} \quad [3.6]$$

3.3. Thermal analysis

In thermal analysis physical and chemical properties like enthalpy, heat capacity, mass, and expansion of samples are measured as a function of temperature.

The thermogravimetric analysis (TGA) gives the mass change of a sample as a function of temperature. In differential thermal analysis (DTA) the temperature of a sample is compared to the temperature of an inert reference material during a defined temperature program. The temperature of the sample and the reference should be identical until a thermodynamic process (e.g. melting, decomposition, phase transition) occurs in the sample. These changes in the sample can be either endothermic or exothermic and can be detected in relation to the inert material.

For the investigations described here, TGA and DTA were applied simultaneously. Alumina crucibles were used for the samples. Prior to all of the measurements a correction measurement was carried out with empty alumina crucibles. This general procedure is used to eliminate errors caused by the crucibles and furnace in the thermal analysis device. The samples were ground, weighted and filled into the crucibles. The second empty alumina crucible was used as reference for the measurements. The measurements were carried out in air atmosphere.

The amounts of calcium hydroxide ($Ca(OH)_2$) and calcium carbonate ($CaCO_3$) in samples of cement and concrete were determined by simultaneous DTA/TGA (STA 409, NETZSCH, Selb, 30 °C - 1000 °C, heating rate 10 °C/min, air). Decomposition reactions were registered at characteristic temperatures with corresponding mass losses that were assigned to the loss of

water and carbon dioxide. The first thermal effects that were detected can be assigned to losses of water that is chemically or physically bound and to the decomposition of ettringite and C-S-H. $Ca(OH)_2$ decomposes to calcium oxide, CaO between 430 and 530 °C, $CaCO_3$ loses CO_2 between 650 and 900 °C [46, 47]. Figure 3.2 shows an example of a DTA/TGA measurement of a clinker and a cement paste. Due to the high mass losses in the temperature range between 50 and 400 °C, the reference mass for the calculation was set at 550 °C as described in the literature. [48]. The contents of $Ca(OH)_2$ and $CaCO_3$ of the samples were calculated by using equations 3.7 and 3.8.

$$\mathbf{Ca(OH)_2 \rightarrow\ CaO\ +\ H_2O} \qquad \mathbf{\%Ca(OH)_2 = [H_2O_{[Ca(OH)2]loss} * (74/18)]/M_{550°C}} \qquad \mathbf{[3.7]}$$

74g/mol 56g/mol 18g/mol

$$\mathbf{CaCO_3 \rightarrow\ CaO\ +\ CO_2} \qquad \mathbf{\%Ca(OH)_2 = [CO_{2loss} * 100/44]/M_{550°C}} \qquad \mathbf{[3.8]}$$

100g/mol 56g/mol 44g/mol

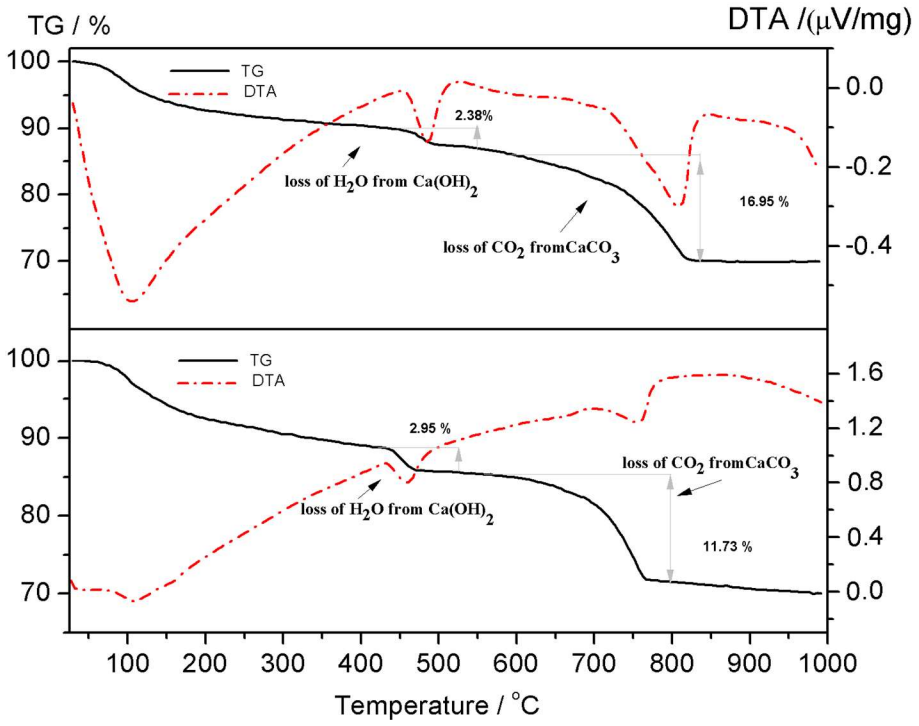

Fig 3.2: Thermal analysis of a carbonated clinker sample (top, C_3S-0.6) and a limestone-rich cement paste (bottom, Z92-0.4), showing typical decomposition effects.

3.4. Carbonation depth measurements

Concretes have high pH values (> 11) due to high amounts of $Ca(OH)_2$. During the carbonation, the concrete reacts with CO_2 from the atmosphere and its pH value decreases to 8.5-9. Phenolphthalein is a well-known indicator which is very sensible to changing pH

values and can therefore be used to indicate the pH values in concrete. In concrete chemistry this is commonly applied by spraying an alcoholic solution of phenolphthalein on concrete surfaces. If the area where the phenolphthalein solution is applied turns pink/violet the pH value is about 11. If the surface remains colorless, the pH value is ~ 8.5 or lower which means that carbonation has occurred. The color changes in a carbonated sample are shown in figure 3.3.

Fig 3.3: Sample sprayed with 1 % phenolphthalein in ethanol. The violet colored regions are not carbonated, transparent regions are carbonated.

In this work a solution of 1 % phenolphthalein in ethanol was used. The phenolphthalein solution is applied to fresh fracture surfaces. For further characterizations samples were taken from the carbonated zones.

3.5. Porosimetry Measurements

Porosity was determined by using the Mercury Intrusion Porosimetry (MIP). The volume of mercury intruded under controlled pressure into a porous sample is measured according to DIN 66133 [48]. The measurements were carried out at high mercury pressures up to 400 MPa (Pascal 140/440 Thermo Scientific Company). The samples were taken from edges of cement pastes after carbonation and dried at 40 °C until a constant weight was obtained. At the lowest filling pressure, it is assumed that there is no pore filled with mercury. The bulk volume of the sample was determined using Archimedes law. The pressure was increased to the maximum and mercury was forced to penetrate into all pores in the sample accessible to mercury. The volume of mercury required to fill all accessible pores is considered the total pore volume. The ratio between the total pore volume and bulk volume gives the percentage of porosity of the sample. The radius of pores can be also determined by MIP using the Washburn equation 3.9:

$$P = \frac{2\gamma cos\theta}{r} \qquad \textbf{[3.9]}$$

P is the external mercury pressure (N/m^2), γ is the surface tension of mercury

(0.48N/m at 20 °C), θ is the contact angle between solid and mercury (≈141°), and r is the pore access radius (m) [49].

3.6. Equipment for high temperature synthesis

The syntheses of clinker phases were carried out in vertical tube furnaces (Carbolite) and in high-frequency induction furnaces.

Two induction furnaces (Fig. 3.4), with high frequency generators (AXIO 10/450 and Tru-Heat HF 5010, Hüttinger) were used. The specifications of the high-frequency induction furnace are given below.

Output power: 10 kW

Working frequency: 50-450 kHz

Power supply: 400 V, 50 Hz

Connectivity:12.5 KW

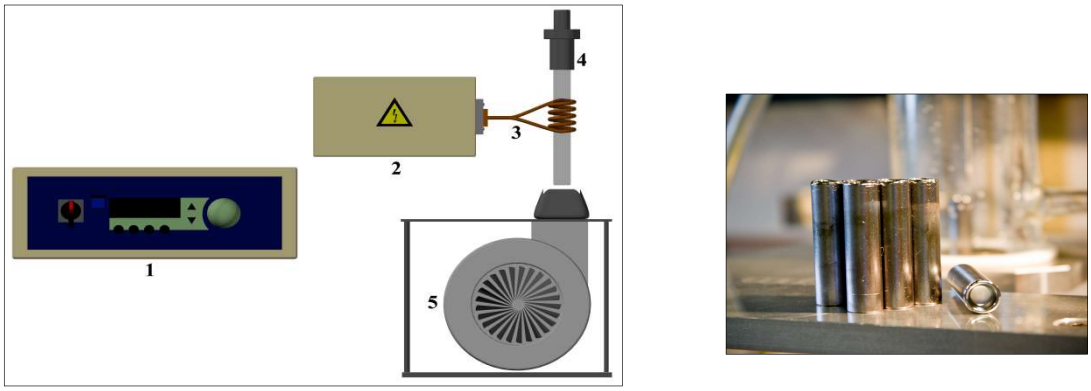

Fig 3.4: Left: Schematic construction of a high-frequency induction furnace (1: generator, 2: outer circuit, 3: copper coil, 4: quartz glass reactor, 5: radial fan) [50]. **Right**: sealed tantalum crucibles.

The generator, the external circuit and the inductor each have an independent connection for cooling water. The flow of cooling water for each device is supplied with approx. 250-300 l / h (20 °C). For the cooling of the quartz glass reactor a radial fan was used. The main advantage of high-frequency induction furnaces are the high temperatures that can be reached (>2000 °C). In this study, 1900 °C was chosen as the maximum reaction temperature. To measure the temperatures a pyrometer was used (LINSEIS, 900 nm). The whole system was controlled using the Lab VIEW software [51]. Sealed tantalum crucibles were used.

The vertical tube furnace consists of a corundum tube which is surrounded by an electric resistor of SiC. The maximum temperature achievable with this kind of furnaces is 1500 °C. Alumina crucibles were used for these syntheses.

3.7. Carbonation chamber (Carbobox)

The carbonation of samples was carried out in a closed chamber (carbobox). Technical grade CO_2 gas was used. The carbonation chamber is located in a climate-controlled room at 20 °C. A relative humidity of 65 % was adjusted by using aqueous NH_4NO_3 solution inside the carbonation chamber.

4. STATE OF THE ART

The amount of clinker phases in cement can be significantly reduced by the use of substitution materials, typically reactive materials such as pozzolans, fly ash, blast furnace slag, or calcined clay [2 - 7, 52 - 54]. Inert substitution materials like micro-silica can also be applied [55, 56]. The drawback of these substitution materials are the limited availabilities of fly ash and blast furnace slag and the high cost of micro-silica, which is therefore taken for special applications only [56 - 61]. For decades, highly available and low cost rock flour, such as limestone powder has been used as substitution material, too. Portland limestone cement CEM II-LL with an addition up to 35 % limestone is widely chosen in Europe in accordance with the European cement standard EN 197-1. For instance, in 2012 nearly 27% of the CEM II produced in Europe was Portland limestone cements [61]. The use of blended cements with up to 15 wt.-% limestone addition is allowed in the USA since 2013 and in Canada since 2008 [62, 63].

The performance of concrete is influenced in particular by the clinker content, the water-cement ratio (w/c-ratio), and the grain size distribution [64 - 66]. For a sufficient workability of new cement mixtures, the use of high performance super plasticizers was investigated by several work groups [2, 4 - 7, 34, 64 - 69].

For the introduction of the clinker-reduced eco-friendly cements all industrial standards developed for conventional cements regarding durability and mechanical properties have to be fulfilled. Therefore, the deterioration mechanisms were investigated [2, 4 – 7, 29, 33, 35, 61 70].

For steel reinforced concretes the carbonation resistance is especially important to ensure long-term stability. Carbonation is simply defined as the reaction between atmospheric or dissolved CO_2 and cement pastes, mortars, or concretes which result in chemical and physical changes [9, 10, 14, 32, 71,72]. In theory, all calcium- and alkali metal-ion containing phases can react with CO_2. CO_2 reacts with the dissolved ions inside the pores [14, 72, 33]. $Ca(OH)_2$ is discussed to be the most important compound susceptible to carbonation, but other hydration products like C-S-H phases and ettringite also react with CO_2 [32, 36, 71, 73 -76]. The final products of the carbonation reactions are $CaCO_3$ and silica gel ($SiO_2 \cdot H_2O$) [32, 33, 36, 70, 77 - 79]. Carbonation mainly affects the pH- value and, to a lesser extend the porosity of the concrete. The effects of porosity changes are complex. It is discussed that the formation of silica gel causes an increase [70] and the formation of calcium carbonate a decrease of the porosity [32, 71, 72, 80, 81].

The carbonation rate and the order in which the different phases react with CO_2 is discussed controversially. In some studies, the carbonation of $Ca(OH)_2$ and C-S-H phases are reported to occur simultaneously [32, 81], although from a thermodynamically point of view, the carbonation of $Ca(OH)_2$ should be favored [33].

The evaluation of the carbonation resistance of concretes under natural CO_2 exposition (0.04 % in air) is very time-consuming (months to years). Therefore, many researchers investigate accelerated carbonation reactions using high CO_2-concentration ranging from 1 to 50 % CO_2 on sufficiently hydrated samples. There is no consensus on the exact procedure of accelerated carbonation tests in Europe [82].

The phenolphthalein test indicates a carbonation depth corresponding to a pH value and is commonly related to carbonation models, which are based on the diffusion processes in the porous structures assuming a sharp carbonation front [81]. Meanwhile, different studies show that the carbonation front is not sharp but gradual. Partially carbonated regions of the specimen cannot be detected properly using this test. In order to have better results, not only the diffusion processes but also chemical interactions must be taken into account [32, 71, 72, 80, 8].

Different techniques are used to investigate the carbonation behavior of cement pastes [32, 33, 36, 71 - 90]. Common methods to study the formation of calcium carbonate in cement pastes and mortars are thermal analysis (DTA / TGA) and X-ray powder diffraction (XRD), as done by Cole et al. [88]. Different authors investigated the carbonation of C-S-H phases. All of the C-S-H phases investigated in these studies were synthesized differently. Due to the amorphous nature of the C-S-H phases they are difficult to compare. Crystalline calcium-silica hydrates like tobermorite were used instead [73, 86, 87]. Only a few authors investigated the carbonation of amorphous pastes of the hydrated clinker phases [89]. It was found that the primary reaction product of CO_2 with mortar and C-S-H pastes is not calcite, the most stable polymorph of $CaCO_3$, but rather a poorly crystalline or amorphous modification besides crystalline vaterite and aragonite. It was concluded that vaterite and aragonite form first and transform into calcite over time which is accordance with the Ostwald rule. Additionally, the formation of vaterite seems to be favored at higher pH values [89]. The carbonation of 11 Å tobermorite was studied by Sauman and Ikeda et al. [73, 90]. They observed vaterite as the first modification formed, which transformed to calcite either directly or via aragonite. Sauman stated that vaterite is more stable at low CO_2 partial pressures, while calcite dominates at higher CO_2 contents. Slegers et al. used XRD and infrared spectroscopy

(IR) to determine the carbonation of hydrated C_3S. They described that in "young" pastes vaterite was the polymorph precipitated first, followed by aragonite. Further on they observed that during the carbonation the signals in the IR spectra corresponding to the C-S-H phases disappeared prior to the $Ca(OH)_2$-signals [89]. Garbev et al. used Raman spectroscopy in combination with XRD to investigate the carbonation of C-S-H phases with different Ca/Si ratios obtained by mechanochemical synthesis [86]. They observed that the initial carbonation products were always amorphous and transformed to vaterite or aragonite over time. Vaterite can be found when the Ca/Si ratio is ≥ 0.67 and aragonite was present when the Ca/Si ratio was ≤ 0.50. Previous works of Nishikawa et al. and Groves et al. showed similar results on hardened cement pastes [75, 85]. Nishikawa et al. observed the formation of vaterite as the only polymorph when ongoing carbonation reduced the Ca/Si ratio from 1.5 to 1.0 [75]. Groves et al. found vaterite and calcite to be the only crystalline polymorphs of $CaCO_3$ observed when the Ca/Si ratio was higher than 1.0 [85]. Villain et al. observed stable, metastable and amorphous forms of $CaCO_3$ and mentioned that the thermal stability of carbonation products of C–S–H was lower than that of calcite [81]. In general, it is assumed that the carbonation of C–S–H is a function of the Ca/Si ratio. Samples with different Ca/Si ratios have different condensation/crystallization rates. C–S–H with lower Ca/Si ratios form more silica gel when $Ca(OH)_2$ is not present as a buffer phase [7, 32, 87].

The carbonation reactions of eco-friendly cement pastes with high limestone content depend on external factors, e.g. relative humidity, temperature, and concentration of CO_2 [77, 91 - 93] as well as internal factors including the water/cement (w/c) ratio, the cement type, supplementary cementitious materials, and the amount of filler materials. The effects of limestone on the carbonation were subject to several studies. It is discussed controversially if a reduction of hydration products like C-S-H and $Ca(OH)_2$ in eco-friendly cements affects the carbonation mechanisms compared to ordinary Portland cement. Several authors report that the carbonation resistance of concrete with a limestone substitution up to 20 wt.-% is similar to that of ordinary Portland cement [94, 95]. Other authors state that a limestone substitution will lead to an increase of the carbonation rate [28, 97-98]. On the contrary, Tsivilis et al. observed no reduction of the carbonation resistance for 35% limestone addition [99]. Lollini et al. found that the carbonation resistance is decreased remarkably for a 30 % substitution and is negligible for a 15% substitution [100]. Schmidt et al. reported that concretes with limestone addition show a slightly higher carbonation depth than concretes without limestone addition but have a better carbonation resistance when compared to mixtures with blast

furnace slag and fly ash [96]. Barker et al. proposed that the carbonation resistance of eco-friendly cements is directly related to the compressive strength [101]. Similar results were found by Dhir et al. for Portland cements with up to 50 wt.-% limestone addition. [28]. Hainer et al. performed several studies on water-reduced limestone-rich cements and found slightly lower carbonation resistances but the same compressive strengths, compared to ordinary Portland cement. He also reported that the w/c-ratio is the key parameter for cements with high limestone contents. The mechanical properties and carbonation resistance are highly dependent on the w/c-ratio [2, 4, 5, 61].

In general, limestone fillers improve the hydration rate of cement and therefore increase the strength at early ages [53, 54, 59, 60]. The cement pastes include mainly $Ca(OH)_2$, C-S-H phases and some sulphate containing phases like ettringite (AFt phases) and monosulphoaluminate (AFm phases) as minor component. From a chemical point of view, limestone does not have puzzolanic properties and is thought to be inert. But it was shown that it reacts with the alumina phases of cement and forms hemi- and monocarboaluminate hydrate with no significant changes on the strength of the resulting concrete [102]. According to thermodynamical calculations, in the very early stages of carbonation the sulphate containing phases play a key role, because SO_4^{2-} ions compete with CO_3^{2-} ions. The amount of monosulphoaluminate decreases, while the amount of hemicarboaluminate increases. Monosulphoaluminate becomes unstable in solution due to a release of SO_4^{2-} ions and converts to ettringite [102 - 106]. Damidot et al. found that calcium hemicarboaluminate is stable only over a limited range of CO_2 activities, while the calcium monocarboaluminate is more stable and can exist also in the presence of limestone. In the presence of limestone AFm phases readily transform to carboaluminate phases. Ettringite and AFt will become stable indirectly [106]. The amount of ettringite reaches the highest level when the monocarboaluminate appears. The hemicarboaluminate reacts to monocarboaluminate with increasing amount of carbonate. When all hemicarboaluminate is disappeared the calcite formation begins from the carbonation reactions [33,103-106].

In limestone-containing systems the hemi- and monocarboaluminates form preferentially. About 1 % limestone addition slow down the formation of monosulphoaluminate [107]. With higher addition of limestone (up to 20 %) the formation of ettringite and monocarboaluminate are observed after hydration over 90 days [60]. This can be due to partial replacement of SO_4^{2-} ions with CO_3^{2-} ions in ettringite or AFt [33, 60, 103, 105 - 107].

The comparison of the different studies is difficult because carbonation is a sequence of complex chemical reactions which can be affected by the conditions of exposure and by other experimental parameters. The most important experimental difficulties are; he difference in chemical compositions, the changes of the microstructure during carbonation
and the conditions of the exposure. As mentioned above [4, 5, 6, 32, 31, 72];

- Cements have a wide range of compositions. These differences together with different w/c-ratios can result in different amounts of hydration products which are directly related to carbonation.
- Unhydrated clinker phases like C_2S or C_3S are often neglected especially in accelerated carbonations experiments. Additional C-S-H and $Ca(OH)_2$ may form in ongoing reaction parallel to carbonation.
- The formation of other carbonation products (e.g. Na_2CO_3, $MgCO_3$) are mostly neglected, too.
- Other substitutions materials like pozzolans may cause other reaction products and change the compositions of concretes.
- Generally the formation of $CaCO_3$ causes an increase of volume which reduces the porosity.
- The formation of silica gel increases the porosity but it is seen at the later stages of carbonation.
- The formation of $CaCO_3$ during carbonation is directly related to the CO_2 concentrations. The differences in the concentrations can lead to different results between the natural and the accelerated carbonation of concrete.
- Too low or too high humidity can lower the carbonation rate.
- Finally, temperature changes also affect the stability of phases and the kinetics of the carbonation.

5. INVESTIGATION OF CARBONATION REACTIONS IN LIMESTONE-RICH CEMENT PASTES

5.1. Experimental program

5.1.1. Starting materials and mix design approach

The objective of this work is the investigation of the carbonation behavior of cement pastes with a reduced clinker content and an addition of limestone in the range of 0-50 wt. %. For the evaluation of the carbonation of limestone-rich paste samples of ordinary Portland cements that are commercially available were selected. Table 5.1 shows the chemical analysis provided by the manufactures of different Portland cements Z1 (CEM I 52.5 R, Dyckerhoff, Göllheim), Z2 (CEM I 42.5 N, Dyckerhoff, Göllheim) and Z3 (CEM I 52.5 R, Spenner, Erwitte) which were used to prepare the cement pastes.

Table 5.1: Composition of commercially available Portland cement used for cement pastes (Z1, Z2, and Z3); data from the suppliers.

Chemical content	Z1, CEM I 52.5 R, Dyckerhoff, Göllheim	Z2, CEM I 42.5 N, Dyckerhoff, Göllheim	Z3, CEM I 52.5 R, Spenner, Erwitte
Calcium oxide (CaO, %)	63.25	63.11	64.61
Iron oxide (Fe_2O_3, %)	2.92	2.96	2.67
Aluminium oxide (Al_2O_3, %)	4.50	4.57	4.21
Soluble silica (SiO_2, %)	20.31	20.29	21.31
Sulphuric anhydrite* (SO_3 %)	3.10	3.07	3.69
Magnesium oxide (MgO, %)	2.12	2.12	0.96
Sodium oxide (Na_2O, %)	0.12	0.13	0.19

Potassium oxide (K_2O, %)	0.81	0.74	0.57
Titanium oxide (TiO_2, %)	0.21	0.21	0.22
Phosphorus pentoxide (P_2O_5, %)	0.17	0.18	0.12
Loss of ignitation , % (LI)	1.48	2.39	0.76

* present as anhydrite ($CaSO_4$), hemihydrate ($CaSO_4 \cdot 0.5H_2O$), and gypsum ($CaSO_4 \cdot 2H_2O$),

Table 5.2 shows the limestone fillers obtained from different suppliers (KSM1, KSM2, KSM3, KSM4). Polycarboxylate ether (LZF Mapei-Betontechnik) and Glenium Ace 430 (BASF) were used as super plasticizer and potato based starch (Foxcrete) was used to avoid water secretion in some mixtures. Darmstadt city tap water was used to produce the samples.

Table 5.2: Phase composition (in %) of limestone powders; data from the suppliers.

Limestone Type	SiO_2	Al_2O_3	Fe_2O_3	CaO	MgO	$CaCO_3$	Supplier
KSM1	7.6	2.2	1.1	48.6	0.9	86.7	Dyckerhoff, Göllheim
KSM2	0.4	0.2	0.1	54.1	0.4	97.8	Brilon
KSM3	3.2	1.1	0.6	53.1	0.5	94.8	Schäfer
KSM4	0.3	0.1	0.1	55.1	0.2	98.1	SH Minerals

5.1.2. Preparation and characterization of cement pastes

Cement pastes with and without addition of limestone were prepared. The samples without limestone addition were investigated as references. The choice of the samples was as follows:

- cement pastes with commercial cement from different sources with a common w/c ratio of 0.5 to guarantee similar behavior of different batches of the basic material.
- cement pastes with the commercial cement Z1 with different w/c ratios to evaluate the w/c ratios needed for the eco-friendly cements.
- cement/limestone mixtures with limestone contents of 10-50 % and different w/c ratios.
- mixtures with identical limestone content and one w/c ratio but limestone powders from different commercial sources.

The test specimens were prepared according to DIN EN 196-1 [1]. Three prismatic test specimens with the dimensions of 40 mm × 40 mm × 160 mm were produced for each mixing recipe. For the paste samples water and cement were mixed for about 90 seconds. After that the cement pastes were scraped from the edges of the bowl and mixed for another 120 seconds. Super plasticizer or stabilizers were added if required. The cement pastes were placed into the molds on the vibrating table. The vibrating table was started at medium speed for 120 seconds, the remaining cement pastes were added within the first 60 seconds. For the samples with 0.5 and 0.6 water-cement ratio stabilizers were needed to avoid water secretion. A super plasticizer was needed for samples with a w/c ratio of 0.3 for sufficient workability. The compositions of the samples produced are shown in Table 5.3. The sample names Z1, Z2 and Z3 correspond to cement pastes without limestone addition. After mixing, the samples were covered with foil for 24 hours and casted in forming dies. After that the foil was removed and the samples were stored and cured in a water bath for 28 days at 20 °C according to DIN EN 196-1[1]. For reproducibility selected samples were prepared and characterized for a second time. In order to have fully hydrated samples selected mixtures were stored in water for 90 days. These experiments were repeated as well.

Table 5.3: Composition of cement pastes prepared from commercial cement, limestone, water, plasticizer, and stabilizer.

Sample ID	Cement %	Total amount of cement and limestone, g	Water, g	Plasticizer, g	Stabilizer, g	w/c
Z1-0.5	10 (Z1)	1216	608	-	1	0.50
Z2-0.5	100 (Z2)	1216	608	-	2	0.50
Z3-0.5	100 (Z3)	1216	608	-	1	0.50
Z1-0.6	100 (Z1)	1084	650	-	5	0.60
Z1-0.4 *	100 (Z1)	1384	554	-	-	0.40
Z80-0.4*	90 (Z1)	1384	554	-	-	0.40
Z81-0.4	80 (Z1+KSM1)	1384	554	-	-	0.40
Z82-0.4*	70 (Z1+KSM1)	1384	554	-	-	0.40
Z83-0.4*	60 (Z1+KSM1)	1384	554	-	-	0.40
Z84-0.4 *	50 (Z1+KSM1)	1384	554	-	-	0.40
Z90-0.4	70 (Z2+KSM1)	1384	554	-	-	0.40

Z91-0.4	70 (Z3+KSM1)	1384	554	-	-	0.40
Z92-0.4	70 (Z1+KSM2)	1384	554	-	-	0.40
Z93-0.4	70 (Z1+KSM3)	1384	554	-	-	0.40
Z94-0.4	70 (Z1+KSM4)	1384	554	-	-	0.40
Z1-0.35 *	100 (Z1)	1487	520	-	-	0.35
Z82-0.35*	70 (Z1+KSM1)	1487	520	-	-	0.35
Z83-0.35*	60 (Z1+KSM1)	1487	520	-	-	0.35
Z84-0.35*	50 (Z1+KSM1	1487	520	-	-	0.35
Z1-0.30 *	100 (Z1)	1606	482	5	-	0.30
Z82-0.30*	70 (Z1+KSM1)	1606	482	9	-	0.30
Z83-0.30*	60 (Z1+KSM1)	1606	482	11	-	0.30
Z84-0.30*	50 (Z1+KSM1)	1606	482	14	-	0.30

* These samples were selected and produced again. They were also stored in water for 90 days.

After curing, all of the samples were analyzed by X-ray powder diffraction to determine the content of crystalline phases in the cement pastes. The amounts of $Ca(OH)_2$ and $CaCO_3$ were obtained by thermal analysis for selected samples. The maximum amount of $Ca(OH)_2$ that could be expected was calculated using equations 2.1, 2.2, 2.4, and 2.7. The results of the experiments are shown in Table 5.4.

Table 5.4: Expected and determined amounts of $Ca(OH)_2$ and $CaCO_3$ after 28 and 90 days curing in a water bath and crystalline phases identified by X-ray powder diffraction.

Sample ID	$Ca(OH)_2$ %, max. theo.	$Ca(OH)_2$ %, DTA/TGA exp.	$CaCO_3$ %, DTA/TGA exp.	Major phases	Minor phases
Z1-0.6	27.20	24.95	6.66	$Ca(OH)_2$ C-S-H ettringite	$CaCO_3$ (calcite) C_3S C_2S $C_2(AF)$
Z1-0.5	27.20	23.81	5.89		
Z2-0.5	27.26	24.05	6.19		
Z3-0.5	26.36	22.39	1.66		
Z1-0.4	27.20	19.60	5.41		
Z1-0.4 N*	27.20	21.03	6.33		
Z1-0.4 90 days**	27.20	24.18	5.97		

Z80-0.4	24.82	17.69	12.49		
Z81-0.4	22.38	15. 19	14.65		
Z82-0.4	19.86	13.76	27.58		
Z83-0.4	17.27	-	-		
Z83-0.4 N*	17.27	16.46	33.67		
Z83-0.4 90 days**	17.27	16.85	33.01	$Ca(OH)_2$ C-S-H ettringite $CaCO_3$ (calcite)	C_3S C_2S $C_2(AF)$ $C_4A\bar{C}H_{11}$
Z84-0.4	14.61	9.25	38.35		
Z84-0.4 N*	17.27	13.98	39.79		
Z84-0.4 90 days**	14.61	14.71	44.62		
Z90-0.4	19.88	-	-		
Z91-0.4	19.25	-	-		
Z92-0.4	19.86	13.99	32.35		
Z93-0.4	19.86	-	-		
Z94-0.4	19.86	-	-		
Z1-0.35	27.20	-	-		
Z1-0.35 N*	27.20	17.13	5.32	$Ca(OH)_2$ C-S-H ettringite	$CaCO_3$ (calcite) C_3S C_2S $C_2(AF)$
Z1-0.35 90 days**	27.20	20.31	5.91		
Z82-0.35	19.86	-	-		
Z82-0.35 N*	19.86	18.44	20.94	$Ca(OH)_2$ C-S-H ettringite calcite	C_3S C_2S $C_2(AF)$ $C_4A\bar{C}H_{11}$ $C_2(AF)$ $C_4A\bar{C}H_{11}$
Z82-0.35 90 days**	19.86	18.95	22.32		$C_4A\bar{C}H_{11}$

Z83-0.35	17.27	12.67	30.18	$Ca(OH)_2$ C-S-H ettringite calcite	C_3S C_2S $C_2(AF)$ $C_4A\bar{C}H_{11}$
Z83-0.35 N*	17.27	16.46	34.26		$C_2(AF)$ $C_4A\bar{C}H_{11}$
Z83-0.35 90 days**	17.27	16.59	33.20		$C_2(AF)$ $C_4A\bar{C}H_{11}$
Z84-0.35	14.61	9.96	31.49		C_3S C_2S $C_2(AF)$ $C_4A\bar{C}H_{11}$
Z84-0.35 N*	14.61	13.65	39.97		C_2S $C_4A\bar{C}H_{11}$
Z84-0.35 90 days**	14.61	14.05	39.51		$C_4A\bar{C}H_{11}$
Z1-0.30	27.20	-	-	$Ca(OH)_2$ C-S-H ettringite	$CaCO_3$ (calcite) C_3S C_2S $C_2(AF)$
Z1-0.30 N*	27.20	16.02	6.36		
Z1-0.30 90 days**	27.20	17.51	5.79		
Z82-0.30	19.86	-	-	$Ca(OH)_2$ C-S-H ettringite	C_3S C_2S $C_2(AF)$ $C_4A\bar{C}H_{11}$
Z82-0.30 N*	19.86	17.18	27.18		C_2S $C_2(AF)$ $C_4A\bar{C}H_{11}$
Z82-0.30 90 days**	19.86	16.51	25.57		C_2 $C_4A\bar{C}H_{11}$

Z83-0.30	17.27	-	-	$Ca(OH)_2$ C-S-H ettringite calcite	C_3S C_2S $C_2(AF)$ $C_4A\bar{C}H_{11}$
Z83-0.30 N*	17.27	16.25	34.26		$C_2(AF)$ $C_4A\bar{C}H_{11}$
Z83-0.30 90 days**	17.27	14.56	36.52		$C_2(AF)$ $C_4A\bar{C}H_{11}$
Z84-0.30	14.61	9.17	34.92		C_3S C_2S $C_2(AF)$ $C_4A\bar{C}H_{11}$
Z84-0.30 N*	14.61	14.54	40.14		$C_4A\bar{C}H_{11}$
Z84-0.30 90 days**	14.61	13.56	42.24		$C_4A\bar{C}H_{11}$

*These synthese were repeated were and the samples stored in water for 28 days.
**These samples were stored in water 90 days in order to have sufficient hydration.

The comparison of the theoretical and the determined amounts of $Ca(OH)_2$ shows the expected results for cement pastes without limestone addition. Samples with a high w/c-ratio show a high degree of hydration. With decreasing w/c-ratios the degree of hydration is decreasing as well. Longer curing in water increases the degree of hydration as seen for the samples stored in water for 90 days. Compared to the samples without limestone addition the hydration rates for the samples with limestone are always higher. On the one hand this is due to the increased w/c-value of these samples, because they contain lower amounts of clinker phases. On the other hand it has been discussed in the literature that the limestone powder acts as a very fine filler material which decreases the porosity of the pastes [32, 71, 72, 80, and 81]. The XRD measurements show that the samples consist mainly of $Ca(OH)_2$, $CaCO_3$, ettringite, C-S-H phases, as well as some unreacted clinker phases like C_3S, C_2S, and $C_2(AF)$. Selected X-ray powder patterns are shown in figure 5.1 and 5.2. $CaCO_3$ is formed during the preparation and hydration of the pastes due to a reaction with carbon dioxide from air. Cement mixtures with limestone contain higher amounts of $CaCO_3$ as calcite.

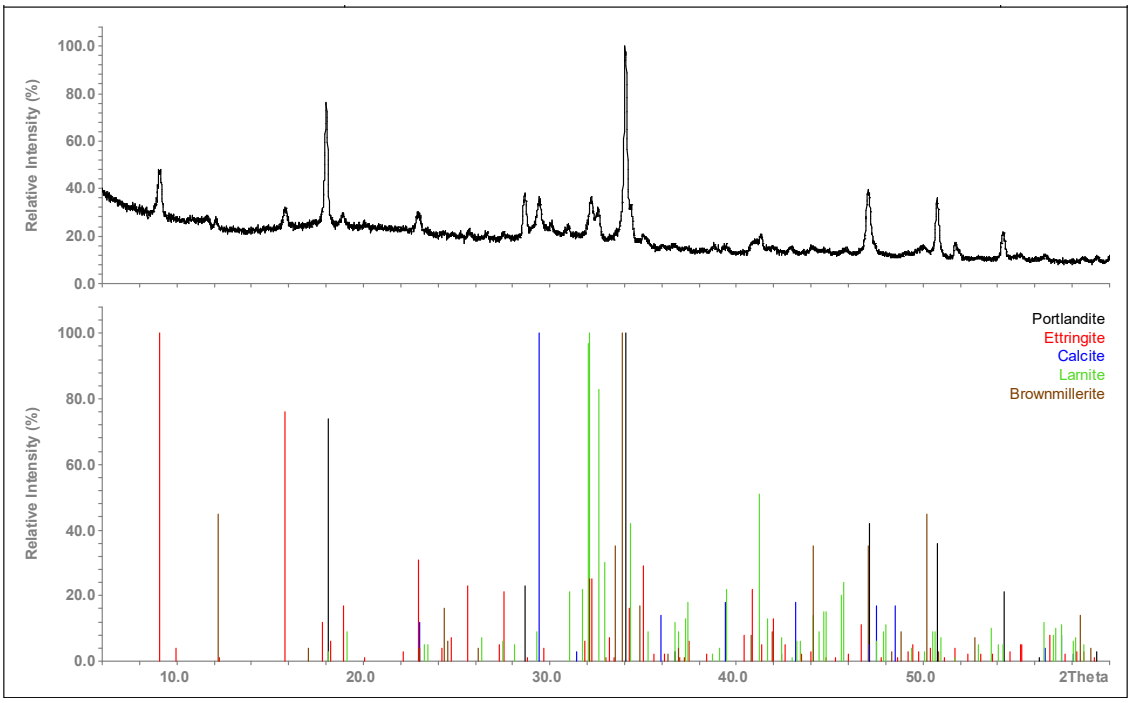

Figure 5.1: X-ray powder pattern of Z1-0.4, (top: experimental, bottom: data from literature [11, 12, 15, 108, 109, 111])

When figures 5.1 and 5.2 are compared it can be seen easily that the samples with limestone additions also contain monocarboaluminate ($(Ca_4Al_2(CO_3)(OH)_{12}\cdot 5H_2O)$). It is assumed that it is formed through the reaction between limestone and aluminate phases. This finding disproves the assumption that limestone is a completely inert material.

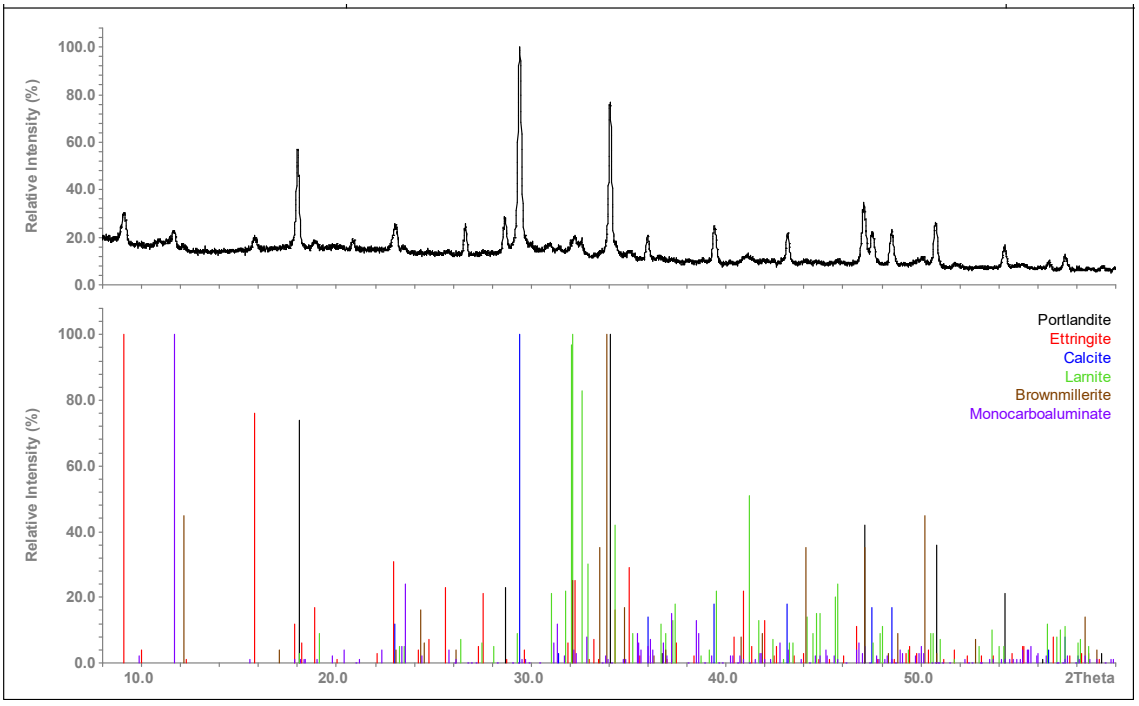

Figure 5.2: X-ray powder pattern of Z82-0.4 (top: experimental, bottom: pattern data from literature [12, 15, 108 - 111]).

5.1.3. Carbonation of cement pastes

5.1.3.1. Experimental procedure

Accelerated carbonation reactions were carried out under controlled conditions inside a closed chamber ("Carbobox") with a concentration of CO_2 of two vol. % and relative humidity of 65 % at 20 °C. The carbonation depths of the samples were determined using phenolphthalein solution. Samples were taken from the carbonated zones of the paste prisms. The amounts of $Ca(OH)_2$ and $CaCO_3$ were determined by thermal analysis and X-ray powder diffraction. The results are given in Table 5.5.

The carbonated samples consist of different modifications of $CaCO_3$, e.g. calcite, vaterite, and aragonite. Calcite and vaterite were observed in almost all samples. Especially high amounts of vaterite were detected in samples without limestone addition. Aragonite exists as a minor phase in carbonated cement pastes. SiO_2 (mainly quartz) was seen in samples with higher amounts of limestone. SiO_2 is present in commercial limestone sources and can be also formed during carbonation process of C-S-H phases.

Table 5.5: Amounts of $Ca(OH)_2$ and $CaCO_3$ after 28 days of accelerated carbonation.

Sample ID	$Ca(OH)_2$ %, DTA/TG	$CaCO_3$ %, DTA/TG	Major Phases	Minor Phases
Z1-0.5	-	52.89	calcite vaterite	C_3S C_2S $C_2(AF)$ ettringite
Z2-0.5	3.12	50.98	calcite vaterite $Ca(OH)_2$	C_3S C_2S $C_2(AF)$ ettringite C-S-H $Ca(OH)_2$
Z3-0.5	5.10	54.21	calcite vaterite $Ca(OH)_2$	C_3S C_2S $C_2(AF)$ ettringite

				C-S-H $Ca(OH)_2$
Z1-0.6	-	56.82	calcite vaterite	C_3S C_2S $C_2(AF)$
Z1-0.4	12.20	20.48	$Ca(OH)_2$ calcite vaterite C-S-H	C_3S C_2S $C_2(AF)$ ettringite
Z1-0.4 N	19.55	8.44	$Ca(OH)_2$ calcite ettringite C-S-H	$C_4A\bar{C}H_{11}$
Z1-0.4 90 days	21.78	11.92	$Ca(OH)_2$ calcite ettringite C-S-H	$C_4A\bar{C}H_{11}$
Z80-0.	5.07	35.03	calcite vaterite	aragonite $Ca(OH)_2$
Z81-0.4	-	52.73	calcite vaterite SiO_2 (quartz)	aragonite vaterite
Z82-0.4	-	63.15	calcite SiO_2(quartz)	aragonite vaterite
Z83-0.4	-	-	Calcite SiO_2(quartz) calcite	aragonite vaterite $Ca(OH)_2$
Z83-0.4 N	8.78	55.96		
Z83-0.4 90 days	9.59	56.37		
Z84-0.4	-	64.05	Calcite vaterite SiO_2 (quartz)	aragonite vaterite

Z84-0.4 N	1.79	65.80	calcite SiO_2 (quartz)	aragonite vaterite $Ca(OH)_2$
Z84-0.4 90 days	5.72	64.71		
Z92-0.4	0	61.55	calcite	vaterite C_3S C_2S $C_2(AF)$
Z1-0.35 N	18.46	8.86	$Ca(OH)_2$ calcite ettringite C-S-H	
Z1-0.35 90 days	20.67	7.83		
Z82-0.35 N	14.82	38.83	$Ca(OH)_2$ calcite ettringite C-S-H	vaterite C_2S $C_2(AF)$
Z82-0.35 90 days	13.61	39.21		
Z83-0.35	-	62.66	calcite SiO_2 (quartz)	
Z83-0.35 N	12.95	50.32	calcite $Ca(OH)_2$ SiO_2(quartz)	vaterite aragonite C_2S $C_2(AF)$
Z83-0.35 90 days	13.58	51.43	calcite $Ca(OH)_2$ SiO_2 (quartz)	vaterite aragonite C_3S C_2S $C_2(AF)$
Z84-0.35	-	66.20	calcite SiO_2 (quartz)	C_3S C_2S $C_2(AF)$
Z84-0.35 N	4.78	60.35	calcite $Ca(OH)_2$ SiO_2 (quartz)	vaterite aragonite C_2S $C_2(AF)$

Z84-0.35 90 days	8.85	62.64	calcite $Ca(OH)_2$ SiO_2 (quartz)	vaterite C_2S $C_2(AF)$
Z1-0.30 N	14.51	9.88	$Ca(OH)_2$ calcite ettringite C-S-H	vaterite C_2S $C_2(AF)$
Z1-0.30 90 days	15.99	9.59		
Z82-0.30 N	14.53	32.85		
Z82-0.30 90 days	14.62	33.21	$Ca(OH)_2$ calcite ettringite C-S-H	calcite C_2S $C_2(AF)$
Z83-0.30 N	9.43	58.46	calcite $Ca(OH)_2$ SiO_2 (quartz)	aragonite C_2S $C_2(AF)$
Z83-0.30 90 days	12.02	52.45	Calcite $Ca(OH)_2$	SiO_2 (quartz)
Z84-0.30	-	59.29	calcite	SiO_2 (quartz) ettringite
Z84-0.30 N	8.58	55.73	Calcite $Ca(OH)_2$	
Z84-0.30 90 days	9.82	56.81	Calcite $Ca(OH)_2$	

5.1.3.2. Quantitative determination of $CaCO_3$

The amount of $CaCO_3$ formed by carbonation of $Ca(OH)_2$ was calculated assuming a reaction between $Ca(OH)_2$ and CO_2 according to equation 5.1. For that purpose, the amounts of $Ca(OH)_2$ and $CaCO_3$ before and after 28 days of carbonation were determined by thermal analysis. After that, the stoichiometric factor from equation 5.2 was multiplied with the difference in the content of $Ca(OH)_2$ before and after 28 days of accelerated carbonation.

$$\mathbf{Ca(OH)_2 + CO_2 \rightarrow CaCO_3 + H_2O} \qquad \mathbf{[5.1]}$$

74 g/mol 44 g/mol 100 g/mol 18 g/mol

$$\% CaCO_{3\,(CH)} = (\% Ca(OH)_{2\,before} - \% Ca(OH)_{2\,after}) * 100/74 \quad [5.2]$$

The amount of $CaCO_3$ formed by carbonation of other phases was determined by subtracting the amount of $CaCO_3$ before carbonation and the amount of $CaCO_3$ formed from $Ca(OH)_2$ from the experimentally observed total amount of $CaCO_3$ as shown in equation 5.3.

$$\% CaCO_{3\,(others)} = CaCO_{3(total)} - (CaCO_{3\,(CH)} + CaCO_{3(before)}) \quad [5.3]$$

Table 5.7: Amount of $CaCO_3$ from carbonation of $Ca(OH)_2$ and from carbonation of hydration products, determined by DTA/TGA

Sample ID	$CaCO_3$ % from carbonation of $Ca(OH)_2$ %	$CaCO_3$ % from carbonation of other phases
Z1-0.5	40.00	7.00
Z2-0.5	35.16	9.63
Z3-0.5	29.05	23.50
Z1-0.6	41.92	8.24
Z1-0.4	12.40	2.67
Z1-0.4 N	2.49	0.62
Z1-0.4 90 days	4.03	1.92
Z80-0.4	21.20	1.34
Z81-0.4	25.52	12.56
Z82-0.4	23.12	12.45
Z83-0.4 N	12.90	9.39
Z83-0.4 90 days	12.20	11.16
Z84-0.4	15.54	10.16
Z84-0.4 N	20.48	5.53
Z84-0.4 90 days	15.10	4.99
Z92-0.4	23.50	5.70
Z1-0.35 N	-	5.77
Z1-0.35 90 days	-	2.52
Z82-0.35 N	6.08	5.81

Z82-0.35 90 days	8.97	2.92
Z83-0.35	21.29	11.19
Z83-0.35 N	5.90	10.06
Z83-0.35 90 days	5.06	13.17
Z84-0.35	16.73	17.98
Z84-0.35 N	14.90	5.48
Z84-0.35 90 days	8.74	14.39
Z1-0.30 N	2.54	0.98
Z1-0.30 90 days	2.55	1.25
Z82-0.30 N	4.45	1.22
Z82-0.30 90 days	3.18	4.46
Z83-0.30 N	11.46	12.74
Z83-0.30 90 days	4.27	11.66
Z84-0.30	15.41	8.96
Z84-0.30 N	10.01	5.58
Z84-0.30 90 days	6.28	8.29

As seen in table 5.7, not only $Ca(OH)_2$ is carbonated but also a remarkable amount of other hydrated phases.

5.2. Conclusion

Carbonation depths (phenolphthalein test) and porosities of the first batch of samples were determined after 28 days of accelerated carbonation. Selected results are shown in figure 5.3 where the carbonation depth and the porosity are depicted together with the original content of $Ca(OH)_2$ as determined before the carbonation was started. The content of $Ca(OH)_2$ before the carbonation is used to test the general assumption that the carbonation resistance is mainly dependent on the amount of $Ca(OH)_2$ that is present in the samples. By comparing the samples Z1-0.6, Z1-0.5 and Z1-0.4, it can be seen that the sample with the lowest w/c ratio has the lowest carbonation depth. It can also be seen that the cement pastes with 50 % limestone substitution (Z84-0.4, Z84-0.35 and Z84-0.30) have lower porosities and

carbonation depths with decreasing w/c ratios. The cement paste with 50 % limestone substitution and 0.30 w/c ratio has a lower carbonation depth than Z1-0.6 and Z1-0.5.

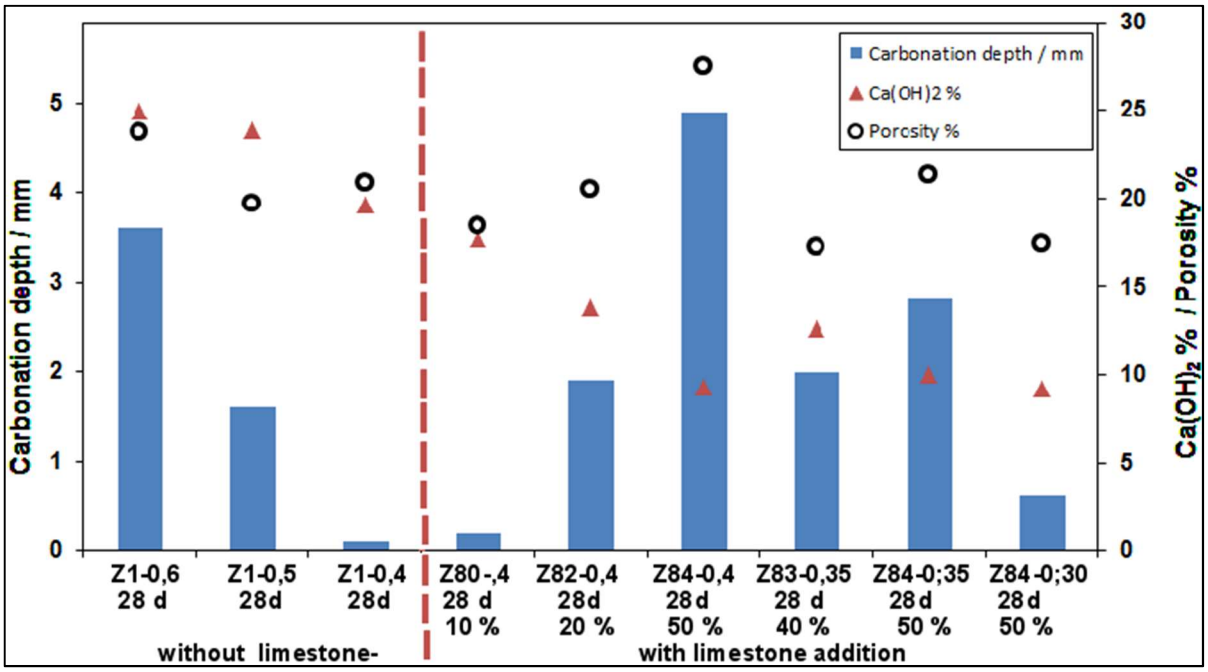

Figure 5.3: Content of $Ca(OH)_2$, porosity measurements, and carbonation depth of selected cement pastes (with different limestone and w/c ratios) after 28 days accelerated carbonation.

Repeating the sample preparation for samples with w/c ratios 0.6 and 0.5 [15] under identical conditions gave reproducible results. To further investigate the influence of the w/c ratio on the carbonation resistance, samples without limestone addition but different w/c values were examined more closely. In figure 5.4 it can be seen, that a w/c of less than or equal to 0.4 leads to low carbonation depths which are comparable to each other. Simultaneously, the $Ca(OH)_2$-content before the carbonation does not change dramatically with decreasing water content. It is assumed that the formation of capillary pores, which are formed due to high water contents, are responsible for the high carbonation depths.

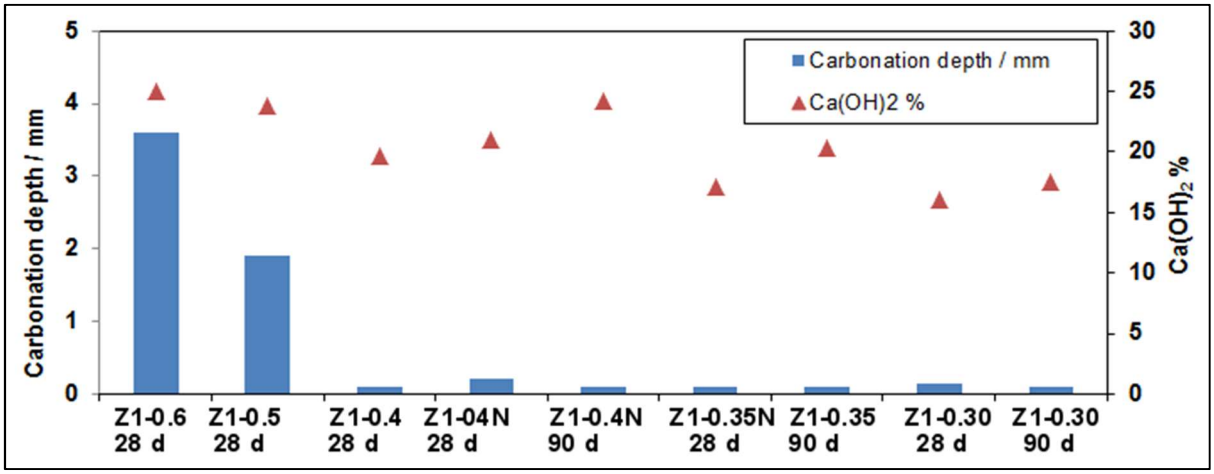

Figure 5.4: Content of $Ca(OH)_2$ and carbonation depth of cement pastes without limestone with different w/c ratios after 28 days accelerated carbonation.

In figure 5.5 samples with a constant w/c ratio of 0.4 and increasing amount of limestone are compared to samples with the same w/c ratio but without limestone addition. The $Ca(OH)_2$-content is compareable for all cement /limestone mixtures, but at the same time the carbonation depths increase strongly with increasing content of limestone. The reason can be found in the ratio of clinker phases to water content. This ratio increases for the samples with increasing w/c (water/cement) values. In mixtures with high limestone additions higher amounts of water are available for the hydration of the clinker phases than in comparable cement without limestone addition.

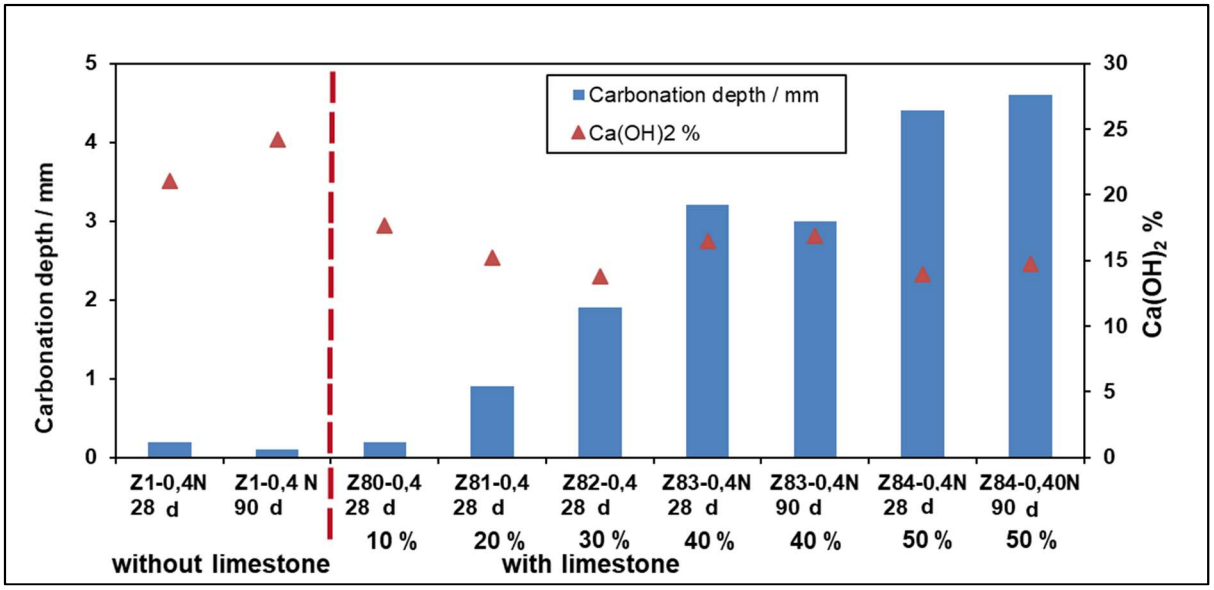

Figure 5.5: Content of $Ca(OH)_2$ and carbonation depths of cement pastes with different amounts of limestone (0-50 %) at a constant w/c ratio (0.40) after 28 days of accelerated carbonation.

A further reduction of the quantity of water increases the carbonation resistance as can be seen in figures 5.6 and 5.7 where cement pastes with limestone additions of 30 %, 40 %, and 50 %, and w/c ratios of 0.35 and 0.30 are compared to cement pastes without additions but with matching w/c ratios.

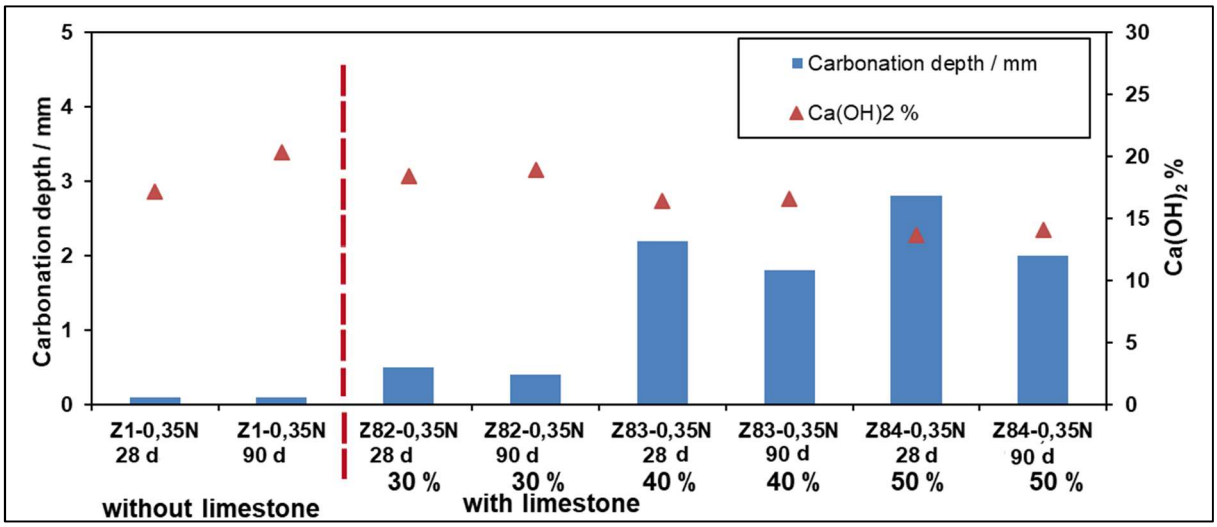

Figure 5.6: Content of $Ca(OH)_2$ and carbonation depth of cement pastes with different amounts of limestone (0-50 %) at a constant w/c ratio (0.35) after 28 days of accelerated carbonation.

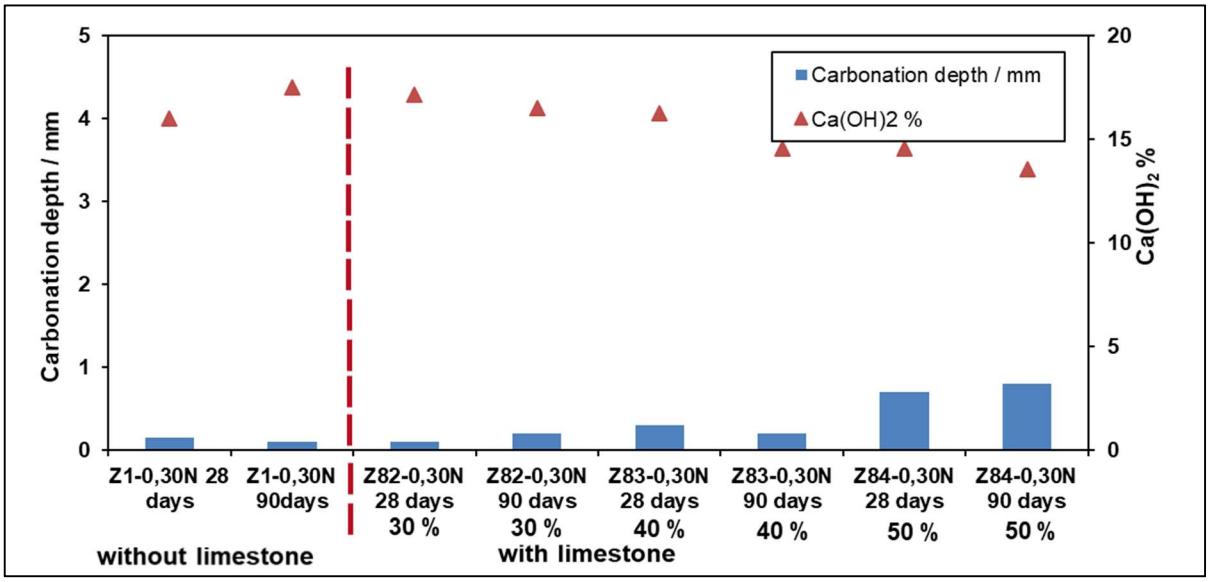

Figure 5.7: Content of $Ca(OH)_2$ and carbonation depths of cement pastes with different amounts of limestone addition (0-50 %) at constant w/c ratio (0.30) after 28 days of accelerated carbonation.

From these investigations it can be concluded, that the carbonation reactions are not solely dependent on the amount of $Ca(OH)_2$ initially formed. Figures 5.3-5.6 show that the w/c ratio plays an important role as well. For most of the samples investigated the amount of $Ca(OH)_2$ formed does not vary strongly. It can be seen, that a decreasing w/c ratio results in lower carbonation depths, even for samples with high limestone contents. The results show that the carbonation depths are more dependent on the w/c ratio than on the initial amount of $Ca(OH)_2$. Generally, that means eco-friendly cements with high amounts of limestone addition can show similar carbonation resistance as commercial cements as long as the w/c-ratio is adjusted.

The experimental investigations of these complex materials pose different challenges. The phenolphthalein test used for the determination of the carbonation depths can only give a rough estimate instead of exact data, because only the pH of the surface of the test specimens are determined. Zones of the specimen considered to be fully carbonated (phenolphthalein colorless, pH < 9) can still contain significant amounts of $Ca(OH)_2$ as determined by XRD and DTA/TGA. Moreover, no information on the nature of the hydration products and their reaction products are available. Also, there is no chance to distinguish between the carbonation of different hydrated phases in the cement paste samples. In table 5.7, it is shown that hydrated phases other than $Ca(OH)_2$ can form carbonate, too. However, neither the sequence nor the speed of the individual carbonation reactions can be determined with this experimental approach. To gain a deeper insight into these reactions, more detailed investigations are necessary. For that reason the main clinker phases were synthesized and investigated individually as described in the following chapter.

6. INVESTIGATION OF PURE CLINKER PHASES

6.1. Preparation and synthesis of pure clinker phases

6.1.1. Ca_3SiO_5

Ca_3SiO_5 (C_3S) can be synthesized at high temperatures according to equation 6.1. Ca_3SiO_5 is not stable at temperatures below 1250 °C and rapid cooling or quenching is necessary to avoid decomposition of Ca_3SiO_5 to CaO and Ca_2SiO_4 [8, 13].

$$\mathbf{3\ CaO + SiO_2 \rightarrow Ca_3SiO_5} \qquad \mathbf{[6.1]}$$

$CaCO_3$ (Merck, 99.95 % purity), SiO_2 (Sigma Aldrich, 99.90 %) and $Al(OH)_3$ (Grüssing, 98.5 % purity) powders were used as starting materials. $CaCO_3$ was calcined at 1000 ° C for one hour in a tube furnace to yield CaO. CaO and SiO_2 were then weighed stoichiometrically with 1% Al_2O_3 and mixed in a ball-mill. Al_2O_3 was added to stabilize the triclinic modification of Ca_3SiO_5. The mixtures were pressed into pellets. The amounts of the powders used for an experiment are given in table 6.1. Each of the experiments yielded one gram of final product.

Table 6.1: Amounts of starting materials for Ca_3SiO_5.

Composition	CaO, mg	SiO_2, mg	Al_2O_3, mg
C_3S	733.71	266.29	-
C_3S with 1 % Al_2O_3	729.04	260.96	10

Pressed pellets were filled into tantalum crucibles. After that the tantalum crucibles were sealed and heated to 1900 °C for one hour in an induction furnace under argon atmosphere. Afterwards, the hot crucible was quenched immediately in water. The powders obtained were characterized by X-ray powder diffraction. The data were fitted using the Rietveld method (figure 6.1).

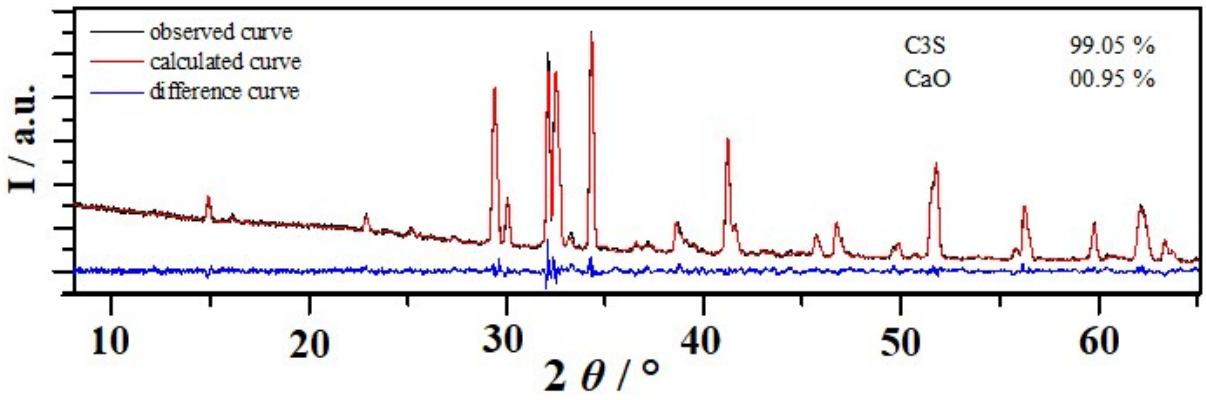

Figure 6.1: X-ray powder data after Rietveld refinement of Ca_3SiO_5 based on the structural model of the triclinic polymorph [11]. X-ray powder pattern (black) and Rietveld fit (red), difference curve in blue (R_{exp}; 3.82 %, R_{wp}; 4.91 %, R_p; 3.54, GOF: 1.29).

As seen in figure 6.1, the triclinic modification of Ca_3SiO_5 was synthesized almost phase pure. However, there is a small detectable amount of CaO (0.95 %), but no Ca_2SiO_4 was observed.

6.1.2. Ca_2SiO_4

Ca_2SiO_4 was synthesized by solid state reaction. As starting materials $CaCO_3$ (Merck, 99.95 % purity), SiO_2 (Sigma Aldrich 99.90 % purity) and B_2O_3 (Merck, 99.0% purity) were used. $CaCO_3$ was calcined to give CaO, then, CaO and SiO_2 were stoichiometrically weighed and 1.5 % B_2O_3 was added to stabilize the β-modification which is the reactive form of Ca_2SiO_4. The amounts of the powders used for an experiment can be seen in table 6.2, again resulting in one gram of final product each.

Table 6.2: Amounts of starting materials for Ca_2SiO_4.

Composition	CaO, mg	SiO_2, mg	B_2O_3, mg
C_2S (Ca_2SiO_4)	651.12	348.88	-
C_2S with 1.5 % B_2O_3	641.42	343.58	15

The weighed powders were mixed with a ball-mill. Afterwards the powders were pressed into pellets and filled into alumina crucibles. A vertical tube furnace (Carbolite) was used to perform the solid state reaction between CaO and SiO_2 according to equation 6.2.

$$2\ CaO + SiO_2 \rightarrow Ca_2SiO_4 \qquad \textbf{[6.2]}$$

The alumina crucibles were heated up to 1300 °C and held eight hours at that temperature. Ca_2SiO_4 is stable from room temperature to its melting point at 2130 °C. There are no

decomposition reactions in this temperature range so that it was cooled slowly (within eight hours) to room temperature. The powders obtained were taken out from the alumina crucible and characterized using X-ray powder diffraction. A quantitative phase determination was carried out using the Rietveld method (figure 6.2).

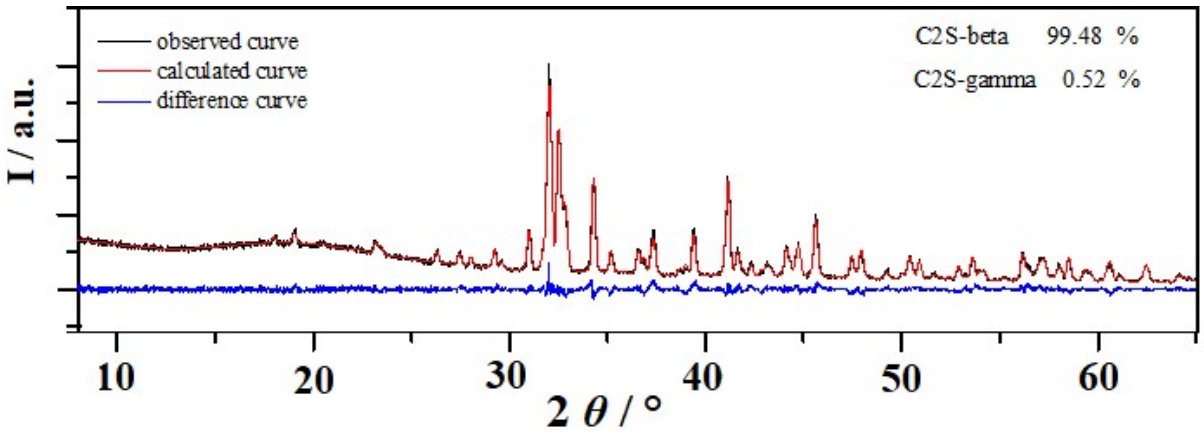

Figure 6.2: X-ray powder data after Rietveld refinement of Ca_2SiO_4 based on the β-and γ-modifications [12, 112]. X-ray powder pattern (black) and Rietveld fit (red) of a Ca_2SiO_4 sample, difference curve in blue (R_{exp}: 5.43 %, R_{wp}: 6.57 %, Rp: 4.87, GOF: 1.21).

The procedure described yielded Ca_2SiO_4 without impurities. The desired β-Ca_2SiO_4 was obtained with a phase purity of 99.48 %, a small amount of γ- Ca_2SiO_4 was usually found as side product.

6.1.3. $Ca_3Al_2O_6$

$Ca_3Al_2O_6$ can be easily synthesized by solid state reaction according to equation 6.3.

$$3\ CaCO_3 + 2\ Al(OH)_3 \rightarrow Ca_3Al_2O_6 + 3\ H_2O + 3\ CO_2 \qquad \textbf{[6.3]}$$

$CaCO_3$ (Merck, 99.95 % purity), $Al(OH)_3$ (Grüssing, 98.5 % purity) and $Na_2B_4O_7$ (Alfa Aesar, 98.5 % purity) were used as starting materials. $Na_2B_4O_7$ was used to decrease the sintering temperature. The amounts used for an experiment can be seen in table 6.3.

Table 6.3: Amounts of starting materials for $Ca_3Al_2O_6$.

Composotion	$CaCO_3$, mg	$Al(OH)_3$, mg	$Na_2B_4O_7$, mg
C_3A	1110.20	577.35	-
C_3A with 1% $Na_2B_4O_7$	1099.10	571.15	10

$CaCO_3$, $Al(OH)_3$ and $Na_2B_4O_7$ were weighed stoichiometrically. The weighed powders were mixed in a ball-mill, pressed into pellets, and filled into alumina crucibles. The pellets were

heated to 1200 °C within eight hours, held at this temperature for another eight hours and then cooled slowly back to room temperature. The powders obtained were characterized by X-ray powder diffraction. The observed data was fitted with the Rietveld method (figure 6.3).

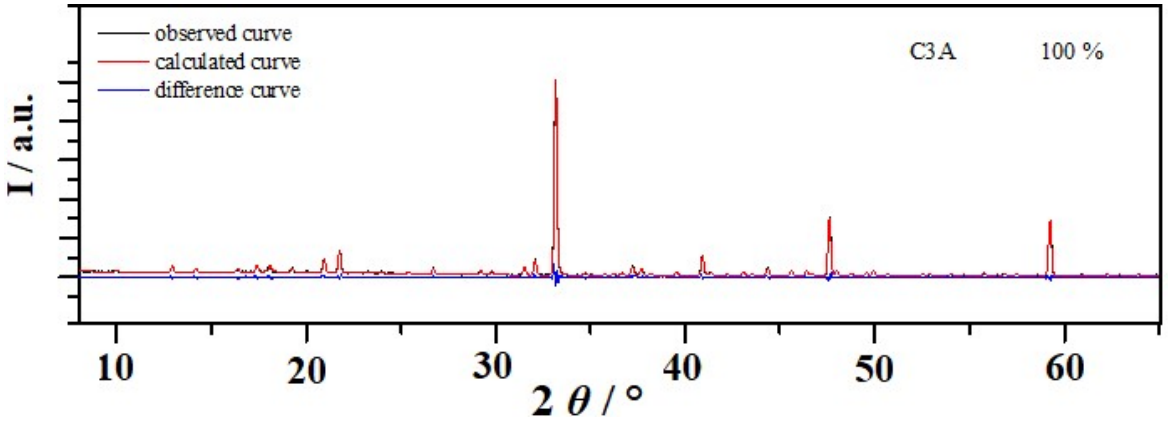

Figure 6.3: X-ray powder data after Rietveld refinement based on the structure model of $Ca_3Al_2O_6$ [107]. X-ray powder pattern (black) and Rietveld fit (red), difference curve in blue. (R_{exp}: 7.15 %, R_{wp}:11.57 %, R_p: 8.20, GOF:1.64).

As shown in figure 6.3 $Ca_3Al_2O_6$ was obtained as phase-pure sample. The pellets were ground finely for subsequent investigations.

6.1.4. $Ca_2(Al,Fe)_2O_5$

For $Ca_2(Al,Fe)_2O_5$ ($C_2(AF)$) different Al/Fe ratios are possible. For the samples in this study only phases with an Al/Fe ratio of one were prepared according to equation 6.4.

$$2\ CaCO_3 + Al(OH)_3 + 1/2\ Fe_2O_3 \rightarrow Ca_2(Al,Fe)_2O_5 \qquad \textbf{[6.4]}$$

As starting materials powder of $CaCO_3$ (Merck, 99.95 % purity), Fe_2O_3 (Alfa Aesar 98.5 % purity) and $Al(OH)_3$ (Grüssing, 98.5 % purity) were used. The amounts of the powders used for an experiment are given in table 6.4.

Table 6.4: Amounts of starting materials for $Ca_2(Al,Fe)O_5$.

Composition	$CaCO_3$, mg	Fe_2O_3, mg	$Al(OH)_3$, mg
Ca_2AlFeO_5	823.04	328.58	321.00

$CaCO_3$, $Al(OH)_3$ and Fe_2O_3 were weighed stoichiometrically. The starting materials were mixed in a ball-mill, pressed into pellets, filled in alumina crucibles and heated in a vertical tube furnace with the same sintering procedure as described for $Ca_3Al_2O_6$. After the reaction the products were characterized by X-ray powder diffraction. The results of a Rietveld fit are given in figure 6.4

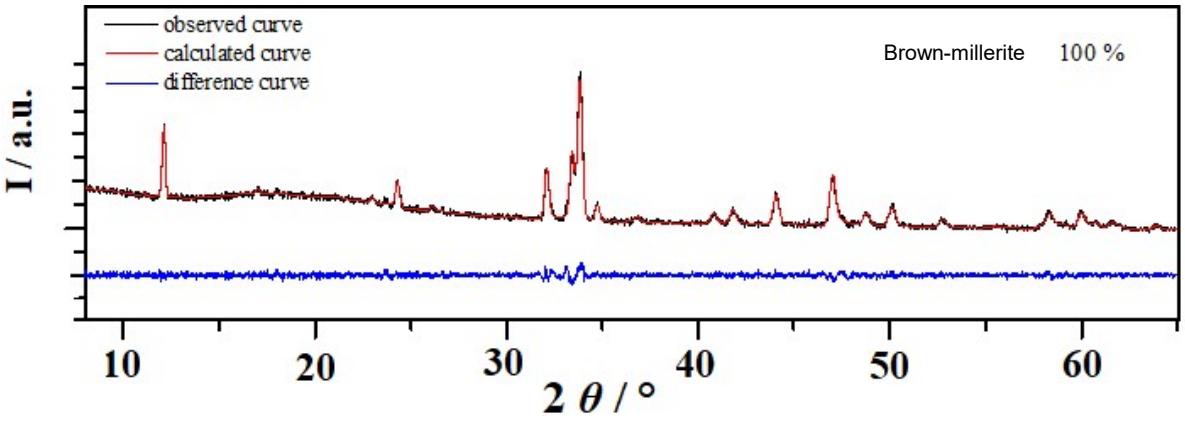

Figure 6.4: X-ray powder data after Rietveld refinement of Ca_2AlFeO_5 based on crystal structure data [15]. X-ray powder pattern (black) and Rietveld fit (red) of a Ca_2AlFeO_5 sample, difference curve in blue (R_{exp}: 2.50 %, R_{wp}: 2.59 %, R_p: 2.01, GOF: 1.04).

6.1.5. Synthesis of Ettringite

Ettringite ($Ca_6Al_2[(OH)_{12}|SO_4)_3 \cdot 26H_2O$) can form in calcium-rich, alkaline environments, and is found as a minor mineral in rocks [114]. Ettringite formation is a pH-controlled reaction (at a pH above 10) of compounds containing calcium, aluminum, and sulphate ions. In this study, ettringite was synthesized using $Ca_3Al_2O_6$ and gypsum according to equation 6.5.

$$Ca_3Al_2O_6 + 3\ CaSO_4 \cdot 2\ H_2O + 26\ H_2O \rightarrow Ca_6Al_2[(OH)_{12}|(SO_4)_3] \cdot 26\ H_2O \qquad \textbf{[6.5]}$$

During the reaction the pH values must remain above 10 as seen in figure 6.5. $Ca_3Al_2O_6$ and gypsum were ground and mixed with water. The pH value of the solutions was controlled with NaOH solution (0.1 mol/l) to avoid precipitation of undesired phases. The mixture was stored in a desiccator under N_2 to avoid reaction with CO_2 in air. However, even while the reaction is fast at the beginning, the complete reaction takes approximately one week. In conventional concretes ettringite partially contains Fe^{3+} ions and other impurities. AFt phases are derived from pure ettringite with a partial substitution of Al by Fe and SO_4^{2-} by other ions as CO_3^{2-}.

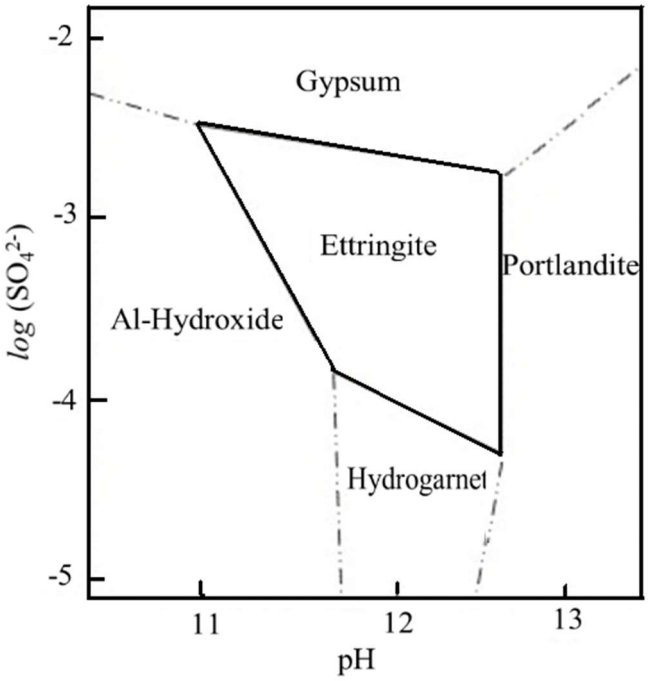

Figure: 6.5: Stability of ettringite depending on the concentration of SO_4^{2-} and the pH-value [115].

After storing in the desiccator under N_2 atmosphere for one week, the solidified mixture was analyzed by X-ray powder diffraction. XRD patterns were fitted for quantative analysis using the Rietveld method. The results are shown in figure 6.6.

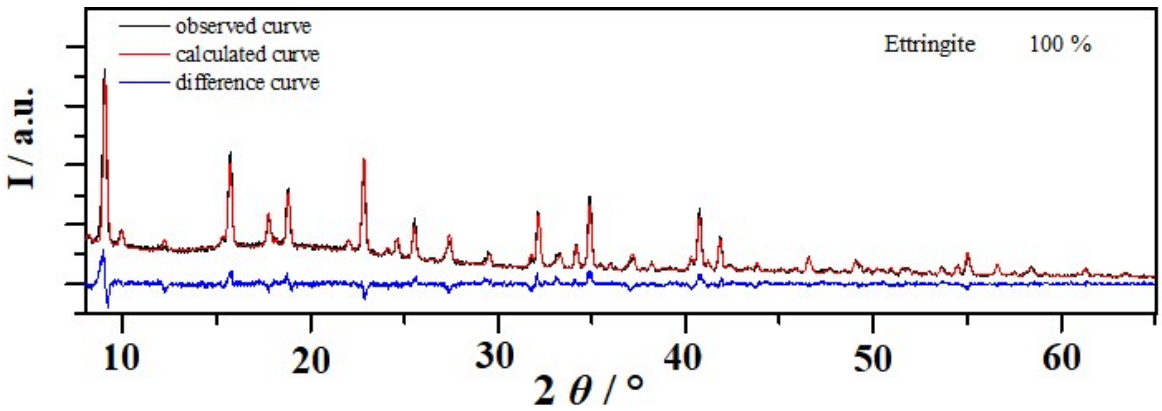

Figure 6.6: X-ray powder data after Rietveld refinement of ettringite based on structure data of ettringite [108]. X-ray powder pattern (black) and Rietveld fit (red) of an ettringite sample, difference curve in blue. (R_{exp}: 2.50 %, R_{wp}: 2.59 %, R_p: 2.01, GOF: 1.04).

6.2. Hydration and carbonation of pure clinker phases

6.2.1. Preparation of cement pastes from pure phases

For the investigation of the carbonation reactions of hydrated pure clinker phases, the powders synthesized were ground and mixed with different amounts of distilled and degassed water. After mixing, all the samples were hydrated for 28 days in an argon-filled desiccator with aqueous solution of NH_4NO_3.

To investigate the influence of the specimen preparation and sample geometry, different samples were prepared.

To allow for direct comparison with the cement pastes investigated earlier the samples were analyzed after 28 days of hydration and carbonation. Thus, the pure clinker phases (2g) were hydrated in plastic tubes (10 mm diameter) with w/c ratios of 0.4, 0.5 and 0.6.

Prior to the time dependent carbonation, the samples were prepared according to the following procedures:

- Hydrated samples with a w/c value of 0.5, 0.4 and 0.6 were pressed into pellets (10 tons, 10 mm diameter, 1 mm high) and stored under CO_2 atmosphere (2 % CO_2, 65 % relative humidity, 20 °C) for different time spans (0, 1, 2, 4, 7, 14, 21 and 28 days) Prior to the analyses the pellets were ground completely into homogeneous powders.
- Hydrated samples in form of cylindrical blocks (10 mm diameter, 30 mm high) were prepared. For these experiments one cylindrical sample of each clinker phase was investigated. Samples for the analysis were broken out of the cylinder approximately 1 mm from the edges after different time intervals (0, 1, 2, 4, 7, 14, 21 and 28 days).
- For each pure clinker phase eight portions of one gram were filled into 5 mL polystyrene cups. The samples were hydrated within these cups. After 28 days of hydration the small cups were placed inside the “carbobox”. After different time intervals (0, 1, 2, 4, 7, 14, 21 and 28 days) the content of one cup of each sample was ground for analysis.
- A model cement with a composition of 81 % C_3S, 12 % C_3A, 2 % C_2S, 5 % $CaSO_4{\cdot}2H_2O$ was prepared in 5 mL polystyrene cups. The model cement samples were hydrated and carbonated as described above.

After hydration all samples were analyzed by X-ray powder diffraction to identify the crystalline phases. The amounts of $Ca(OH)_2$ and $CaCO_3$ were calculated using thermal analysis.

6.2.2. Hydration of clinker phases for direct comparison with the cement paste samples.

Prior to the carbonation reaction the pure clinker phases were hydrated as described above. To determine the hydration rates, first the theoretical amount of $Ca(OH)_2$ was calculated, assuming fully hydrated samples of C_2S and C_3S samples and an average composition of $CaO{\cdot}2SiO_2{\cdot}4H_2O$ (equations 6.6 and 6.7) for the C-S-H phases.

$2\ Ca_3SiO_5 + 7\ H_2O \rightarrow 3\ CaO{\cdot}\ 2SiO_2\ {\cdot}4\ H_2O + 3\ Ca(OH)_2$ **[6.6]**

2*22 8 g/mol 18 g/mol 360 g/mol 74 g/mol

$\%\ Ca(OH)_{2(theoretical)} = [(3*74)/(360+(74*3)]*100 \rightarrow 38.14\%$

$2Ca_2SiO_4 + 5\ H_2O \rightarrow 3CaO{\cdot}\ 2SiO_2\ {\cdot}4H_2O + Ca(OH)_2$ **[6.7]**

2*172 g/mol 18 g/mol 360 g/mol 74 g/mol

$\%\ Ca(OH)_{2(theoretical)} = [(74)/(360+74)] * 100 \rightarrow 17.05\ \%$

Table 6.5 shows the results of the DTA/TGA and XRD (Fig 6.8) measurements of the hydrated C_2S and C_3S samples and the estimated hydration rates (pure clinker phases (2g) in plastic tubes (10 mm diameter), different w/c ratios). In figure 6.8 a representative powder pattern of hydrated C_3S with a w/c ratio of 0.6 is shown.

Table 6.5: Results of DTA/TGA and XRD measurements of the hydration products C_2S and C_3S and estimated hydration rates after 28 days.

Sample ID	w/c	Hydration rate %	$Ca(OH)_2$ %, max. theo.	$Ca(OH)_2$ %,	$CaCO_3$ %,	crystalline phases
C_2S-0.4	0.4	81.18	17.05	13.95	-	$Ca(OH)_2$ C-S-H unreacted C_2S
C_2S-0.5	0.5	70.91	17.05	12.10	5.67	$Ca(OH)_2$ C-S-H unreacted C_2S calcite
C_2S-0.6	0.6	65.51	17.05	11.17	0.99	$Ca(OH)_2$ C-S-H unreacted C_2S
C_3S-0.4	0.4	70.79	38.14	27.01	-	$Ca(OH)_2$ C-S-H unreacted C_3S

C_3S-0.5	0.5	68.32	38.14	26. 07	-	$Ca(OH)_2$ C-S-H unreacted C_3S
C_3S-0.6	0.6	78.97	38.14	30.12	2.44	$Ca(OH)_2$ C-S-H unreacted C_3S calcite

Upon hydration, $Ca(OH)_2$ and C-S-H phases are formed from C_2S and C_3S. Small amounts of unreacted phases and $CaCO_3$ can be found as well (table 6.5 and figure 6.8).

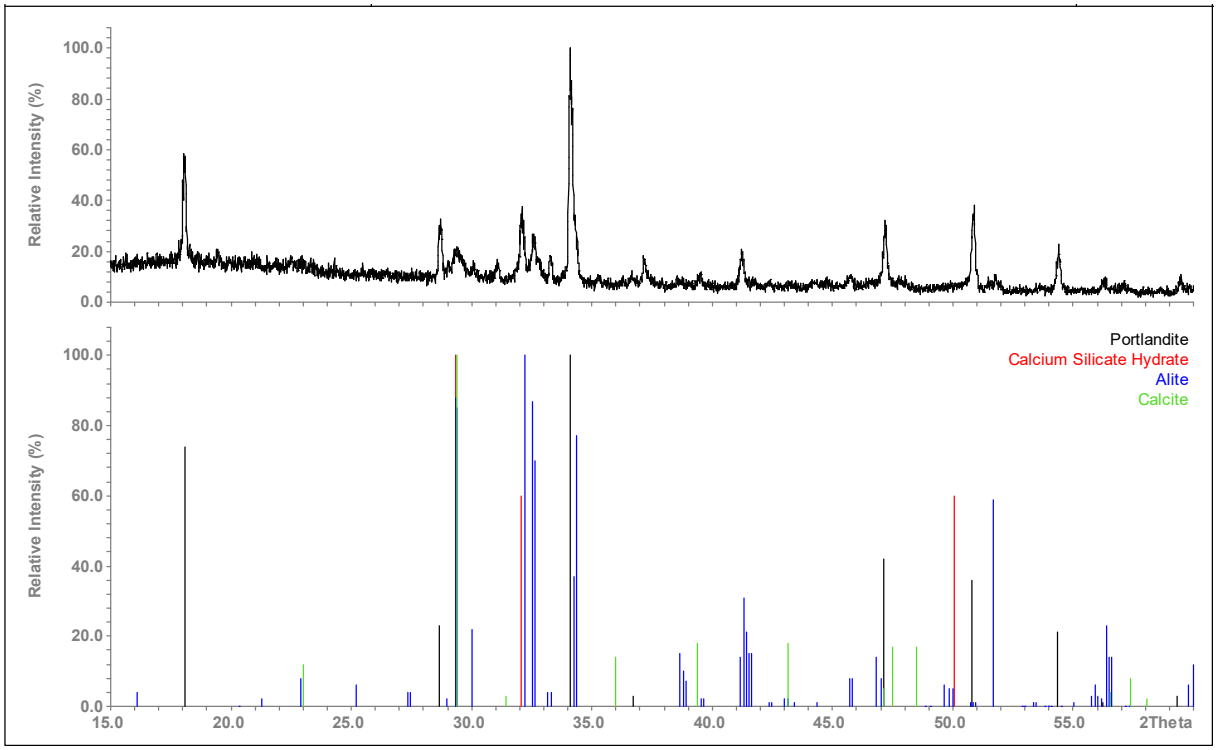

Figure 6.8: X-ray powder pattern of hydrated C_3S with a w/c ratio of 0.6; underneath theoretical line patterns from literature [11, 109, 111, 116]

As shown in table 6.6, the main hydration product of $C_2(AF)$ and C_3A is hydrogarnet ($(Ca_3(Al,Fe)_2(OH)_{12}$). About 80% hydrogarnet is formed. The results of qualitative and quantitative phase analysis of hydrated $C_2(AF)$, C_3A and ettringite are shown in table 6.7.

Table 6.6: Results from qualitative and quantitative phase analysis of hydrated based on the structure models ($C_2(AF)$, C_3A and ettringite) [15, 113, 108].

Sample ID	w/c	hydration product %	crystalline phases
$C_2(AF)$	0.4	81.41 % hydrogarnet ($Ca_3(Al,Fe)_2(OH)_{12}$)	unreacted $C_2(AF)$
$C_2(AF)$	0.5	82.49 % hydrogarnet ($Ca_3(Al,Fe)_2(OH)_{12}$)	unreacted $C_2(AF)$
C_3A	0.4	83.57 % hydrogarnet ($Ca_3Al_2(OH)_{12}$)	unreacted C_3A
C_3A	0.5	84.34 % hydrogarnet ($Ca_3Al_2(OH)_{12}$)	unreacted C_3A
Ettringite	-	100 % ettringite	Ettringite

Hydrogarnet ($Ca_3(Al,Fe)_2(OH)_{12}$) formed by hydration of $C_2(AF)$ and C_3A can differ in its iron content. It can be assumed that iron ions substitute part of the aluminum ions. The X-ray powder pattern of hydrated $C_2(AF)$ and C_3A are similar, as shown in figure 6.9. The high background in the powder pattern of $C_2(AF)$ is due to fluorescence effects produced by the iron atoms in combination with $Cu_{K\alpha 1}$-radiation.

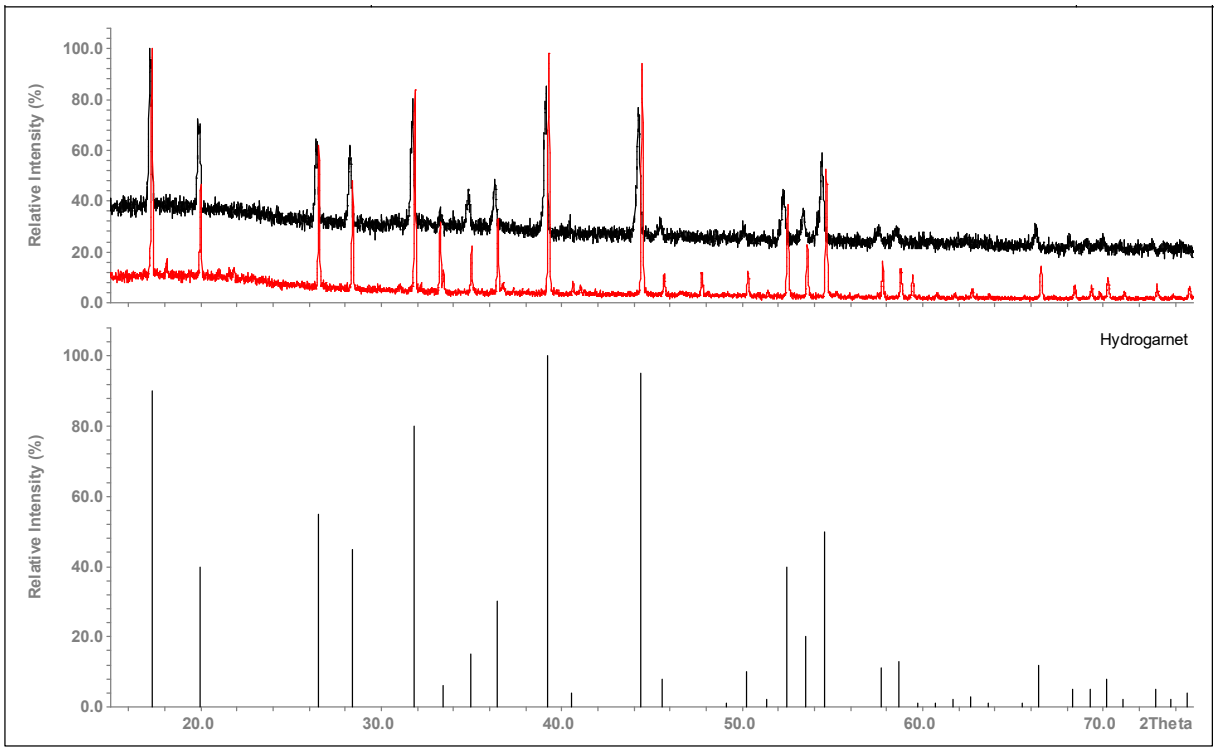

Figure 6.9: X-ray patterns of hydrated $C_2(AF)$ (black) and C_3A(red) (w/c ratio 0.4), underneath a theoretical line pattern from literature for hydrogarnet [118].

The first set of experiments was carried out in the same manner as done for the cement pastes (see chapter 5.1.3). Accelerated carbonation reactions of the hydrated samples were run under controlled conditions inside a closed chamber ("carbobox" at 2 vol. % CO_2 and 65 % relative humidity at 20 °C) for 28 days. The samples were taken from the carbonated zones at the surfaces.

After 28 days, vaterite and calcite were found as main products in C_2S and C_3S samples. Aragonite was also observed in some of the samples as a minor phase. The results of DTA/TGA and XRD measurements of sample of C_2S and C_3S after 28 days of accelerated carbonation are shown in table 6.7.

Table 6.7: Results of DTA/TGA and XRD measurements of hydrated C_2S and C_3S after 28 days of accelerated carbonation.

Sample ID	w/c	$Ca(OH)_2$ / %	$CaCO_3$ / %	crystalline phases
C_2S-0.4	0.4	2.43	43.19	vaterite calcite aragonite $Ca(OH)_2$ unreacted C_2S C-S-H
C_2S-0.5	0.5	-	51.41	vaterite calcite C-S-H unreacted C_2S
C_2S-0.6	0.6	-	57.63	vaterite calcite C-S-H unreacted C_2S
C_3S-0.4	0.4	-	55.13	vaterite calcite C-S-H unreacted C_3S
C_3S-0.5	0.5	-	66.85	vaterite calcite C-S-H unreacted C_3S
C_3S-0.6	0.6	6.23	50.15	vaterite calcite $Ca(OH)_2$ unreacted C_3S C-S-H

Carbonation reactions of hydrated $C_2(AF)$ and C_3A result in carbonate formation. Two polymorphs of $CaCO_3$, vaterite and calcite, were found as main carbonation products. The results of DTA/TGA and XRD measurements of hydrated C_3A and $C_2(AF)$ after 28 days of accelerated carbonation are shown in table table 6.8.

Table 6.8: Phase analysis of hydrated C_3A and $C_2(AF)$ after 28 days of accelerated carbonation.

Sample ID	phase ratios	crystalline phases
C_3A-0.4	50.82 % hydrogarnet, 16.24 % C_3A, 13.81 % calcite, 19.14 % vaterite	hydrogarnet unreacted C_3A calcite vaterite
Ettringite	69.45 % ettringite, 25.83% bassanite 4.72 % calcite	ettringite bassanite calcite
$C_2(AF)$ 0.5	30.16% hydrogarnet, 50.95% vaterite, 17.38% unreacted $C_2(AF)$ 1.51% calcite	hydrogarnet vaterite unreacted $C_2(AF)$ calcite

During the carbonation reaction, ettringite tends to form calcium sulphate ($CaSO_4 \cdot 0.5\ H_2O$) at pH values below 11 (see figure 6.5.) The quantative phase analysis of the product mixture is shown in figure 6.10.

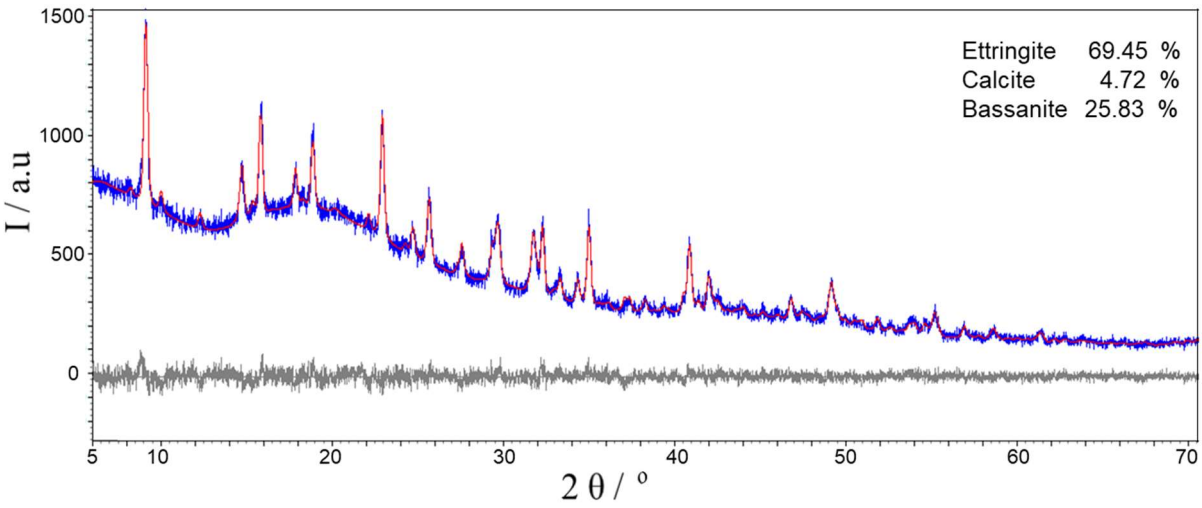

Fig 6.10: X-ray powder pattern (blue) and Rietveld fit (red) of a carbonated sample of ettringite, difference curve in grey. The positions of the reflections of three crystalline phases present in the sample (ettringite, calcite, basanite) are indicated by markers below the traces. (R_{exp}: 3.76 %, R_{wp}: 8.45 %, R_p: 5.71, GOF:2.24).

These experiments show that all single phases are prone to carbonation. After 28 days, calcite can be found as the main carbonation product for all samples. The drawback of these investigations is that time-resolved information cannot be obtained.

6.2.3. Time-dependent carbonation of pure clinker phases

To study the carbonation behavior of C-S-H and $Ca(OH)_2$ in more detail, pure $Ca(OH)_2$, hydrated C_3S, $C_2(AF)$, and C_3A were also investigated at shorter time intervals as well. To that purpose powders of freshly precipitated and dried $Ca(OH)_2$ and hydrated C_3S with different w/c values were pressed into pellets (10 tons, 10 mm diameter, 1 mm height) and stored under CO_2 (same conditions as described above) for different time spans (1, 2, 4, 7, 14, 21 and 28 days; prior to the analyses the pellets were ground completely into homogeneous powders). The results of the accelerated carbonation reactions are shown in table 6.9 and 6.10. For comparability cylindrical block samples of C_3S (10 mm diameter, 30 mm height; samples for the analyses were broken out of the cylinders approximately 1 mm from the edges) were investigated under the same conditions as well (tables 6.11, 6.12)

Table 6.9: Carbonation of pellets of $Ca(OH)_2$ at different time spans. The amounts of $Ca(OH)_2$ and $CaCO_3$ were determined by DTA/TGA.

Sample ID	$Ca(OH)_2$ %	$CaCO_3$ %,
$Ca(OH)_2$	98.11	1.16
$Ca(OH)_2$ 1 day	95.89	4.10
$Ca(OH)_2$ 2 days	94.30	5.70
$Ca(OH)_2$ 4 days	92.30	7.58
$Ca(OH)_2$ 7 days	90.70	9.30
$Ca(OH)_2$ 14 days	89.64	10.36
$Ca(OH)_2$ 21days	86.46	13.54
$Ca(OH)_2$ 28 days	85.15	14.85

To differentiate between the amount of $CaCO_3$ formed by carbonation of $Ca(OH)_2$ and carbonation of other phases the following procedure was applied: the amount of $Ca(OH)_2$ of each investigated sample was determined from the DTA/TGA experiments for each day (Table 6.10, column A and C). Secondly, the amounts of $Ca(OH)_2$ and $CaCO_3$ observed at

day zero were defined as the initial amount of $Ca(OH)_2$ and $CaCO_3$ within the sample. Column B (Table 6.11) shows the differences between the initial amounts of $Ca(OH)_2$ minus the remaining amounts of $Ca(OH)_2$ measured each day. These differences were then multiplied with a stoichiometric factor according to equation 6.8. That results in the amount of $CaCO_3$ formed by carbonation of $Ca(OH)_2$ (Table 6.10, column D).

$$\mathbf{Ca(OH)_2 + CO_2 \rightarrow CaCO_3 + H_2O} \quad \textbf{[6.8]}$$

74 g/mol 44 g/mol 100 g/mol 18 g/mol

$$\mathbf{\%\ CaCO_{3\,(CH)} = (\%CH_{initial} - \%CH_{after})*100/74}$$

The amount of $CaCO_3$ formed by carbonation of C-S-H (Table 6.11, column E) was determined by subtracting the initial amount of $CaCO_3$ at day zero and the amount of $CaCO_3$ formed from $Ca(OH)_2$ (column D) from the experimentally observed total amount of $CaCO_3$ (Table 6.10, column C, equations 6.9).

$$\mathbf{\%CaCO_{3(C\text{-}S\text{-}H} = CaCO_{3(total)} - (CaCO_3)_{(CH)} + CaCO_{3(initial)})} \quad \textbf{[6.9]}$$

Table 6.10: Carbonation of hydrated pellets of C_3S at different time spans. The amounts of $Ca(OH)_2$ and $CaCO_3$ were determined by DTA/TGA.

Sample ID Cylinder Blocks	$Ca(OH)_2$ %, DTA / TGA **A**	$Ca(OH)_2$, % reacted with CO_2 **B**	$CaCO_3$ %, DTA / TGA **C**	$CaCO_3$ %, from carbonation of $Ca(OH)_2$ **D**	$CaCO_3$ % from carbonation of C-S-H **E**
C_3S-0.5 day zero	27.40	-	2.71	-	-
C_3S-0.5 1 day	22.72	4.68	9.60	6.31	0.57
C_3S-0.5 2 days	21.80	5.60	10.50	7.56	0.23
C_3S-0.5 4 days	21.41	5.99	12.45	8.08	1.65
C_3S-0.5 7 days	21.19	6.21	13.01	8.38	1.91
C_3S-0.5 14 days	20.15	7.25	15.18	9.87	2.60
C_3S-0.5 21 days	17.14	10.26	19.30	13.85	2.74
C_3S-0.5 28 days	12.29	15.11	27.58	20.40	4.47

Table 6.11 : Carbonation of hydrated C_3S cylindrical blocks at different time spans. The amounts of $Ca(OH)_2$ and $CaCO_3$ were determined by DTA/TGA.

Sample ID Cylinder Blocks	$Ca(OH)_2$ %, DTA / TGA **A**	$Ca(OH)_2$, % reacted with CO_2 **B**	$CaCO_3$ %, DTA / TGA **C**	$CaCO_3$ % from carbonation of $Ca(OH)_2$ **D**	$CaCO_3$ % from carbonation of C-S-H **E**
C_3S-0.6 day zero	30.12	-	2.44	-	-
C_3S-0.6 1 day	11.60	18.52	37.81	25.00	10.36
C_3S-0.6 2 days	11.07	19.05	41.00	25.7	11.16
C_3S-0.6 4 days	10.18	19.94	44.53	26.91	15.71
C_3S-0.6 7 days	7.89	22.23	48.68	30.01	16.54
C_3S-0.6 14 days	7.59	22.53	49.91	30.41	17.12
C_3S-0.6 21 days	8.40	21.72	49.25	29.32	17.49
C_3S-0.6 28 days	6.23	23.85	50.15	32.25	15.46
C_3S-0.5 day zero	29.79	-	5,65	-	-
C_3S-0.5 1 day	17.15	12.64	38.64	17.16	15.83
C_3S-0.5 2 days	16.44	13.35	46.91	18.02	23.23
C_3S-0.5 4 days	16.15	13.64	46.59	18.41	22.52
C_3S-0.5 7 days	12.97	16.82	52.63	22.70	24.27
C_3S-0.5 14 days	12.06	17.73	54.80	23.93	25.21
C_3S-0.5 21 days	7.49	22.30	59.80	30.15	24.00
C_3S-0.5 28 days	5.60	24.19	60.32	32.65	27.62

The results of the carbonation reactions presented in tables 6.9, 6.10 and 6.11 are differing strongly and indicate a relationship of the sample preparation and geometry. The very low carbonation rate of $Ca(OH)_2$ can be attributed to an insufficient amount of moisture within the pellets. In addition the pressure for forming the pellets was probably too high, resulting in very dense samples. The C_3S samples investigated were hydrated with different amounts of water to simulate two different w/c values, and in different sample geometry (pellets vs. cylindrical block).

The data shows that the carbonation of $Ca(OH)_2$ is slower for the pellet samples. Additionally it can be seen, that the other phases (in case of C_3S corresponding C-S-H phases) are being carbonated from the very beginning, in parallel to the carbonation of $Ca(OH)_2$.

Hydrated C_3A and $C_2(AF)$ samples were also investigated under the same conditions at shorter time intervals. Both hydrated C_3A and $C_2(AF)$ pellets and cylinder blocks were stored under two Vol. % CO_2 concentrations and 65 % relative humidity at 20 °C for different time spans (1, 2, 4, 7, 14, 21 and 28 days). The results of the accelerated carbonation reactions are shown in table 6.12 and 6.14 for pellet samples and 6.13 cylindrical samples**.**

Table 6.12: Carbonation of hydrated C_3A pellets after different time spans.

Sample ID Pellet	hydrogarnet %	% $CaCO_3$	other crystalline phases
C_3A-0.5 day zero	100	-	-
C_3A-0.5 1day	94.33	5.63	hemicarboaluminate
C_3A-05 2 days	93.70	6.01	hemicarboaluminate
C3A-05 4 days	91.36	8.21	hemicarboaluminate
C3A-05 7 days	89.76	11.13	hemicarboaluminate calcite
C3A-0.5 14 days	89.32	10. 93	hemicarboaluminate calcite
C3A-0.5 21 days	83.04	14.07	hemicarboaluminate calcite
C3A-0.5 28 days	80.12	14.36	hemicarboaluminate calcite

In contrast to the investigations of the reaction products of carbonation after 28 days, the evaluation of samples taken after shorter time intervals shows the appearance of intermediate

carbonation products rather than different modifications of $CaCO_3$. Generally, hemicarboaluminate ($Ca_4Al_2(CO_3)_{0.5}(OH)_{13}\cdot 5.5H_2O$) and monocarboaluminate $Ca_4Al_2(CO_3)(OH)_{12}\cdot 5H_2O$) were observed. Both phases are metastable, over the time they react to $CaCO_3$ and $Al(OH)_3$ (see chapter 2.6.1, equation 2.19). For the pellets of C_3A, the X-ray powder patterns clearly show the existence of hemicarboaluminate next to unreacted hydrogarnet (figure 6.11). After 28 days, a small amount of calcite was observed, too.

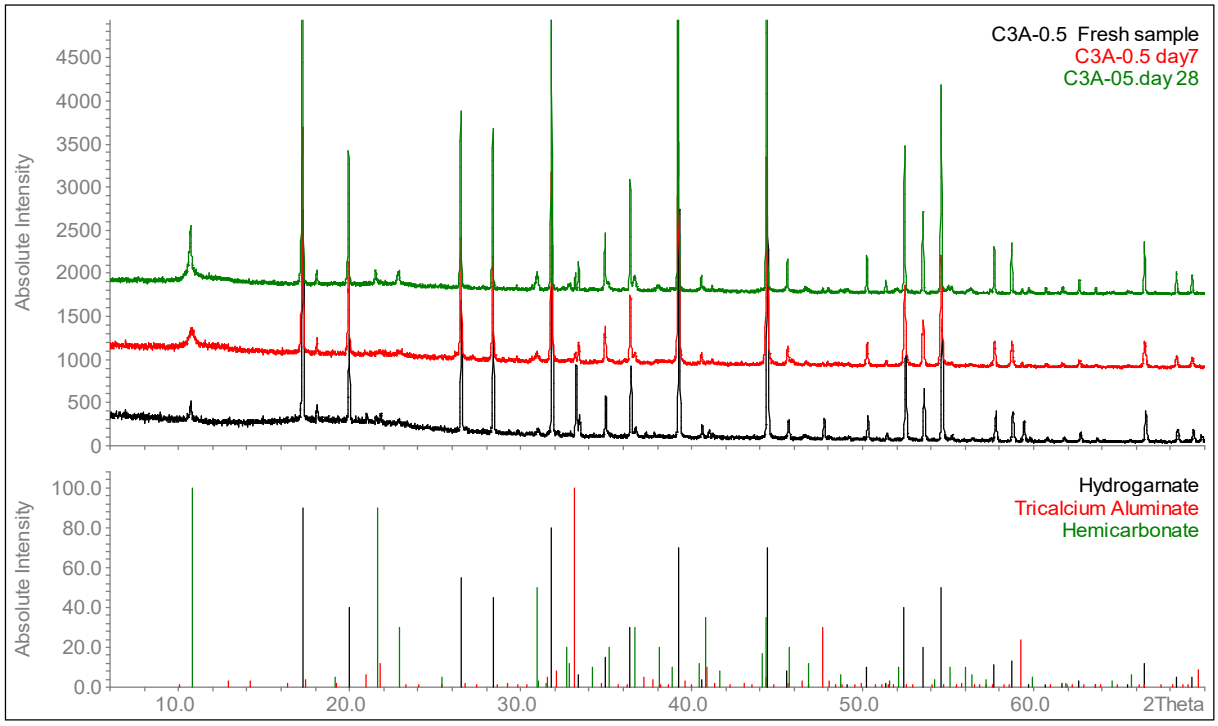

Figure 6.11: X-ray patterns of different C_3A samples (fresh pellet sample (black), after carbonation (red: 7 days, green: 28 days)); bottom pattern data from literature [113, 118, 119]

Table 6.13: Carbonation of hydrated C_3A samples (cylinder block) exposed to CO_2 at different time spans.

Sample ID	hydrogarnet %	% $CaCO_3$	other crystalline phases
C_3A-0.5 day zero	84.15	1.60	hemicarboaluminate
C_3A-0.5 1 day	50.83	35.67	vaterite calcite
C_3A-0.5 2 days	45.61	41.38	vaterite calcite
C_3A-0.5 4 days	38.56	47.79	vaterite calcite
C_3A-0.5 7 days	38.11	48.77	vaterite calcite

C_3A-0.5 14 days	39.74	47.94	vaterite calcite
C_3A-0.5 21 days	36.15	50.93	vaterite calcite
C_3A-0.5 28 days	35.13	52.85	vaterite calcite

The time-dependence of the carbonation reaction of cylindrical samples shows a gradual reaction via intermediate products (figure 6.12). It can be clearly seen that hemicarboaluminate is formed first. With longer reaction time the amount of hemicarboaluminate is decreasing and monocarboaluminate is formed. With the appearance of monocarboaluminate, reflections of calcite can be obtained as well. After 28 days only very small amounts of monocarboaluminate are left in the sample.

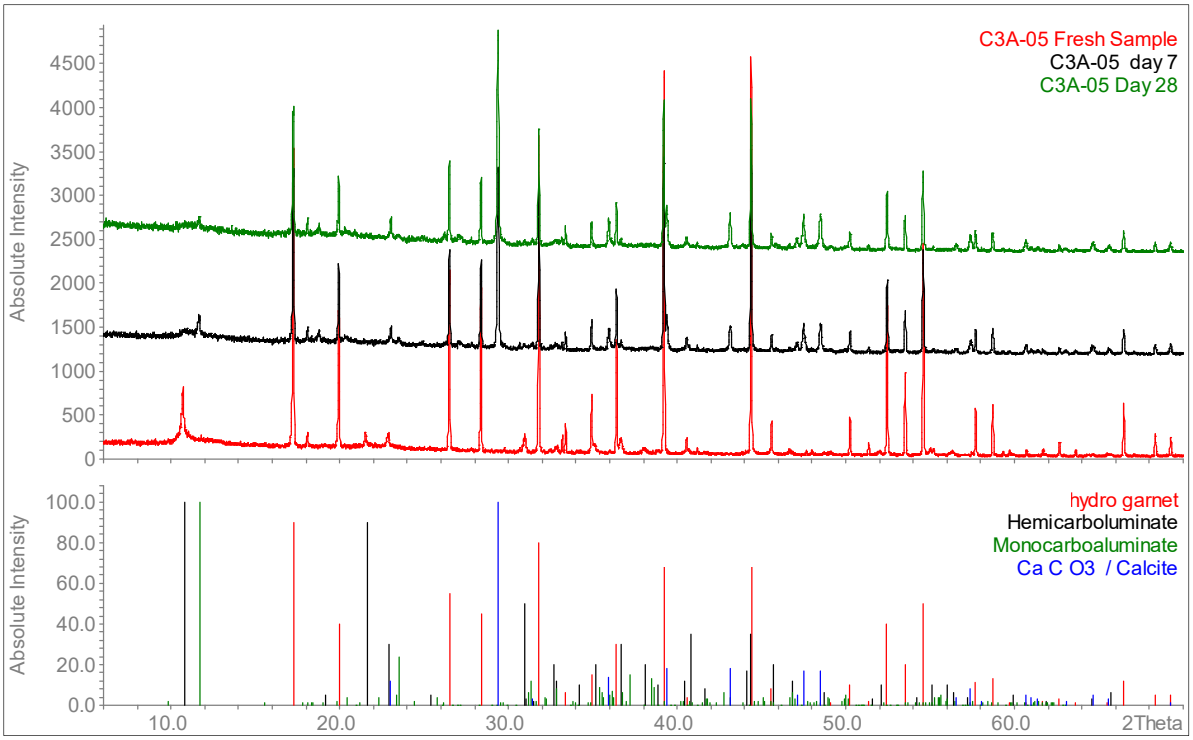

Figure 6.12: X-ray patterns of different C_3A samples (fresh pellet sample (red), after carbonation (black: 7 days, green: 28 days)); bottom pattern data from literature [111, 113, 118, 119]

Table 6.14 Carbonation of hydrated $C_2(AF)$ pellets at different time spans.

Sample ID	Hydrogarnet %	% $CaCO_3$	other crystalline phases
$C_2(AF)$ 0.5 day zero	88.28	5.28	unreacted $C_2(AF)$
$C_2(AF)$ 0.5 1 day	82.97	8.81	unreacted $C_2(AF)$
$C_2(AF)$ 0.5 2 days	80.97	9.12	unreacted $C_2(AF)$

C_2(AF) 0.5 4 days	79.16	8.94	unreacted C_2(AF)
C_2(AF) 0.5 7 days	81.16	8.28	unreacted C_2(AF)
C_2(AF) 0.5 14 days	81.13	8.39	unreacted C_2(AF)
C_2(AF) 0.5 21 days	80.97	9.39	unreacted C_2(AF)
C_2(AF) 0.5 28 days	78.52	12.35	unreacted C_2(AF) hemicarboaluminate

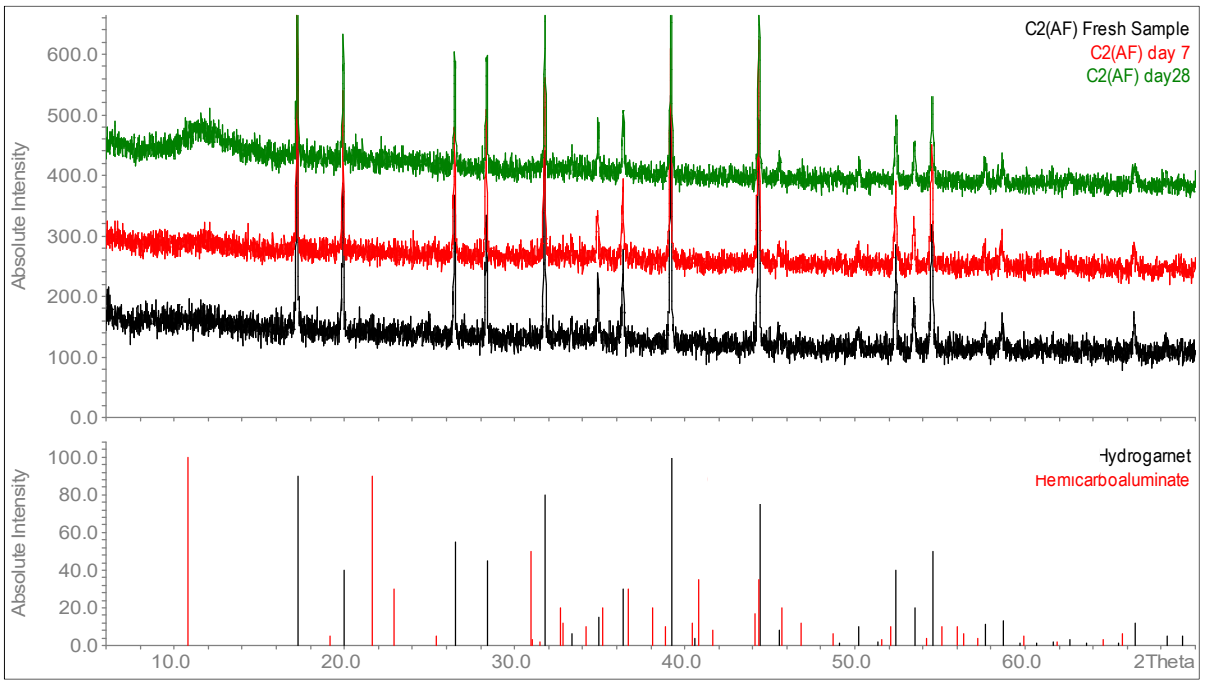

Figure 6.13: X-ray patterns of different C_2(A F) samples (fresh pellet sample (black), after carbonation (red:7 days, green: 28 days)); bottom pattern data from literature [118, 119].

In samples of C_2(AF) the formation of monocarboaluminate and hemicarboaluminate was not observed clearly. The formation of hemicarboaluminate starts in the later stages of the carbonation reaction. Different samples show the influence of the preparation and sample geometry.

6.2.4. Time-dependent carbonation of pure clinker phases in polystyrene cups

To further optimize the sample preparation and geometry eight one-gram portions of each clinker phase were filled into polystyrene cups (5ml). The samples were hydrated within these cups with w/c ratios of 0.4 and 0.5. After 28 days of hydration the small cups were placed inside the “carbobox”. After different time intervals (0, 1, 2, 4, 7, 14, 21 and 28 days) the content of one cup of each sample was ground completely in order to have homogeneous samples for the analyses.

The results of the time-dependent analysis of carbonation of C_2S and C_3S samples are shown in table 6.15 and 6.16. The amounts of $CaCO_3$ resulting from the carbonation of $Ca(OH)_2$ and C-S-H were calculated as described in chapter 6.2.3.

Table 6.15: Carbonation of hydrated C_3S in polystyrene cups after different time spans. The amounts of $Ca(OH)_2$ and $CaCO_3$ were determined by DTA/TGA.

Sample ID	$Ca(OH)_2$ %, DTA / TGA **A**	$Ca(OH)_2$, % reacted with CO_2 **B**	$CaCO_3$ %, DTA / TGA **C**	$CaCO_3$ % from carbonation of $Ca(OH)_2$ **D**	$CaCO_3$ % from carbonation of C-S-H **E**
C_3S-0.4 day zero	33.1	-	5.73	-	-
C_3S-0.4 1 day	15.32	17.78	38.65	29.87	3.05
C_3S-0.4 2 days	11.31	21.79	42.83	36.61	0.49
C_3S-0.4 4 days	9.37	23.73	49.22	39.87	3.60
C_3S-0.4 7 days	9.15	23.95	48.13	40.24	2.16
C_3S-0.4 14 days	9.36	23.74	49.57	39.88	3.96
C_3S-0.4 21 days	8.35	24.75	58.19	41.58	10.88
C_3S-0.4 28 days	7.01	26.09	60.12	43.83	10.56
C_3S-0.5 day zero	32.1	-	4.65	-	-
C_3S-0.5 1day	16.22	15.88	36.24	26.68	4.91
C_3S-0.5- 2 days	11.31	20.79	43.91	34.93	4.33
C_3S-0.5 4 days	9.42	22.68	47.93	38.10	5.18
C_3S-0.5 7 days	9.46	22.64	50.63	38.04	7.94
C_3S-0.5 14 days	9.62	22.48	56,96	37.77	14,54
C3S-0.5 21 days	8.35	23.75	59.83	39.90	15.28
C3S-0.5 28 days	7.25	24.85	63.32	41.75	16.92

Table 6.16: Carbonation of hydrated C_2S in polystyrene cups after different time spans. The amounts of $Ca(OH)_2$ and $CaCO_3$ were determined by DTA/TGA.

Sample ID	$Ca(OH)_2$ %, DTA / TGA **A**	$Ca(OH)_2$, % reacted with CO_2 **B**	$CaCO_3$ %, DTA / TGA **C**	$CaCO_3$ % from carbonation of $Ca(OH)_2$ **D**	$CaCO_3$ % from carbonation of C-S-H **E**
C_2S-0.4 day zero	17.62	-	1.87	-	-
C_2S-0.4 1 day	11.31	6.31	16.36	10.60	2.56
C_2S-0.4 2 days	8.36	9.26	32.60	15.56	13.84
C_2S-0.4 4 days	10. 36	7.26	33.90	12.20	18.50
C_2S-0.4 7 days	11.86	5.76	26.23	9.68	13.35
C_2S-0.4 14 days	8.51	9.11	42.38	15.30	23.88
C_2S-0.4 21 days	6.03	11.59	53.06	19.47	30.39
C_2S-0.4 28 days	5.45	12.17	56.13	20.45	32.48
C_2S-0.5 day zero	18.06	-	3.21	-	-
C_2S-0.5 1 day	12.3	5.76	21. 5	9.68	8.62
C_2S-0.5 2 days	11.5	6.56	24.3	11.02	10.08
C_2S-0.5 4 days	9.3	8.76	27.3	14.72	9.38
C_2S-0.5 7 days	10.13	7.93	25.99	13.32	9.47
C_2S-0.5 14 days	8.14	9.92	52.51	16.67	32.64
C_2S-0.5 21 days	6.45	11.61	54.65	19.50	31.95
C_2S-0.5 28 days	3.25	14.81	56.98	24.88	28.90

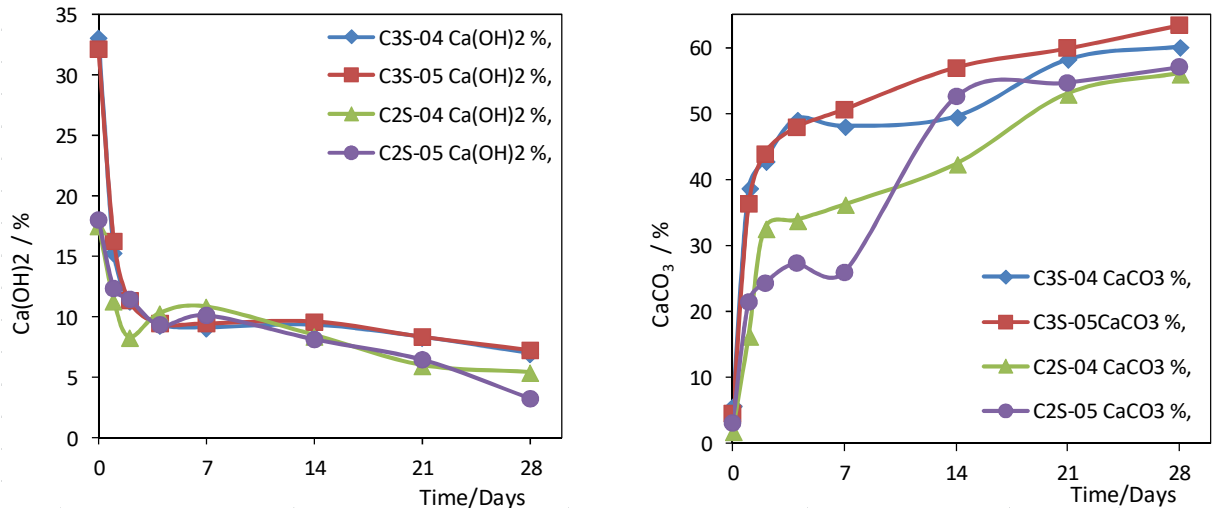

Figure 6.14: Changing content of $Ca(OH)_2$ (left) and $CaCO_3$ (right) in samples of C_3S and C_2S versus time.

Figure 6.14 comprises the data from the tables 6.15 and 6.16. It can be seen that after a fast carbonation reaction at the beginning the speed of carbonation decreases significantly. This can be attributed to a carbonation front decelerating the diffusion of CO_2. After 28 days of carbonation the total amounts of $CaCO_3$ in the hydrated samples of C_2S and C_3S are close to each other. In both samples carbonation of $Ca(OH)_2$ is faster at the beginning as seen in figure 6.15.

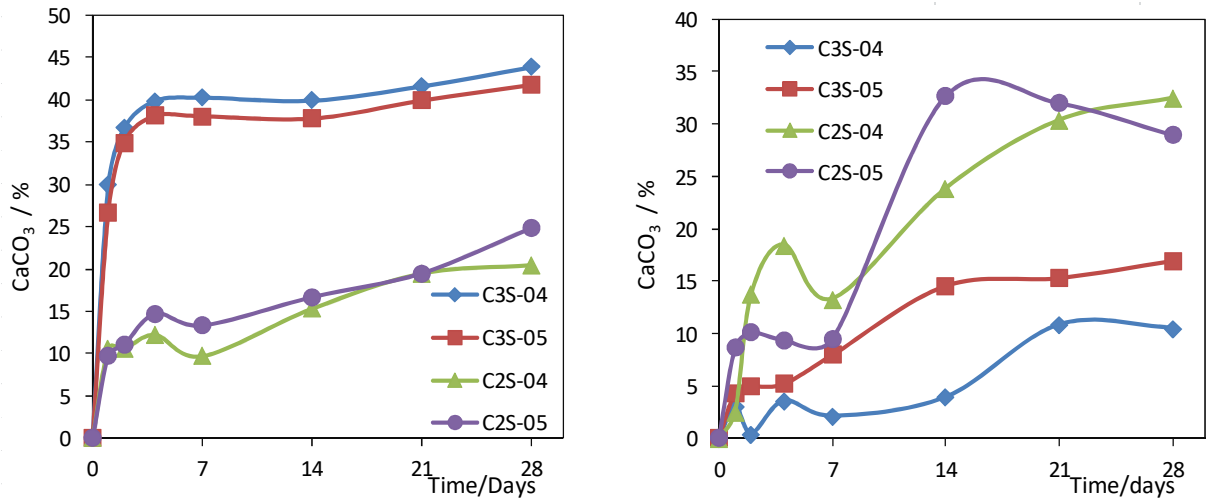

Figure 6.15: $CaCO_3$ content from $Ca(OH)_2$ (left) and $CaCO_3$ content from C-S-H (right) in hydrated samples of C_3S and C_2S in polystyrene cups versus time.

Figures 6.14 and 6.15 also show that the carbonation of $Ca(OH)_2$ and C-S-H occur simultaneously. The amount of $CaCO_3$ formed from carbonation of the C-S-H phases increases day by day. This was observed for samples of C_3S and C_2S, but showed more significantly in carbonated samples of C_2S. At the end of the carbonation process of C_2S, the

amount of $CaCO_3$ formed from carbonation of the C-S-H phases exceeded the amount of $CaCO_3$ formed from carbonation of $Ca(OH)_2$. For the C_3S samples the ratio was reversed, here the amounts of $CaCO_3$ formed from carbonation of $Ca(OH)_2$ were higher than those from carbonation of the C-S-H phases. The carbonation of C_3A and $C_2(AF)$ was also investigated. The results of the analysis of the time-dependence of the carbonation process of C_3A and $C_2(AF)$ are shown in table 6.17 and 6.18.

Table 6.17: Carbonation of hydrated C_3A in polystyrene cups after different time spans.

Sample ID	hydrogarnet %	$CaCO_3$ %,	other crystalline phases
C_3A-0.4 day zero	92.83	2.97	unreacted C_3A hemicarboaluminate
C_3A-0.4 1 day	91.22	7.67	unreacted C_3A hemicarboaluminate
C_3A-0.4 2 days	89.16	7.62	unreacted C_3A hemicarboaluminate
C_3A-0.4 4 days	89.16	6.98	unreacted C_3A hemicarboaluminate mayenite ($Ca_{12}Al_{14}O_{33}$)
C_3A-0.4 7 days	91.2	8.77	unreacted C_3A hemicarboaluminate mayenite
C_3A-0.4 14 days	85.93	13.62	hemicarboaluminate vaterite mayenite
C3A-0.4 21 days	83.21	15.09	unreacted C_3A hemicarboaluminate vaterite calcite mayenite
C_3A-0.4 28 days	85.15	14.75	hemicarboaluminate vaterite calcite mayenite

C_3A-0.5 day zero	90.22	3.65	unreacted C_3A hemicarboaluminate
C_3A-0.5 1 day	88.88	11.32	hemicarboaluminate mayenite vaterite
C_3A-05 2 days	81.25	15.31	hemicarboaluminate mayenite vaterite calcit
C_3A-0.5 4 days	80.87	13.68	hemicarboaluminate mayenite vaterite calcite
C_3A-05 7 days	80.15	14.18	hemicarboaluminate mayenite vaterite calcite
C_3A-0.5 14 days	76.32	21.67	hemicarboaluminate mayenite vaterite calcite
C_3A-0.5 21 days	73.36	22.41	hemicarboaluminate mayenite vaterite calcite
C_3A-0.5 28 days	65.32	29.85	hemicarboaluminate mayenite vaterite calcite

During the carbonation of C_3A (pellet and cylindrical samples), hemicarboaluminate was observed as a metastable carbonate-containing phase. However, no transformation to monocarboaluminate was observed. Reflections of hemicarboaluminate, vaterite, and calcite occur at the same time. The carbonation of the C_3A samples seemed relatively slow. This could be attributed to the formation of a dense carbonation front on the surface of the

specimen. The X-ray powder patterns of C_3A samples with a w/c ratio of 0.4 are shown in figure 6.16.

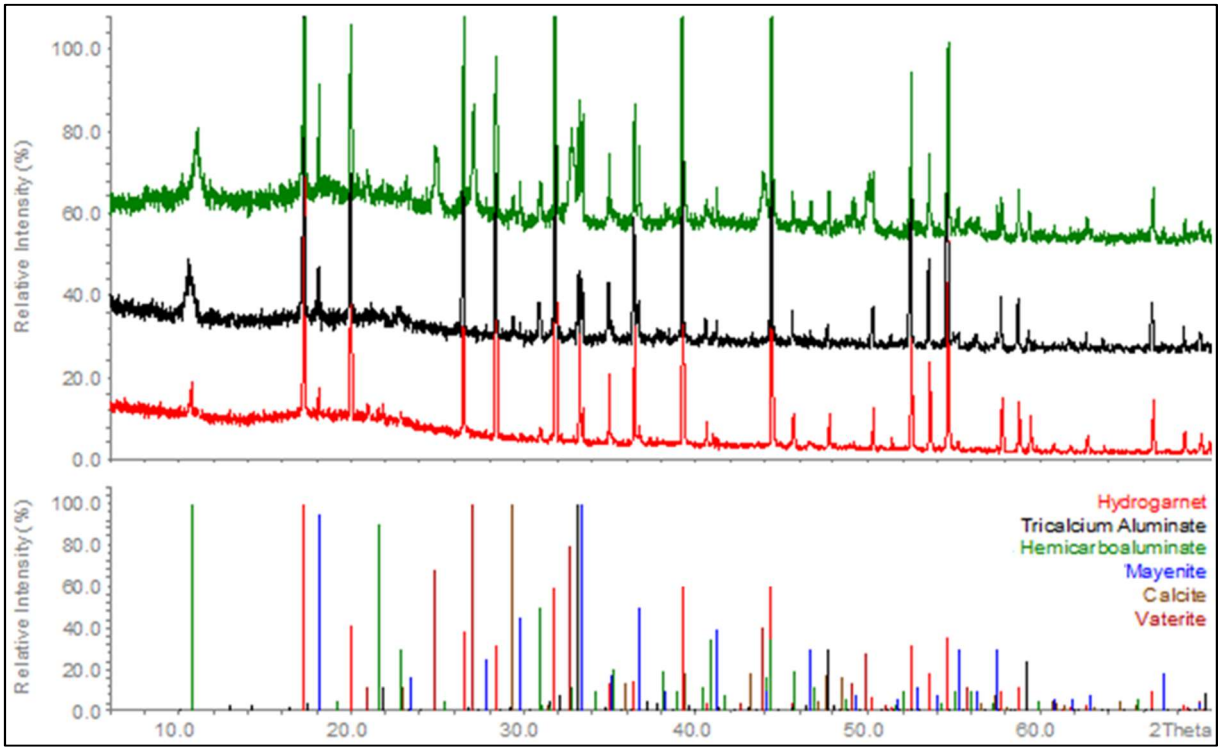

Figure 6.16: X-ray patterns of different C_3A samples (fresh pellet sample (black), after carbonation (red: 7 days, green: 28 days); ; bottom pattern data from literature [110, 111, 113, 118 – 121]

The time dependent carbonation of samples of $C_2(AF)$ shows the same trend as that of C_3A. Reflections of the metastable hemicarboaluminate were also detected in $C_2(AF)$ samples, but no transformation to monocarboaluminate was observed. The intensities of the reflections of hemicarboaluminate decrease slowly at the same time as intensities of reflections of vaterite and calcite increase. The compositions of the samples are shown in table 6.18.

Table 6.18: Carbonation of hydrated $C_2(AF)$ in polystyrene cups at different time spans.

Sample ID	hydrogarnet % DTA/TGA	$CaCO_3$ % DTA/TGA	other crystalline phases
$C_2(AF)$-0.4 day zero	94.68	-	unreacted $C_2(AF)$
$C_2(AF)$-0.4 1day	86.45	9.60	hemicarboaluminate unreacted $C_2(AF)$
$C_2(AF)$-0.4 2 days	81.36	15.30	hemicarboaluminate unreacted $C_2(AF)$ vaterite

C_2(AF)-0.4 4 days	82.45	13.68	hemicarboaluminate unreacted C_2(AF) vaterite
C_2(AF)-0.4 7 days	80.25	14.18	hemicarboaluminate unreacted C_2(AF) vaterite calcite
C_2(AF)-0.4 14 days	75.23	21.67	unreacted C_2(AF) vaterite calcite
C_2(AF)-0.4 21 days	69.61	22.41	unreacted C_2(AF) vaterite calcite
C_2(AF)-0.4 28 days	64.25	29.85	unreacted C_2(AF) vaterite calcite
C_2(AF) -0.5 day zero	93.70	6.70	hemicarboaluminate unreacted C_2(AF)
C_2(AF)-0.5 1day	86.45	10.32	hemicarboaluminate unreacted C_2(AF)
C_2(AF)-0.5 2 days	81.36	14.30	hemicarboaluminate unreacted C_2(AF)
C_2(AF)-0.5 4 days	80.45	16.68	unreacted C_2(AF) vaterite calcite
C_2(AF)-0.5 7 days	80.14	15.18	unreacted C_2(AF) calcite
C_2(AF)-0.5 14 days	65.23	22.67	unreacted C_2(AF) vaterite calcite
C_2(AF)-0.5 21 days	59.51	26.41	unreacted C_2(AF) vaterite calcite
C_2(AF)-0.5 28 days	50.25	39.85	unreacted C_2(AF) calcite

The time-dependent carbonation of samples of ettringite was also investigated. Ettringite decomposes during carbonation. The decomposition of ettringite can be traced in figure 6.17.

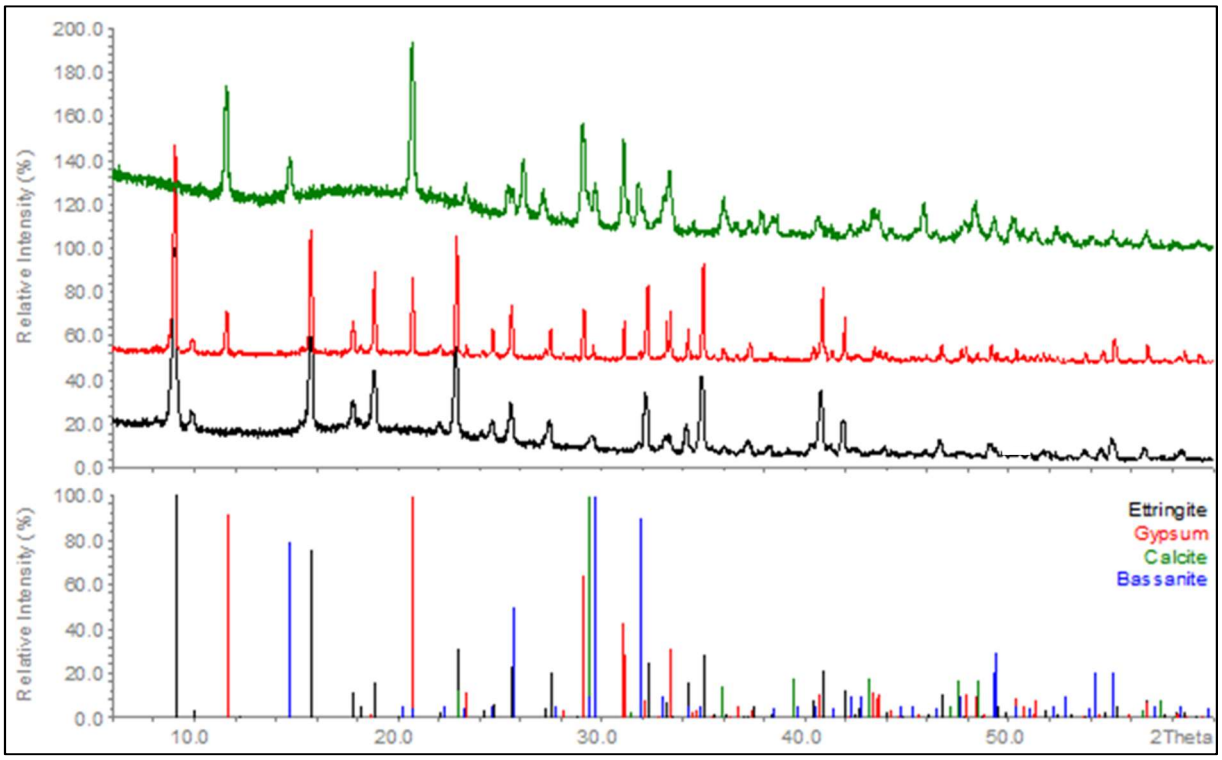

Figure 6.17: X-ray patterns of different ettringite samples (fresh pellet sample (black), after carbonation (red: 7 days, green: 28 days); bottom pattern data from literature [108, 111, 117, 122]

Reflections of calcite and gypsum appear at the same time. With the formation of calcite, ettringite decomposes to sulphate-containing compounds such as gypsum and basanite. After 28 days of accelerated carbonation the reflections of ettringite disappeared.

6.2.5. Time-dependent carbonation of a model cement

To transfer the results from the sample phases to a real system, a model cement was prepared and investigated. The components of the model cement were mixed and filled into small polystyrene cups and mixed with water to reach a w/c value of 0.5. Then, the samples were hydrated for 28 days. Time-dependent carbonation reactions were carried out as described in chapter 6.2.

Table 6.19: Carbonation of a hydrated model cement with w/c ratios of 0.5 at different time spans. The amounts of $Ca(OH)_2$ and $CaCO_3$ were determined by DTA/TGA.

Sample ID Pellet	$Ca(OH)_2$ %	$Ca(OH)_2$ % reacted with CO_2	$CaCO_3$ %	$CaCO_3$ % from carbonation of $Ca(OH)_2$	$CaCO_3$ % from carbonation of others
model cement day zero	32.37	-	-	-	-
model cement 1 day	30.46	1.91	8.69	3.21	5.48
model cement 2 days	29.88	2.49	15.96	4.18	11.78
model cement 4 days	24.35	8.02	25.12	13.47	11.65
model cement 7 days	23.13	9.24	26.33	15.52	10.81
model cement 14 days	22.36	10.01	27.42	16.82	10.60
model cement 21 days	21.41	10.96	33.85	18.41	15.44
model cement 28 days	20.58	11.79	34.93	19.81	15.12

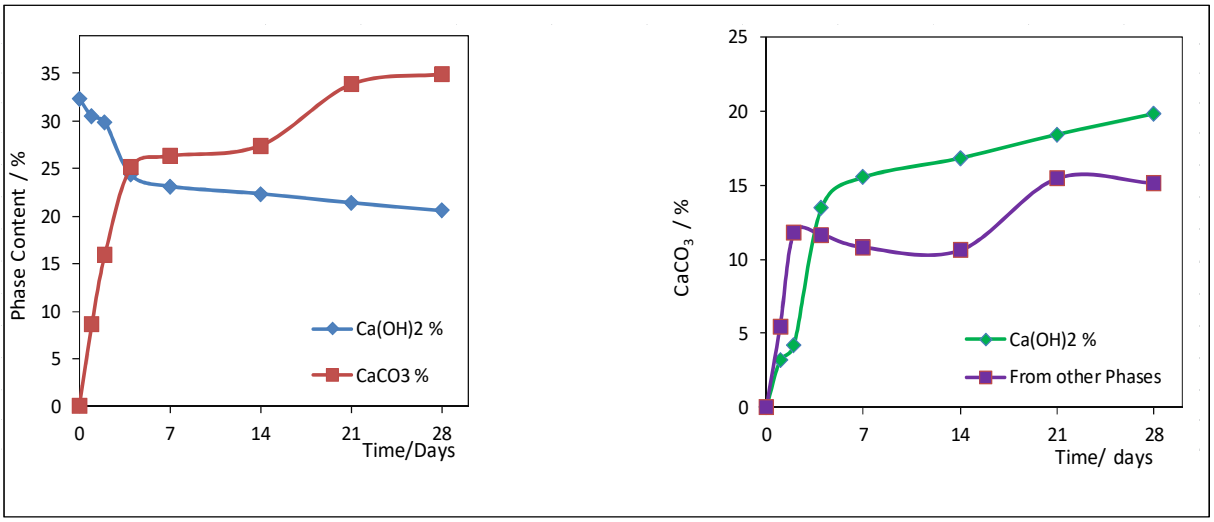

Figure 6.18, left: Amount of $CaCO_3$ (red), $Ca(OH)_2$ (blue). **Right:** $CaCO_3$ from carbonation of $Ca(OH)_2$ (green), and $CaCO_3$ formed from other phases (purple) in the model cement hydrated in polystyrene cups versus time.

The trend seen for the carbonation of a model cement seems similar compared to the carbonation of pure clinker phases. The carbonation reactions of $Ca(OH)_2$ and other phases take place simultaneously, which can be seen in figure 6.19.

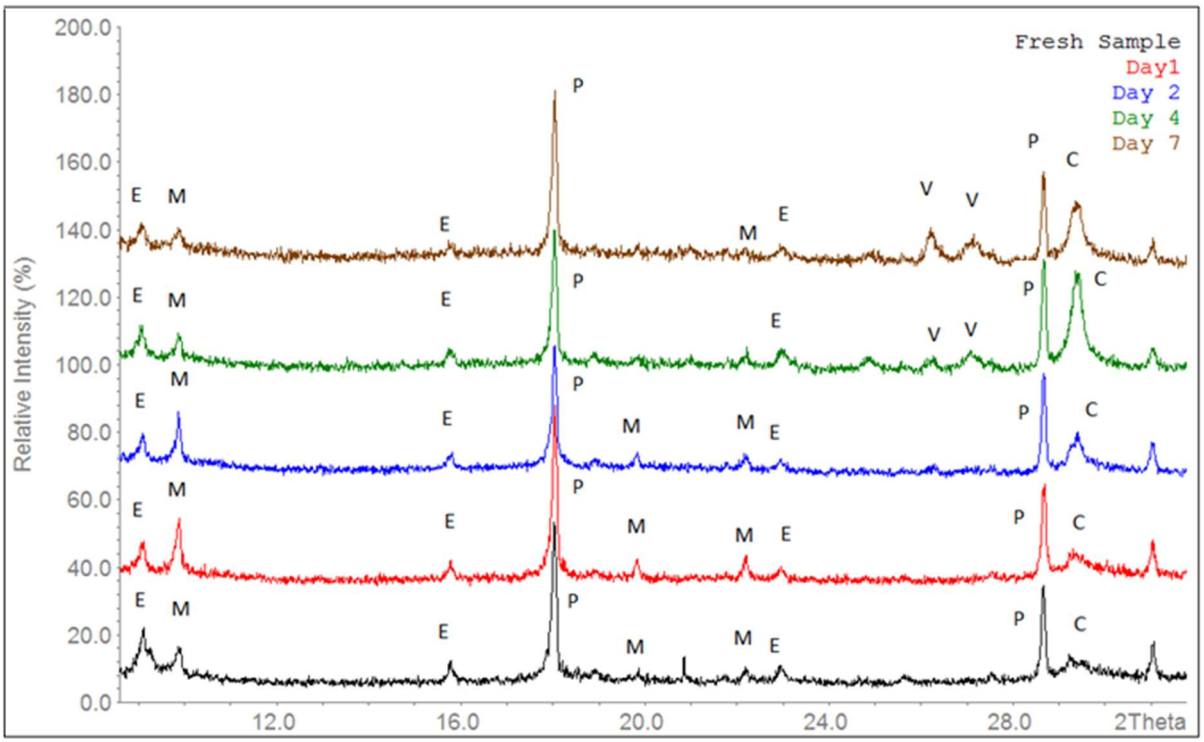

Figure 6.19: X-ray powder patterns of the phases appearing during carbonation of a model cement after different time spans (black curve: fresh sample, red: after one day, blue: after two days, green: after few days, brown: after one week of carbonation; P: portlandite, E: ettringite, M: monocarboaluminate, C: calcite, V: vaterite)

X-ray powder patterns of a hydrated model cement show reflections of portlandite, ettringite, monocarboaluminate and calcite (figure 6.19). At the beginning, the intensities of the reflections of ettringite are higher than those of monocarboaluminate. Then, the intensities of the reflections of monocarboaluminate increase. On the second day of carbonation they become higher in intensity than the reflections of ettringite. The intensities of the reflections of portlandite do not change after one day of carbonation. After the second day, the reflections of calcite are increasing. From the fourth day on reflections of vaterite appear. At the same time, the reflections of monocarboaluminate and ettringite decrease.

These results lead to the following assumption: the early stages of the carbonation process are directly related to SO_4^{2-}-and CO_3^{2-}-containing compounds. This is in accordance with literature [11, 12]. The changes in the reflections of ettringite and monocarboaluminate support this. After an increasing amount of $CaCO_3$ in the form of calcite and vaterite is formed, the intensities of the reflections of ettringite and monocarboaluminate decrease. This may be due to a decrease in pH values.

6.3. Comparison of the carbonated samples and discussion

To compare and simulate the carbonation behavior of concretes, different methods of sample preparation and different geometries of samples were investigated. To allow for a the direct comparison with cement, pastes from commercial cement the clinker powders were mixed with water and filled in plastic tubes for hydration. After 28 days of hydration, they were carbonated for 28 days. The results are plotted in the diagram 6.20.

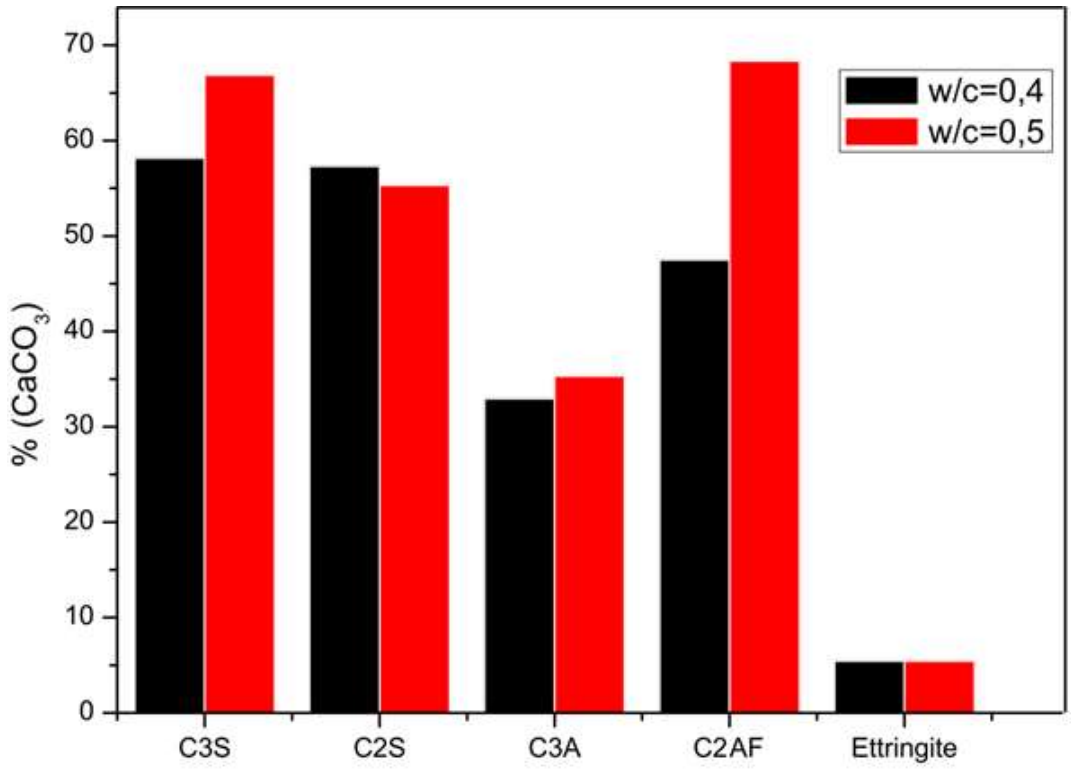

Figure 6.20: Total amount of $CaCO_3$ after hydration and 28 days of carbonation of the individual clinker phases and ettringite with w/c values of 0.4 and 0.5.

The results show that all hydrated clinker phases are carbonated. The carbonation rates of C_3S and C_2S are close to each other. They were affected most from the carbonation. The carbonation of C_3A and $C_2(AF)$ varies strongly from each other. The carbonation rate of $C_2(AF)$ is higher than C_3A . The $C_2(AF)$ sample with a w/c ratio of 0.5 shows the highest carbonation rate of all samples prepared.

When the results of the time dependent carbonation of samples in polystyrene cups are compared, the carbonation rates of C_3S and C_2S are also higher than of the other phases. The carbonation rates of C_3A and $C_2(AF)$ are close to each other with the carbonation rate of $C_2(AF)$ being slightly higher. The carbonate formation in ettringite results in a decomposition. The results for samples with a w/c ratio of 0.4 are shown in figure 6.21.

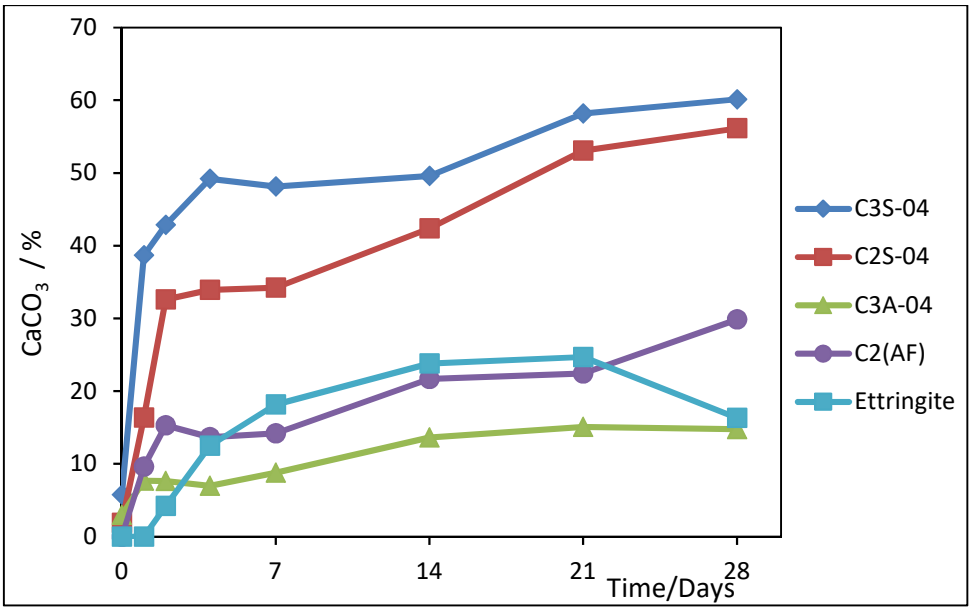

Figure 6.21: Amount of $CaCO_3$ after hydration and carbonation of individual clinker phases and ettringite (w/c: 0.4).

The carbonation rates of the samples with a w/c ratio of 0.5 prepared in polystyrene cups are higher for all of the hydrated clinker phases compared to the samples with a w/c ratio of 0.4. The trends seen for the carbonation reactions of these samples are similar. In addition, samples of the model cement show the same behavior. The formations of the $CaCO_3$ in model cement is lower than in C_3S and C_2S, and close to the individual samples of C_3A and $C_2(AF)$. The results are shown in figure 6.22.

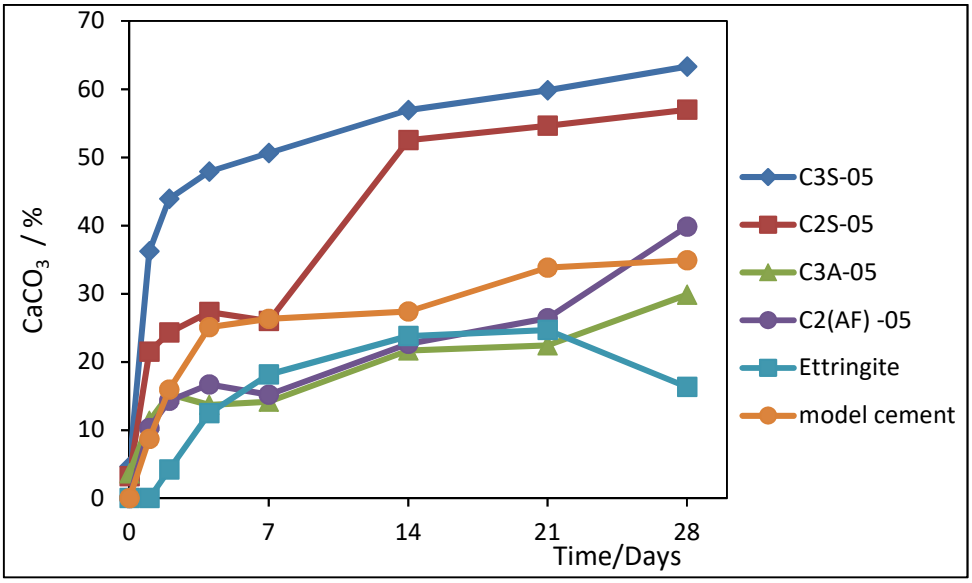

Figure 6.22: Amount of $CaCO_3$ during the carbonation of hydrated single clinker phases and ettringite and model cement (w/c: 0.5)

6.4. First attempt to time-dependent in-situ investigations

For further investigations, in-situ high-resolution synchrotron X-ray diffraction experiments (SyXRD) were performed to analyze the carbonation of cement pastes and clinker phases at the European Synchrotron Facility (ESRF) in Grenoble, France. From the time-resolved in-situ synchrotron investigations a deeper insight into the structural changes during the carbonation of C-S-H phases were expected. For that reason first orienting analyses of a hydrated C_3S sample and two cement mixtures (Z1-05 and Z81-04) were undertaken.

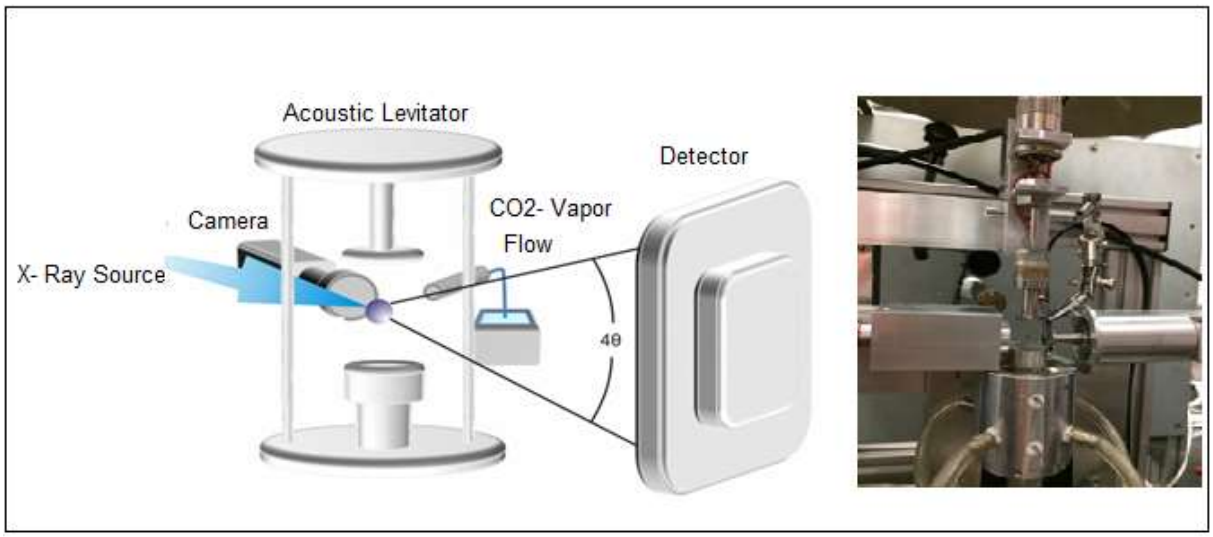

Figure 6.23: Experimental setup for contact-free carbonation using an ultrasonic trap at beamline ID 31, ESRF on a high-resolution synchrotron (λ = 0.20664032 Å) [124].

The in-situ experiments were performed using an ultrasonic trap in order to levitate small sample pellets (2.5- 3.5 mg). The measurements were carried out under a continuous flow of a mixture of water vapor and CO_2 to obtain sufficient humidity and CO_2 concentration for the carbonation reaction. The individual samples were investigated for six to eight hours with about 55 scans per hour.

The synchrotron data of C_3S-0.5, Z1- 0.5 and Z81-0.40 are shown in figures 6.24, 6.25 and 6.26. For all three samples the intensities of the main reflections did not change during the measurements under H_2O / CO_2 stream.

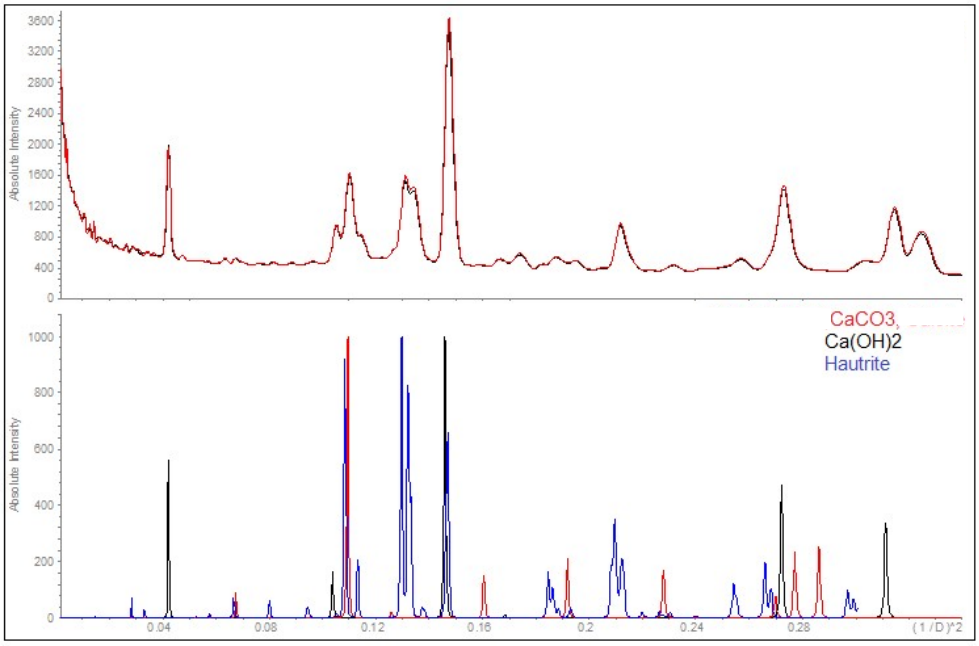

Figure 6.24: Synchrotron X-ray diffraction patterns of C_3S-0.5, black; first measurement, red: 239th measurement, underneath theoretical patterns from literature [118].

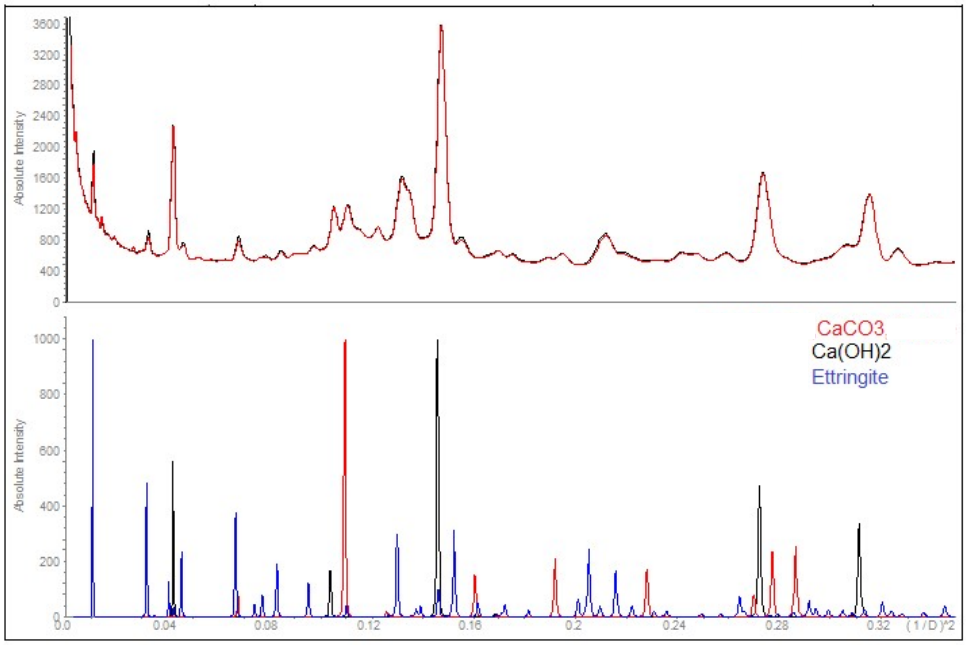

Figure 6.25: Synchrotron X-ray diffraction patterns of Z1-0.5, black; first measurement, red: 253rd measurement, underneath theoretical patterns from literature [118].

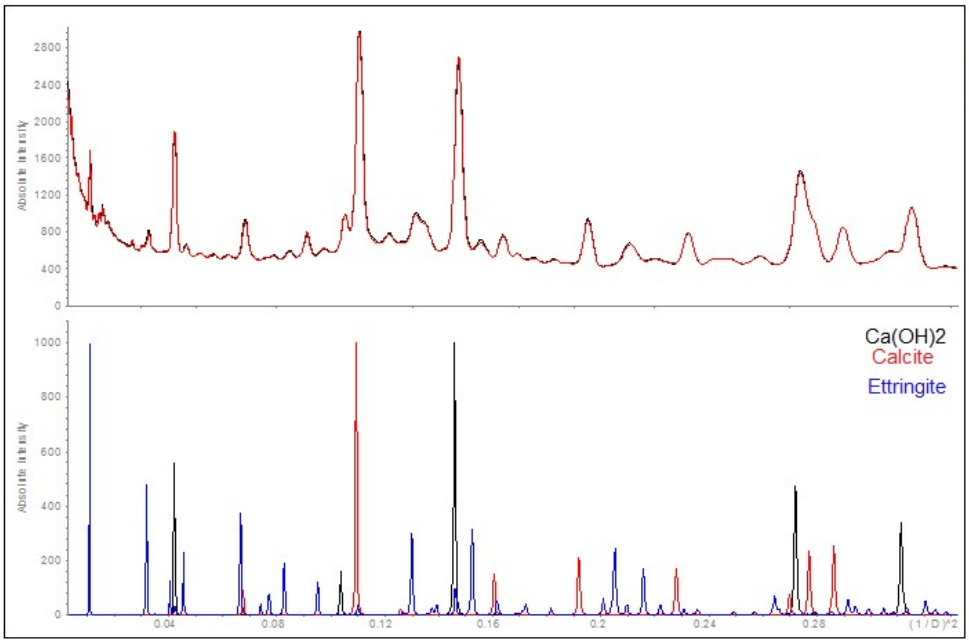

Figure 6.26: Synchrotron X-ray diffraction patterns of Z81-0.4, black; first measurement, red: 389th measurement, underneath theoretical patterns from literature [118].

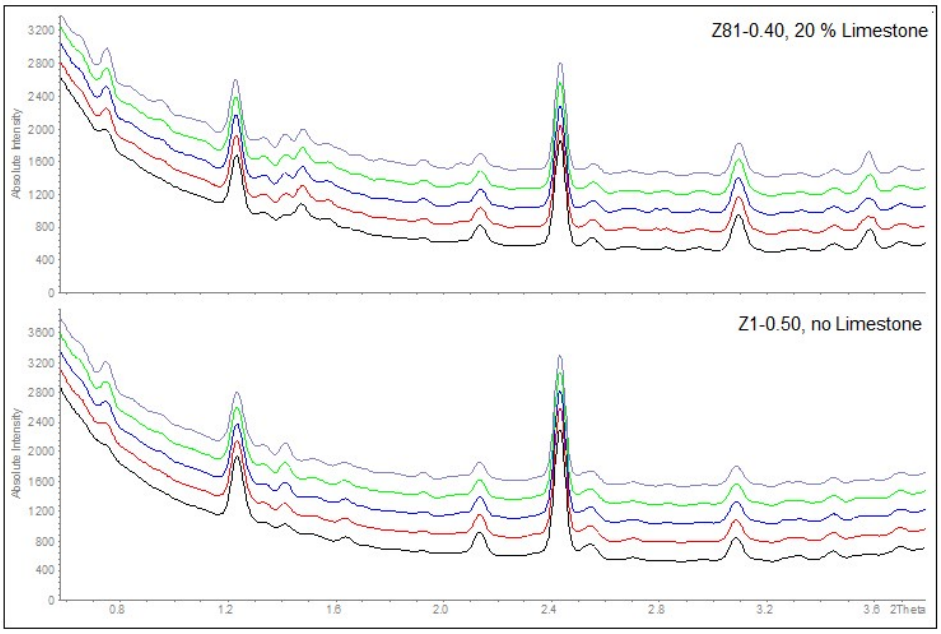

Figure 6.27: Synchrotron X-ray diffraction patterns of Z1 -0.5 and Z81-0.4, black; first measurement, violet: last measurement, underneath theoretical patterns from literature [118]

In the small-angle regions of the diffractograms (figure 6.27) significant intensity variations of the small reflections that are attributed to various C-S-H phases can be recognized. This qualitative view supports our previous findings that the C-S-H phases do react with CO_2 from the very beginning. A sequential carbonation where $Ca(OH)_2$ alone reacts first seems unlikely. In the future time-resolved pair-distribution function (PDF) analyses should be done to understand the carbonation reaction of the C-S-H phases in more detail.

7. CONCLUSIONS

The experimental findings described in this work confirm that new eco-friendly clinker-reduced cements can be designed so that their corrosion resistances resembles to that of conventional cements. It is shown that the water/cement- ratios have to be adjusted to achieve carbonation depths that are similar to the established materials.

In this work, cement pastes made from commercial cement, limestone and water were compared to pure single clinker samples that were laboratory-synthesized. For each cement paste three prismatic samples were prepared and accelerated carbonation was performed in a "carbobox" The carbonation depths were determined by the phenolphthalein test. The samples were characterized before and after carbonation by thermal analysis and X-ray powder diffraction.

Generally a reduction of cement is connected to a reduction of hydration products like portlandite, which is considered to be the most important phase in terms of carbonation reactions. On the first sight, the experiments performed here show lower carbonation resistances than samples from pure Portland cement. However, from the investigations it can be concluded, that the carbonation reactions do not depend directly on the amount of $Ca(OH)_2$ initially formed. The results show that the carbonation depths depend more on the w/c ratio than on the initial amount of $Ca(OH)_2$. This means that eco-friendly cements with high amounts of limestone addition can show similar carbonation resistances compared to commercial cements as long as the w/c-ratios are adjusted.

During the carbonation reactions the formation of different modifications of $CaCO_3$, calcite vaterite and aragonite were observed. The main carbonation products are calcite and vaterite. Aragonite was only found in samples with high additions of limestone. In the course of this investigation it was found that the phenolphthalein test gives an estimate of the carbonation depths that is too rough. Therefore, the results from phenolphthalein tests must be supported and checked with other methods such as DTA/TGA and X-ray powder diffraction.

The main clinker phases Ca_3SiO_5 (C_3S), Ca_2SiO_4 (C_2S), $Ca_3Al_2O_6$ (C_3A), $Ca_2(Al,Fe)O_5$ (C_2AF) and ettringite were synthesized and investigated individually to understand the carbonation of concrete in more detail. Different sample preparations and geometries were applied for the individual clinker phases (cylindrical block, pellets and small cups). The samples in small cups gave the most reasonable results. The hydration of pure clinker phases resulted in the observation of the products: $Ca(OH)_2$ and C-S-H phases from C_3S, C_2S as well

as hydrogarnet ($Ca_3(Al,Fe)_2(OH)_{12}$) from the hydration of C_2AF and C_3A. It was shown that all of the hydrated clinker phases are carbonated. The main carbonation products of clinker phases were calcite and vaterite after 28 days of carbonation. Aragonite was found as a minor phase in some of the samples. For pure clinker phases the carbonation rates mainly depend on the w/c ratio. For the hydrated clinker phases, the samples with a w/c ratio of 0.5 showed the highest carbonation rates. These investigations showed that the hydration and carbonation of single-phase samples yield reaction products comparable to the cement pastes.

The complex nature of cement pastes result in X-ray powder patterns with numerous overlapping reflections making it difficult to detect small amounts of intermediate phases. Here, the investigations of the time-dependent carbonation reactions of the pure clinker phase allowed the observation of intermediate appearing phases in the course of the studied span of time. This was for example observed for the intermediate carbonates (hemicarboaluminate ($Ca_4Al_2(CO_3)_{0.5}(OH)_{13}\cdot 5.5H_2O$) and monocarboaluminate $Ca_4Al_2(CO_3)(OH)_{12}\cdot 5H_2O$)) during the carbonation of hydrated C_2AF and C_3A.

It was also shown that ettringite decomposes to sulphate-containing compounds such as gypsum and bassanite which react to calcite in the course of the carbonation reactions.

The investigation of the pure clinker phases showed that after 28 days of carbonation the total amounts of $CaCO_3$ in the hydrated samples of C_2S and C_3S are similar to each other. For both phases it is clearly seen from the time-dependent investigations that the carbonation of $Ca(OH)_2$ and C-S-H occur simultaneously. The formation of $CaCO_3$ from $Ca(OH)_2$ is fast only at very early stages of the carbonation reaction. After a few days the carbonation rates of C-S-H phases are similar to $Ca(OH)_2$. At the end of the carbonation process of hydrated C_2S, the amount of $CaCO_3$ formed from the C-S-H phases exceeded the amount of $CaCO_3$ formed from of $Ca(OH)_2$. For C_3S the ratio was reversed, here the amounts of $CaCO_3$ formed from of $Ca(OH)_2$ were higher than those from of the C-S-H phases. The model cement samples showed a similar behavior. The detailed investigations presented here unambiguously show the simultaneous carbonation of $Ca(OH)_2$ and C-S-H. Before, simultaneous carbonation was discussed controversially among experts. Often, a gradual carbonation was considered instead with C-S-H phases being carbonated only after all of the $Ca(OH)_2$ was fully transformed to $CaCO_3$. Especially, studies based on theoretical simulations came to this conclusion. Furthermore the time-dependent carbonation reactions for the most important hydrated clinker phases were investigated under the same conditions and compared to each other for the first time. The results show different behaviors for the individual phases, something not

investigated and described in detail before. The findings of this work are important for further research and should be taken into account especially in the future for the theoretical investigations.

8. APPENDIX

Table 1: Thermal analysis data of 28 days cured cement pastes.

Sample ID	Starting mass, mg	Mass at 550 °C	Residual Mass, mg	Loss Chemical Water, mg	Loss of CO_2, mg
Z1-0. 6	25.95	17.83	16.59	1.08	0.52
Z1-0.5	28.57	21.21	19.23	1.23	0.55
Z2-0.5	28.76	20.32	19.42	1.19	0.55
Z3-0.5	27.57	20.68	18.87	1.13	0.15
Z1-0.4	17.60	12.94	12.58	0.62	0.31
Z80-0.4	17.56	12.65	11.75	0.54	0.70
Z81-0.4	26.35	18.69	17.73	0.69	1.21
Z82-0.4	14.55	11.74	9.14	0.39	1.43
Z84-0.4	15.04	11.42	9.47	0.26	1.93
Z92-0.4	12.55	9.43	7.95	0.32	1.34
Z83-0.35	25.64	21.53	17.04	0.66	2.86
Z84-0.35	29.86	23.91	19.83	0.58	3.32
Z84-0.30	29.93	24.71	17.12	0.55	3.80

Table 2: Thermal analysis data of 28 days cured cement pastes after 28 days of accelerated carbonation.

Sample ID	Starting mass, mg	Mass at 550 °C	Residual Mass, mg	Loss Chemical Water, mg	Loss of CO_2, mg
Z1-0.6	27.63	24.51	16.99	0.00	6.14
Z1-0.5	13.35	10.24	8.49	0.00	2.39
Z1-0.5	25.65	19.42	19.01	0.96	0.63
Z2-0.5	29.91	26.13	19.15	0.20	5.87
Z3-0.5	29.61	24.38	19.08	0.30	5.82
Z1-0.4	12.47	11.42	8.74	0.34	1.03
Z80-0.4	11.59	9.66	8.20	0.12	1.49
Z81-0.4	12.15	10.92	8.05	0.00	2.54
Z82-0.4	13.73	12.44	8.25	0.00	3.46
Z84-0.4	12.59	0.49	8.12	0.00	0.14
Z92-0.4	14.36	12.8	9.12	0.00	3.47
Z83-0.35	27.13	24.47	17.23	0.00	6.75
Z84-0.35	29.87	26.84	18.51	0.00	7.83
Z84-0.30	24.46	21.89	16.64	0.00	5.72

Table 3: Thermal analysis data of reproduced cement pastes hydrated for 28 and 90 days.

Sample ID	Starting mass, mg	Mass at 550 °C	Residual Mass, mg	Loss Chemical Water, mg	Loss of CO_2, mg
Z1-0.4 90 days	97.10	70.95	69.33	4.17	1.87
Z1-0.4 N 28 days	129.27	93.33	91.2	4.78	2.19
Z83-0.4 90 days	152.21	119.89	71.26	4.92	17.43
Z83-0.4 N 28 days	113.12	83.9	70.96	3.36	12.44
Z84-0.4 90 days	125.65	93.29	74.45	3.34	18.34
Z84-0.4 N 28 days	132.6	98.91	81.07	3.36	17.34
Z1-0.35 90 days	125.36	102.71	99.54	5.08	2.67
Z1-0.35 N 28 days	124.32	98.96	96.14	4.12	2.32
Z82-0.35 90 days	145.36	117.00	102.42	5.39	14.08
Z82-0.35 28 days	162.32	133.36	117.03	5.98	15.83
Z83-0.35 90 days	128.45	102.14	86.70	4.12	14.94
Z83-0.35 N 28 days	175.12	146.8	124.08	5.88	22.22
Z84-0.35 90 days	186.26	161.82	133.15	5.53	28.17
Z84-035 N 28 days	145.50	109.18	89.46	3.63	19.22
Z1-0.30 90 days	145.57	121.93	118.32	5.19	3.11
Z1-0.30 N 28 days	107.55	85.47	82.58	3.33	2.39
Z82-0.30 90 days	113.45	87.45	77.10	3.51	9.85
Z82-0.30 N 28 days	125.36	96.24	84.22	4.02	11.52
Z83-0.30 90 days	142.36	109.80	91.64	3.89	17.66
Z83-0.30 N 28 days	151.25	115.93	97.93	4.58	17.50
Z84-0.30 90 days	129.36	101.00	81.71	3.33	18.79
Z84-0.30 N 28 days	129.46	84.10	68.73	2.98	14.87

Table 4: Thermal analysis data of 28 and 90 days cured reproduced cement pastes after 28 days of accelerated carbonation.

Sample ID	Starting mass, mg	Mass at 550 °C	Residual Mass, mg	Loss Chemical Water, mg	Loss of CO_2, mg
Z1-0.4 90 days	160.30	119.13	113.39	6.31	6.26
Z1-0.4 N 28 days	116.05	87.83	84.48	4.18	3.27
Z83-0.4 90 days	124.05	101.64	81.00	2.37	25.24
Z83-0.4 N 28 days	103.56	86.61	68.64	1.85	21.35
Z84-0.4 90 days	121.87	103.22	77.99	1.44	29.42
Z84-0.4 N 28 days	129.34	114.66	81.18	0.50	33.24
Z1-0.35 90 days	148.90	113.06	108.16	5.69	3.90
Z1-0.35 N 28 days	108.83	84.31	74.26	3.79	3.29
Z82-0.35 90 days	189.36	149.58	137.19	4.95	25.84
Z82-0.35 28 days	105.00	83.32	71.82	3.00	14.25
Z83-0.35 90 days	180.00	147.94	127.91	4.89	33.52
Z83-0.35 N 28 days	112.06	92.62	74.00	2.92	20.53
Z84-0.35 90 days	122.00	105.51	76.82	2.27	29.12
Z84-035 N 28 days	158.95	131.84	106.64	1.23	28.05
Z1-0.30 90 days	140.50	110.38	105.89	4.29	4.66
Z1-0.30 N 28 days	110.08	86.05	83.62	3.04	3.75
Z82-0.30 90 days	156.06	122.96	106.38	4.37	17.99
Z82-0.30 N 28 days	104.12	83.11	71.89	2.94	12.03
Z83-0.30 90 days	121.30	95.99	80.40	2.81	22.18
Z83-0.30 N 28 days	150.80	124.74	101.00	2.86	32.12
Z84-0.30 90 days	111.06	92.04	72.84	2.20	23.03
Z84-0.30 N 28 days	116.57	96.82	75.89	2.02	23.77

Table 5: Thermal analysis data of hydrated C_2S and C_3S samples for 28 days.

Sample ID	Starting mass, mg	Mass at 550 °C	Residual Mass, mg	Loss Chemical Water, mg	Loss of CO_2, mg
C_2S-0.4	29.72	23.27	23.20	0.79	0
C_2S-0.5	35.92	30.58	29.31	0.90	0.76
C_2S-0.6	41.05	36.80	36.52	1.00	0.16
C_3S-0.4	36.45	28.21	27.01	11.10	0.22
C_3S-0.5	33.12	23.49	21.95	1.49	0
C_3S-0.6	31.45	25.58	24.98	1.87	0.27

Table 6: Thermal analysis data of hydrated C_2S and C_3S samples after 28 days of accelerated carbonation.

Sample ID	Starting mass, mg	Mass at 550 °C	Residual Mass, mg	Loss Chemical Water, mg	Loss of CO_2, mg
C_2S-0.4	28.17	27.24	22.01	0	5.16
C_2S-0.5	30.87	25.19	19.14	0	5.68
C_2S-0.6	34.55	31.81	22.89	0	8.4
C_3S-0.4	33.12	31.74	23.75	0	7.95
C_3S-0.5	28.40	25.51	17.45	0	7.48
C_3S-0.6	36.15	32.47	25.36	0.49	7.17

Table 7: Carbonation of hydrated pellets of C_3S at different time spans. The amounts of $Ca(OH)_2$ and $CaCO_3$ were determined by DTA/TGA.

Sample ID	Starting mass, mg	Mass at 550 °C	Residual Mass, mg	Loss Chemical Water, mg	Loss of CO_2, mg
C_3S-0.5 day zero	35.13	29.72	28.73	1.98	0.35
C_3S-0.5 1 day	30.45	26.16	24.96	1.45	1.11
C_3S-0.5 2 days	34.11	29.41	28.01	1.56	1.36
C_3S-0.5 4 days	32.42	27.7	25.91	1.44	1.52
C_3S-0.5 7 days	32.77	28.43	26.71	1.47	1.63
C_3S-0.5 14 days	36.15	30.88	28.59	1.51	2.05
C_3S-0.5 21 days	31.58	27.07	24.61	1.13	2.30
C_3S-0.5 28 days	34.82	31.39	27.45	0.94	3.81

Table 8: Carbonation of hydrated C_3S cylindrical blocks at different time spans.

Sample ID	Starting mass, mg	Mass at 550 °C	Residual Mass, mg	Loss Chemical Water, mg	Loss of CO_2, mg
C_3S-0.6 day zero	31.45	25.58	24.98	1.87	0.27
C_3S-0.6 1 day	30.32	26.43	22.01	0.75	4.40
C_3S-0.6 2 days	28.51	24.75	19.81	0.67	4.47
C_3S-0.6 4 days	38.4	33.39	26.87	0.83	6.55
C_3S-0.6 7 days	28.88	24.67	19.16	0.47	5.29
C_3S-0.6 14 days	31.60	27.34	21.69	0.50	6.02
C_3S-0.6 21 days	29.52	25.75	20.25	0.53	5.59
C_3S-0.6 28 days	36.34	33.13	25.66	0.50	7.32
C_3S-0.5 day zero	33.45	27.43	26.3	1.99	0.68
C_3S-0.5 1 day	26.11	21.09	16.95	0.88	3.59
C_3S-0.5 2 days	30.08	24.78	19.36	0.99	5.12
C_3S-0.5 4 days	33.24	27.33	21.59	1.07	5.61
C_3S-0.5 7 days	31.90	26.99	20.25	0.85	6.26
C_3S-0.5 14 days	32.02	26.66	19.52	0.78	6.44
C_3S-0.5 21 days	32.10	26.51	19.31	0.48	6.98
C_3S-0.5 28 days	31.57	26.98	19.61	0.41	7.17

Table 9: Carbonation of hydrated C_3S samples in polystyrene cups after different time spans.

Sample ID	Starting mass, mg	Mass at 550 °C	Residual Mass, mg	Loss Chemical Water, mg	Loss of CO_2, mg
C_3S-0.4 day zero	121.20	88.26	85.5	7.11	2.23
C_3S-0.4 1 day	150.55	115.70	95.91	4.31	19.69
C_3S-0.4 2 days	135.40	110.33	88.54	3.04	20.82
C_3S-0.4 4 days	149.21	121.43	97.26	2.77	26.32
C_3S-0.4 7 days	164.75	143.89	112.79	3.20	30.51
C_3S-0.4 14 days	166.59	131.85	104.71	3.00	28.79
C_3S-0.4 21 days	128.90	106.16	79.07	2.16	27.21
C_3S-0.4 28 days	160.60	135.59	100.09	2.31	35.91
C_3S-0.5 day zero	156.00	113.16	111.94	8.84	2.32
C_3S-0.5 1day	102.19	77.55	73.82	3.06	12.38
C_3S-0.5- 2 days	130.32	114.25	92.88	3.14	22.10
C_3S-0.5 4 days	127.96	110.11	88.90	2.52	23.25
C_3S-0.5 7 days	145.07	126.11	101.84	2.90	28.13
C_3S-0.5 14 days	142.95	120.24	90.44	2.81	30.17
C_3S-0.5 21 days	120.47	108.17	81.63	2.20	28.51
C_3S-0.5 28 days	150.15	140.00	102.17	2.47	39.05

Table 10: Carbonation of hydrated C_2S in polystyrene cups after different time spans.

Sample ID	Starting mass, mg	Mass at 550 °C	Residual Mass, mg	Loss Chemical Water, mg	Loss of CO_2, mg
C_2S-0.4 day zero	140.73	113.10	122.89	8.91	0.00
C_2S-0.4 1 day	102.19	77.49	73.82	5.74	2.97
C_2S-0.4 2 days	130.32	100.24	92.88	7.29	7.05
C_2S-0.4 4 days	127.96	101.09	88.9	5.99	11.19
C_2S-0.4 7 days	145.07	116.11	101.84	6.53	13.47
C_2S-0.4 14 days	142.95	115.23	100.44	6.27	13.92
C_2S-0.4 21 days	120.47	97.14	81.63	5.06	14.49
C_2S-0.4 28 days	149.15	121.37	102.17	6.08	18.68
C_2S-0.5 day zero	126.80	111.18	110.14	4.89	1.57
C_2S-0.5 1 day	143.11	12.85	130.26	120.36	3.90
C_2S-0.5 2 days	134.21	13.74	120.47	104.21	3.37
C_2S-0.5 4 days	149.10	15.50	133.60	113.56	3.02
C_2S-0.5 7 days	159.00	15.15	143.85	121.84	3.55
C_2S-0.5 14 days	126.63	20.54	106.09	78.62	2.10
C_2S-0.5 21 days	102.17	17.92	84.25	64.00	1.32
C_2S-0.5 28 days	105.41	12.53	92.88	70.11	0.73

Table 11: Carbonation of hydrated C_3A samples in polystyrene cups after different time spans.

Sample ID	Starting mass, mg	Mass at 550 °C	Residual Mass, mg	Loss Chemical Water, mg	Loss of CO_2, mg
C_3A-0.4 day zero	112.30	82.96	80.99	18.53	0.00
C_3A-0.4 1 day	103.25	26.88	71.26	18.42	2.25
C_3A-0.4 2 days	65.70	49.35	46.49	16.35	1.42
C_3A-0.4 4 days	150.00	112.75	108.27	26.22	3.49
C_3A-0.4 7 days	147.58	110.18	10.32	26.41	3.78
C_3A-0.4 14 days	141.60	108.38	99.21	22.94	7.21
C_3A-0.4 21 days	133.27	100.47	91.16	20.63	7.47
C_3A-0.4 28 days	148.49	112.01	100.81	21.96	9.82
C_3A-0.5 day zero	131.32	79.37	79.30	17.98	0.00
C_3A-0.5 1 day	144.33	108.11	94.62	20.00	10.86
C_3A-05 2 days	106.15	81.80	69.01	10.74	10.49
C_3A-0.5 4 days	104.36	80.29	70.56	11.18	9.67
C_3A-05 7 days	170.55	130.39	119.66	17.81	7.07
C_3A-0.5 14 days	152.06	115.38	115.85	16.41	13.56
C_3A-0.5 21 days	133.27	100.35	91.16	20.80	7.89
C_3A-0.5 28 days	148.49	111.76	100.81	22.04	9.62

Table 12: Carbonation of hydrated $C_2(AF)$ samples in polystyrene cups after different time spans.

Sample ID	Starting mass, mg	Mass at 550 °C	Residual Mass, mg	Loss Chemical Water, mg	Loss of CO_2, mg
$C_2(AF)$-0.4 day zero	107.69	82.28	80.82	22.45	0.00
$C_2(AF)$-0.4 1day	158.63	128.52	116.34	34.51	5.86
$C_2(AF)$-0.4 2 days	212.35	164.83	151.48	43.34	12.46
$C_2(AF)$-0.4 4 days	188.33	147.24	131.91	39.74	10.08
$C_2(AF)$-0.4 7 days	190.16	153.86	142.91	37.90	10.24
$C_2(AF)$-0.4 14 days	216.94	172.47	157.00	41.73	18.37
$C_2(AF)$-0.4 21 days	124.60	95.92	87.79	19.24	9.47
$C_2(AF)$-0.4 28 days	167.12	140.79	119.58	26.81	19.04
$C_2(AF)$ -0.5 day zero	142.93	111.80	109.75	32.89	0.00
$C_2(AF$)-0.5 1day	166.71	129.85	123.57	36.34	6.63
$C_2(AF)$-0.5 2 days	167.15	130.04	121.81	34.01	9.14
$C_2(AF)$-0.5 4 days	135.20	117.60	114.53	27.26	8.64
$C_2(AF)$-0.5 7 days	153.50	122.70	114.53	30.50	8.83
$C_2(AF)$-0.5 14 days	175.15	143.78	128.46	28.91	15.36
$C_2(AF)$-0.5 21 days	195.00	163.69	160.39	28.07	19.04
$C_2(AF)$-0.5 28 days	170.85	148.54	120.12	21.51	26.08

Table 13: Carbonation of hydrated model cement samples with w/c ratio of 0.5 in polystyrene cups after different time spans.

Sample ID	Starting mass. mg	Mass at 550 °C	Residual Mass. mg	Loss Chemical Water. mg	Loss of CO_2. mg
model cement day zero	156.00	113.10	122.89	8.91	0
model cement 1 day	102.19	77.49	73.82	5.74	2.97
model cement 2 days	130.32	100.24	92.88	7.29	7.05
model cement 4 days	127.96	101.09	88.9	5.99	11.19
model cement 7 days	145.07	116.11	101.84	6.53	13.47
model cement 14 days	142.95	115.23	100.44	6.27	13.92
model cement 21 days	120.47	97.14	81.63	5.06	14.49
model cement 28 days	149.15	121.37	102.17	6.08	18.68

9. LITERATURE

[1] U.S. Geological Survey. Mineral commodity summaries 2016. U.S. Geological Survey. Cement. **2016**. 44-45.

[2] S. Hainer. Karbonatisierungsverhalten von Betonen unter Einbeziehung klinker-reduzierter Zusammensetzungen. Ph. D. thesis. Technische Universität Darmstadt. **2015**.

[3] Fib Bulletin 67. Guidelines for Green Concrete Structures. International Federation for Structural Concrete Bulletin. **2012**. 1562-3610..

[4] T. Proske. S. Hainer. M. Jakob. H. Garrecht. C. A. Graubner. *Beton- und Stahlbetonbau.* **2012.** 401– 413.

[5] T. Proske. S. Hainer. M. Jakob. H. Rezvani. C. A. Graubner. *Cem. Concr. Res.*. **2013**. 51. 38–46.

[6] E. Gartner. *Cem. Concr. Res.*. **2004**. 34 (9). 1489–1498.

[7] H. Müller. M. Haist. M. Vogel. *Constr. Build. Mater.* **2014**. 67. 321–337.

[8] P. C. Aïtcin. Binders for durable and sustainable concrete. London. Taylor & Francis. **2008.**

[9] J. Bensted. P. Barnes. Structure and performance of cements. 2nd ed.. London. Spon Press **2002**.

[10] H. F. W. Taylor. Cement chemistry. 2nd ed. London. Thomas Telford. **1997**.

[11] A. G. de La Torre. R. N. de Vera. Cuberos. J.M. Antonio. A.G. Miguel Aranda. *Cem. Concr. Res.* **2008**. 38. 1261–1269.

[12] K. H. Jost. B. Ziemer. R. Seydel. *Acta Crystallogr. B.* **1977**. 33. 1696–1700

[13] A.Wesselsky. O. M. Jensen. *Cem. Concr. Res.*. **2009**. 39. 973-980.

[14] J. Stark. B. Wicht. Dauerhaftigkeit von Beton. 2. aktualisierte und erweiterte Auflage. Berlin. Heidelberg. Springer Vieweg. **2013.**

[15] C. B. Vanpeteghem. R.J. Angel. J. Zhao. N. L. Ross. G. J. Redhammer. F. Seifert. *Phys. Chem. Miner.*. **2008**. 35. 493–504.

[16] K. M. A. Malik. J. W. Jeffery. *Acta Crystallogr. B. **1976**.* 32. 475–480.

[17] T. Yano. K. Urabe. H. Ikawa. T. Teraushi. N.Ishizawa. S. Udagawa. *Acta Crystallogr. C.* **1993**. 49. 1555–1559.

[18] N. A. Yamnova. H. Sarp. T. Egorov. K. Yu. D. Yu. Pushcharovskii. *Kristallografiya*. **1993**. 38. 73-78.

[19] E. Bonaccorsi. S. Merlino. A.R. Kampf. *J. Am. Ceram. Soc.*. **2005**. 88. 505–512.

[20] T. Armbruster. *Eur. J. of Mineral.*. **2001**. 13. 577–590.

[21] S. Merlino. E. Bonaccorsi. H.F.W. Taylor. *Cem. Concr. Res.*. **2004**. 34. 1481–1488.

[22] J. A.Gard. H. F. W. Taylor. *Acta Crystallogr.*. **1960**. 13. 785–793.

[23] Y. Dai. E. J. Post. *Amer. Mineral.* **1995**. 80. 841–844.

[24] H. Mamedov. N.V. Belov. *Vses. Mineral. Obshchest.*. **1956**. *85*. 13-38.

[25] G. Krassimir „Struktur. Eigenschaften und quantitative Rietveldanalyse von hydrothermal kristallisierten Calciumsilikathydraten (C-S-H-Phasen)“ Dissertatiton. Karlsruhe. **2004.**

[26] J.A. Gard. K. Luke. H.F.W. Taylor. *Sov. Phys. Crystallogr.*. **1981**. 26. 1218-1223.

[27] J.A. Gard. T. Mitsuda. H.F.W. Taylor. *Miner. Mag.*. **1975**. 40. 312.

[28] R. K. Dhir. M. C. Limbachiya. M. J. McCarthy. A. Chaipanich. *Mater. Struct.*. **2007**. 40. 459–473.

[29] H. F. W Taylor. C. Famy. K.L. Scrivener. *Cem. Concr. Res.*. 31. 683–693.

[30] B. Bary. A. Sellier. *Cem. Concr. Res.*. **2004**. 34 (10). 1859–1872

[31] M. A. Peter. A. Muntean. S. A. Meier. M. Böhm. *Cem. Concr. Res.*. **2008**. 38. 1385–1393.

[32] A. Morandeau. M. Thiéry. P. Dangla. *Cem. Concr. Res.*. **2016.** 56. 153–170

[33] F. P. Glasser. T. Matschei. Proceedings of the 12th International Conference on the Chemistry of Cements (ICCC). Montreal. **2007**.

[34] A. Griesser “Cement-superplasticizer interactions at ambient temperatures: rheology. phase composition. pore water and heat of hydration of cementitious systems” Ph. D. thesis. Zurich. **2002**.

[35] F. Al-Neshawy “Computerised prediction of the deterioration of concrete building facades caused by moisture and changes in temperature” Ph. D. thesis. Espoo. **2013.**

[36] A. K. Ramezanianpour “Cement Replacement. Properties. Durabilty. Sustainability” Springer Verlag. Berlin. **2014**.

[37] DIN EN 197-1 Zement–Teil 1. *Zusammensetzung. Anforderungen und Konformitätskriterien von Normalzement*. **2004**. 197-1.

[38] K. Scrivener. R. Snellings. B. Lothenbach “A practical guide to microstructural analysis of cementitious materials” Boca Raton. CRC Press. **2016**.

[39] T. Hartmann. Labnote. Stoe StadiP. Stoe & Cie GmbH. Darmstadt. **2013**.

[40] International Centre for Diffraction. PDF-2 Data Release 2001 Sets. 1-151. 70-89. 2001

[41] H. M. Rietveld. *Acta Crystallogr.* **1966**. 20. 508–513.

[42] H. M. Rietveld. *J. Appl. Crystallogr.* **1969**. 2. 65–71.

[43] R. A. Young. P. E. Mackie. R. B. von Dreele. *J. App. Crystallogr.* **1977**. 10. 262–269.
[44] D. L. Bish. S. A. Howard. *J. App. Crystallogr.*. **1998**. 21. 86–91.
[45] R. E. Dinniebier. S. J. L. Billinge. Powder Diffraction Theory and practice. The Royal Society of Chemistry. Cambridge. UK. **2008**.
[46] W. Sha. E. A. O'Neill. Z. Guo. *Cem. Concr. Res.*. **1999**. 29. 1487–1489
[47] G. Villain. M. Thiery. G. Platret. *Cem. Concr. Res.*. **2007**. 37. 1182–1192. 4
[48] K. Scrivener. R. Snellings. B. Lothenbach. A practical guide to microstructural analysis of cementitious materials. Boca Raton. CRC Press. **2016**.
[49] DIN 66133: Determination of pore volume distribution and specific surface area of solids by mercury intrusion; **1993**.
[50] Hüttinger Elektronik GmbH & Co. KG. Freiburg
[51] National Instrument. LabVIEW (Laboratory Virtual Instrumentation Engineering Workbench) v8.2.1. **2007**.
[52] M. Schneider. M. Romer. M. Tschudin. H. Bolio. *Cem. Concr. Res.*. **2011**. 41. 642–650.
[53] B. Lothenbach. K. Scrivener. R.D. Hooton. *Cem. Concr. Res.*. **2011**. 41 1244–1256.
[54] M. Antoni. J. Rossen. F. Martirena. K. Scrivener. *Cem. Concr. Res.*. **2012**. 42. 1579–1589.
[55] S.V. B. Reddy. S. Rao. Experimental studies on compressive strength of ternary blended concretes at different levels of micro silica and ggb. Materials Todays. Proceedings B. **2016**. 3752-3760.
[56] D. Mostofinejad. F.Nosouhian. H. Nazari-Monfared. *Constr. Build. Mater.*. **2012**. 117. 107–120.
[57] N. Voglis. G. Kakali. E. Chaniotakis. S. Tsivilis. *Cem. Concr. Compos*.. **2005**. *27.191–*196.
[58] T. Vuk. V. Tinta. R. Gabrovšek. V. Kaučič. *Cem. Concr. Res.*. **2001**. 31. 135–139.
[59] B. Lothenbach. G. Le Saout. E. Gallucci. K. Scrivener. *Cem. Concr. Res.*. **2008**. 38. 848–860.
[60] V.L. Bonavetti. V.F Rahhal. E.F. Irassar. *Cem. Concr. Res.*. **2001**. 31. 853–859.
[61] S. Palm. T. Proske. M. Rezvani. S. Hainer. C. Müller. C. A. Graubner. *Cons. Build. Mater.*. **2016**. 119. 308–318
[62] ASTM C595 / C595M-17. Standard Specification for Blended Hydraulic Cements. ASTM International. West Conshohocken. PA. **2017**.
[63] CAN/CSA-A3000-08. CAN/CSA-A3000-08: Cementitious Materials Compendium. Canadian Standards Association. **2008.**

[64] C. V. Nielsen. M. Glavind. *J. Adv. Concr. Tech.*. **2007**. 3-12.
[65] S. Fennis "Design of ecological concrete by particle packing optimisation" PhD Thesis. Delft University of Technology. Netherlands. Gildeprint. **2010**.
[66] S. Fennis "Measuring the packing density to lower the cement content in concrete". in "Tailor made concrete structures: new solutions for our society". London. UK. Taylor & Francis Group. **2008**.
[67] J. Plank. E. Sakai. C. W. Miao. C. Yu. J. X. Hong. *Cem. Concr. Res.*. **2015**. 78. 81–99.
[68] H. Keller. J. Plank. *Cem. Concr. Res.*. **2013**. 54. 1–11.
[69] F. Mittermayr. M. Rezvani. A. Baldermann. S. Hainer. P. Breitenbücher. J. Juhart. *Cem. Concr. Comp.* **2015**. 55. 364–373.
[70] H.-M. Ludwig „Zur Rolle der Phasenumwandlung bei der Frost- und Frost- Tausalz-Belastung von Beton" Dissertation. Weimar. **1996**.
[71] P. H.R. Borges. J. O. Costa. N. B. Milestone. C. J. Lynsdale. R. E. Streatfield. *Cem. Concr. Res.*. **2010**. 40. 284–292.
[72] M. Castellote. L. Fernandez. C. Andrade. C. Alonso. *Mater. Struct.* 42 (4). pp. 515–525.
[73] Z. Šauman. *Cem. Concr. Res.*. **1971**. 1. 645–662.
[74] K. Suzuki. Y. Uno. *Cem. Concr. Res.*. **1994**. 55-61.
[75]T. Nishikawa. K. Suzuki. S. Ito. K. Sato. T. Takebe. *Cem. Concr. Res.*. **1994**. 6–14.
[76] C. Xiantuo. Z. Ruizhen. C. Xiaorong. *Cem. Concr. Res.*. **1994**. 1383–1389.
[77] B. Lagerblad. "Carbon dioxide uptake during concrete life cycle - State of the art" CBI report. Swedish Cement and Concrete Research Institute. Stockholm. **2005**.
[78] T. Kobayashi. R. Chikamatsu. A. Izobuchi. K. Ichise. "Study on the basic properties of low carbon concrete with high amount of admixture". Proceedings of the First International Conference on Concrete Sustainability. Japan Concrete Institute. Tokyo. **2013**.
[79] J.J. Chen. J. Thomas. H. F.W. Taylor. *Cem. Concr. Res.*. **2004**. 1499–1519.
[80] M. Thiery. G.Villain. P. Dangla. G. Platret. *Cem. Concr. Res.*. **2007**. 1047–1058.
[82] A. T. Harrison. M.R.Jones. M.D. Newlands. S. Kandasami. G. Khanna. *Mag. Concr. Res.*. **2012**. 737–747.
[83] Y. Ji. Y. Yuan. J. Shen. Y. Ma. S. Lai. *Wuhan Univer.. Technol.-Mat. Sci. Edit.*. **2010**. 515-522.
[84] M. Antoni "Investigation of cement substitution by blends of calcined clays and limestone". Ph. D. thesis. Ecole polytechnique Federale de Lausanne. Lausanne. **2013**.
[85] G.W. Groves. A. Brough. I. G. Richardson. M. C. Dobson. *J. Am. Cer. Soc.*. **1991**. 74. 2891–2896.

[86] K. Garbev. P. Stemmermann. L. Black. C. Breen. J. Yarwood. B. Gasharova. *J. Am. Cer. Soc.*. **2007**. 90. 900–907.

[87] L. Black. C. Breen. J. Yarwood. K. Garbev. P. Stemmermann. B. Gasharova. *J. Am. Ceram. Soc.*. **2007**. 90. 908–917.

[88] W. F. Cole. B. Kroone. *Nature 184. Brit. Assoc.*. **1959**. 57. 4688.

[89] P. A. Slegers. P. G. Rouxhet. *Cem. Concr. Res.*. **1976**. 6. 16381-388.

[90] Y. Ikeda. Y. Yasuike. M. Kumagai311. Y. Park. *J. Cer. Soc Jap.*. **1992**. 100 1098-1102.

[91] C. D. Atis. *Constr. Build. Mater.*. **2003.** 17. 147–152

[92] L. de Deukelaire. D. van Nieuwenburg. *Cem. Concr. Res.*. **1993**. 23. 442–452.

[93] L. Fernández-Carrasco. D. Torréns-Martín. Martínez-Ramírez. *Cem. Concr. Comp.*. **2012**. 34 1180–1186.

[94] J. Baron. "The Durability of Limestone Composite Cements in the Context of the French Specifications. Durability of Concrete: Aspects of Admixtures and Industrial. International Seminar". Swedish Council for Building Research. **1986.** 115–122.

[95] Y. Tezuka. D. Gomes. J.M. Martins. J.G. Djanikian "Durability aspects of cements with high limestone filler content". 9th International Congress of the Chemistry of Cement. New Delhi. India. **1992**.

[96] M. Schmidt. Zement-Kalk-Gips. **1992.** 45. 296-301.

[97] J.D. Matthews "Performance of limestone filler cement concrete". London. Taylor & Francis113–47. **1994.**

[98] L. Courard. F. Michel. *Constr. Build. Mater.*. **2014**. 51. 439–44.

[99] S. Tsivilis. G. Batis. E. Chaniotakis. G. Grigoriadis. D. Theodossis. *Cem. Concr. Res.*. **2000**. 30. 1679–1683.

[100] F. Lollini. E. Redaelli. L. Bertolini. *Cem. Concr. Comp.*. **2014**. 46. 32–40.

[101] A.P. Barker. J.D. Matthews "Concrete Durability Specification by Water / Cement or Compressive Strength for European Cement Types" in: "Durability of Concrete: Third International Conference". Nice France. **1994**.

[102] T. Matschei. B.Lothenbach. F. P..Glasser. *Cem. Concr. Res.*. **2007**. 37. 551–558.

[103] T. Matschei "Thermodynamics of cement hydration". Ph. D. thesis. Aberdeen University. **2007**.

[104] T. Matschei. B.Lothenbach. F. P..Glasser. *Cem. Concr. Res.*. **2007**. 118–130.

[105] M. S. Meddah. C. M. Lmbachiya. R.K. Dhir. *Cons. Build. Mater.*. **2014**. 58. 193–205.

[106] D. Damidot. S.J. Barnett. F.P. Glasser. D. Macphee. *Adv. Cem. Res.*. 2004. 16. 69-76.

[107] H.-J. Kuzel. *Cem. Concr. Comp.*. **1996**. 18.195–203.

[108] F. Goetz-Neunhoef. J. Neubauer. *Powder Diffraction*. **2011**. 21. 4-11

[109] O. Chaix-Pluchery. J. Pannetier. J. Bouillot. *J. Solid State Chemistry.* **1987**. 225-234.

[110] M. Francois. G. Renaudin. O. Evrard. *Acta Crystallogr. C.* **1998**. 54. 1214-1217.

[112] E.R. Gobechiya. N.A. Yamnova. A.E. Zadov. V.M. Gazeev. *Kristallografiya.* **2008**. 53. 437-441.

[113] P. Mondal. J. W. Jeffery. *Acta Crystallogr. B.* **1977**. 31. 1696-1700.

[114] E. Alvarez Ayuso. H.W. Nugreten. *Wat. Res.*. **2005**. 39. 65-72.

[115] C.J. Hampson. J.E. Bailey. *Mater. Sci.*. **1992**. 17. 3341–3346.

[116] K. Mahon. H. F. W. Taylor. ICDD 33-306. Aberdeen University. Scotland. **1980**.

[117] H. Schmidt. I. Paschke. D. Freyer. W. Voigt. *Acta Crystallogr. B*. **2011**. 67. 467-475.

[118] L. Smrcok. *J. App. Crystallogr.*.**1987**. 20. 320-322.

[119] T. Runcevski. R.E. Dinnebier. O.V. Magdysyuk. H. Poellmann. *Acta Crystallogr. B*. **2012**. 68.493-500.

[120] S.R. Kamhi. *Acta Crystallogr.*. **1963**. 16. 770-772.

[121] H. Bartl. T. Scheller. *Neues Jahrbuch für Mineralogie. Monatshefte*. **1970**. 547-552.

[122] B.F. Pedersen. D. Semmingsen. *Acta Crystallogr.*. B 38. 1074-1077.

[123] S.M. Antao. I. Hassan. *Canadian Mineralogist*. **2010**. 48. 1225-1236.

[124] M.C Schlegel. A. Sarfraz. U. Müller. U. Panne F. Emmerling. *Angew. Chem. Int. Ed. Engl.*. **2012**. 51. 4993-4996.

Curriculum Vitae

Personal Data

Name	:	Halil YILDIRIM
Adres	:	Hallgarten Straße 54. 60389 Frankfurt am Main. GERMANY
Mobile Phone	:	+49 172 885 97 21
Date of Birth	:	08.05.1985 Darende / TURKEY
Marital Status	:	Single

Work Experience

09/2012–09/2016	Technische Universität Darmstadt. Research Fellow / PhD Candidate
06/2012 – 08/2012	Daiyang SK Metal. Production Engineer. (Tekirdag / Türkei)
04/2011 – 03/2012	Istanbul Maritime & Survey. Quality Engineer. (Istanbul / Türkei)
05/2008 – 06/2008	End Aluminium Metal & Chemistry . Intern. (Kocaeli / Türkei)
07/2007 – 08/2007	Federal-Mogul Corporations & Pistons. Intern. (Kocaeli / Türkei)
08/2006 – 09/2006	Trakya Aluminium Metallurgy. Intern. (Kocaeli / Türkei)

Education

09/2012 – till date **PhD**

Eduard-Zintl-Institut für Anorganische und Physikalische Chemie. Technische Universität Darmstadt

Title of Dissertation: Investigation and Characterization of Eco-friendly Limestone-rich Concretes and their Carbonation Behavior

02/2010 – 04/2012 **Master Degree**

Material Science. Istanbul Technical University (ITU)

Title of Master Thesis: Production of Nickel Pig Iron from Domestic Lateritic Nickel Ores

09/2003 – 08/2008 **Bachelor Degree**

Material Science and Metallurgy Engineering. University of Sakarya

Title of Bachelor Thesis: Production of Ni-Al Metalic- Intermetalic Laminat (MIL) Composites

Darmstadt. den 18. Dezember 2017

Halil YILDIRIM

Halil YILDIRIM

Hallgartenstr. 54. 60389. Frankfurt am Main.
Germany

Erklärung

Ich erkläre hiermit an Eides Statt. dass ich meine Dissertation selbständig und nur mit den angegebenen Hilfsmitteln angefertigt habe.

Darmstadt. den 18. Dezember 2017

_____

Halil YILDIRIM

Halil YILDIRIM

Hallgartenstr. 54. 60389. Frankfurt am Main.
Germany

Erklärung

Ich erkläre hiermit. noch keinen Promotionsversuch unternommen zu haben.

Darmstadt. den 18. Dezember 2017 _____

Halil YILDIRIM